

**JOINT  
RESEARCH  
CENTRE**

# **ANNUAL PROGRESS REPORT ON NUCLEAR DATA 1994**

**INSTITUTE FOR REFERENCE MATERIALS AND MEASUREMENTS**

**GEEL (BELGIUM)**

**June 1995  
EUR 16288 EN**





**JOINT  
RESEARCH  
CENTRE**

**ANNUAL PROGRESS REPORT ON NUCLEAR DATA  
1994**

**INSTITUTE FOR REFERENCE MATERIALS AND MEASUREMENTS**

**GEEL (BELGIUM)**

**June 1995  
EUR 16288 EN**

#### **LEGAL NOTICE**

**Neither the Commission of the European Communities nor any person acting on behalf of the Commission is responsible for the use which might be made of the following information**

# TABLE OF CONTENTS

	Page
<b>EXECUTIVE SUMMARY</b> .....	1
<b>NUCLEAR DATA</b> .....	3
<b>NUCLEAR DATA FOR STANDARDS</b> .....	3
Neutron Data for Standards .....	3
<b>NUCLEAR DATA FOR FISSION TECHNOLOGY</b> .....	8
Neutron Data of Actinides .....	8
Neutron Data of Structural Materials .....	22
<b>NUCLEAR DATA FOR FUSION TECHNOLOGY</b> .....	24
<b>SPECIAL STUDIES</b> .....	30
<b>NUCLEAR METROLOGY</b> .....	44
<b>RADIONUCLIDE METROLOGY</b> .....	44
<b>TECHNICAL APPENDIX</b> .....	57
<b>LIST OF PUBLICATIONS</b> .....	67
<b>GLOSSARY</b> .....	73
<b>CINDA ENTRIES LIST</b> .....	75

**Note:** For further information concerning the Project Nuclear Measurements (Nuclear Data, Nuclear Metrology), please contact A.J. Deruytter, Project Manager, IRMM, Retieseweg, B-2440 Geel, Belgium

**Editor:** H.H. Hansen

## **Executive Summary**

A.J. Deruytter

In 1994, the last year of the third Framework Programme the main objectives of the project "Nuclear Measurements" have been pursued in the subprojects "Nuclear Data" and "Nuclear Metrology" : to improve the neutron standards data set, relative to which partial cross-sections or other quantities, important for fission and fusion technology, are determined; to improve the knowledge of radionuclide decay data for standards applications; to develop nuclear measurement techniques for nuclear and non-nuclear applications.

At the occasion of the International Conference on Nuclear Data for Science and Technology, Gatlinburg May 9-13, 1994 two invited and sixteen contributed papers were presented by IRMM staff.

The Geel linear electron accelerator, GELINA, was operational till end of July 1994 and then the refurbishment was started. The 7 MV Van de Graaff accelerator was operational during the full year.

The improvement of the set of **standard neutron cross-sections** and other quantities selected within the INDC/NEANDC Standards File continued. Total cross-sections have been measured in the frame of the NEA-NSC Interlaboratory collaboration on the  $^{10}\text{B}(n,\alpha)$  Standard Cross Section in order to extend the energy range where this cross-section can be used as a standard. Measurements and analysis in the range 80 eV to 100 keV were obtained at GELINA and additional data at the Van de Graaff accelerator facility in the energy region from 1.5 to 18 MeV using a Be-Li target as a white neutron source. Important additional detailed information on the fission process for  $^{252}\text{Cf}$  and  $^{237}\text{Np}$  was obtained.

Requests from the nuclear science community followed from deficiencies in available experimental data sets, which were detected by careful evaluation efforts in the framework of the Working Party on International Evaluation Cooperation (IEC) of the NEA Nuclear Science Committee (NEA-NSC). These requests are tackled in the framework of a newly formed NEA Working Party on Experimental Activities (WPEA).

In the field of **nuclear data for fission technology** high resolution neutron capture measurements were performed on  $^{58}\text{Ni}$  and analysed. The  $(n,n'\gamma)$  excitation functions for low-lying levels of palladium isotopes were measured for neutron energies between 0.2 and 3.3 MeV, in order to obtain more precise data on the inelastic scattering cross-sections for weakly absorbing fission product nuclides.

A collaboration was started with CEA Saclay and Cadarache to study total and capture cross-sections at GELINA. First measurements were done on  $^{237}\text{Np}$ .

In the field of **nuclear data for fusion technology** the very high resolution total neutron cross-section measurements of natural iron and  $^{27}\text{Al}$  were further

analysed, and the high resolution measurements on vanadium, a candidate for the blanket material in fusion reactors, were completed and the analysis is well underway. Measured and calculated differential and total yield cross-section data of  $^{58}\text{Ni}(n,\alpha)$  and  $^{63}\text{Cu}(n,xp)$  in the range from 2.0 to 15.6 MeV were thoroughly analyzed.

More basic measurements linked to the nuclear data programme were performed, mainly for PhD research. Results are reported under the heading Special Studies : spin assignments of  $^{113}\text{Cd}$  neutron resonances as a contribution to parity-non-conservation (PNC) studies; measurements of (n, charged particle) reactions on chlorine and of high resolution  $^{138}\text{Ba}(n,\gamma)$  cross-sections, for their key-role in astrophysical applications; investigation of fission fragments' mass and energy distribution of several plutonium isotopes.

In the **radionuclide metrology** subprojects highlights were: (1) the production and standardization of two sets of KX-ray fluorescence sources to calibrate X-ray detectors in the low-energy range; (2) neutron fluence monitor sets, irradiated in the High Flux Reactor (HFR) of JRC Petten, were measured and the fluence analysis was performed; (3) background characterization of IRMM low-level HPGe detector was done at the underground facility HADES (SCK, Mol) and MPI für Kernphysik, Heidelberg. Measurements of radionuclide concentrations in a Manchester Clay Standard were performed.

At the 7 MV Van de Graaff accelerator the Hydrogen Nuclear Resonant Reaction Analysis was installed using the resonant reaction  $^1\text{H}(^{15}\text{N},\alpha\gamma)^{12}\text{C}$ . Beam-line, new target area and reaction chambers were installed for the use of a  $^{15}\text{N}^+$ -beam for this hydrogen profiling technique.

At GELINA progress was made towards the equipment of a radiation physics laboratory. Extensive numerical simulations were carried out for the design of the electron beam-line and to predict the properties of the radiation produced by the different effects under consideration, i.e. Smith-Purcell effect, X-ray transition radiation, channeling radiation or parametric X-rays.

## NUCLEAR DATA

### NUCLEAR DATA FOR STANDARDS

The objective of the work on standard nuclear data is to improve the set of neutron data to be used in measurements consistency checks. Competing reactions, angular and kinetic energy distributions of the reaction products have to be studied to increase the reliability of the given standard cross sections. Appropriate research topics are selected from listings of the INDC/NEANDC Standards File. Complementary work is devoted to radionuclide decay data and associated atomic data requested for calibration and reference purposes.

#### **Standard Cross Section Ratio $^{235}\text{U}(n,f)/\text{H}(n,n)$**

F.-J. Hamsch and R. Vogt

The status of the experiment on the determination of the proton recoil events from the hydrogen containing sample has been presented at the International Conference on Nuclear Data for Science and Technology, Gatlinburg, USA. Due to the unexpected results reported in a recent progress report <sup>(1)</sup>, and the crucial point of good counting gas quality, a new ionization chamber with an intrinsic sample changer has been designed. The design is based on a paper by Ito et al. <sup>(2)</sup>. At present the sample changer is mounted between two cathode plates and should be accessible from outside, to perform a sample change without opening of the chamber (Fig. 1). In total five different samples can be placed simultaneously. For background reduction the chamber electrodes are made of high Z-material, tantalum, which has a very small charged particle production cross section.

#### **Investigation of the Correlation of Fission Fragments with Prompt $\gamma$ -ray Emission in $^{252}\text{Cf}(sf)$**

J. van Aarle\*, F.-J. Hamsch, R. Vogt

An investigation of the correlation of fission fragments with prompt  $\gamma$ -ray emission in  $^{252}\text{Cf}(sf)$  has been performed in the present reporting period. The aim of this investigation is to check whether an increased non-statistical high-energy  $\gamma$ -ray yield is found for masses around  $A \approx 132$  as compared to other masses as

---

\* EC Fellow from the University of Marburg, Germany

(1) CBNM Annual Progress Report on Nuclear Data (1992), EUR 15155 EN

(2) N. Ito, M. Baba, S. Matsuyama, I. Matsuyama and N. Hirakawa, Nucl. Instr. Meth. A337 (1994) 474

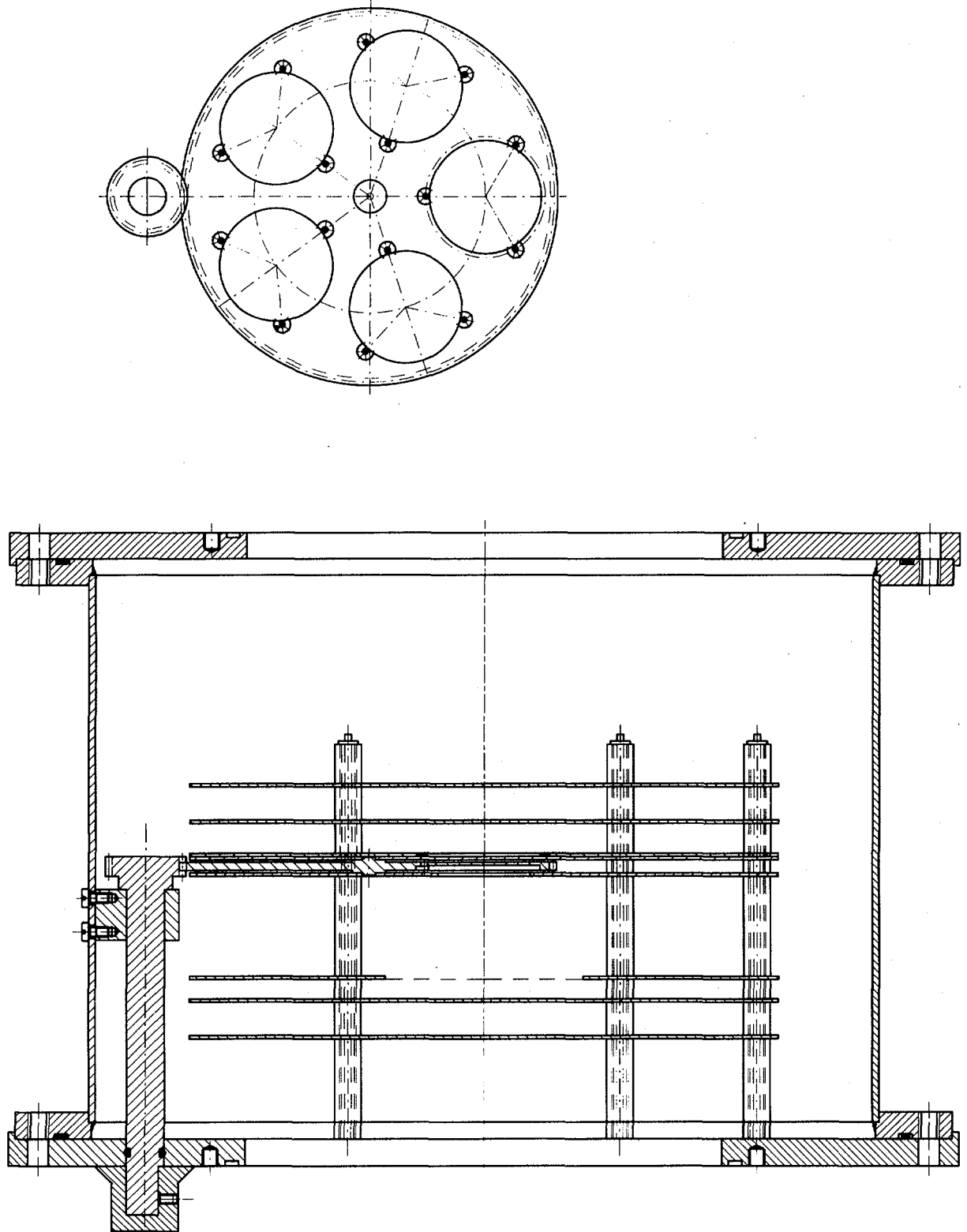


**Fig. 1.** Lower part: Cross-section of the ionisation chamber with the sample changer mounted between two cathode plates. Upper part: Top view of the actual sample positions on the turntable

already seen by other authors <sup>(1-3)</sup>. Furthermore for the determination of the excitation energy of the nascent fragments and of the level density parameters, it is necessary to know the average  $\gamma$ -ray energy as a function of mass and total kinetic energy (TKE). Also in the cold fragmentation region it will be checked whether it is possible to determine fragment charges via specific  $\gamma$ -ray transitions. As fission fragment detector a double Frisch gridded ionization chamber has been used. For the prompt  $\gamma$ -ray detection a HPGe-detector at a distance of 30 cm from the californium source has been taken. The schematical block diagram of the experiment is shown in Fig. 2. The data have been acquired during 6 months with the Delta-t 8 parameter data acquisition system. The data analysis is performed with LISA on a SUN-cluster and is still in progress. About  $2 \cdot 10^7$  events coincident with prompt  $\gamma$ -rays, and  $2 \cdot 10^7$  reference events, where only the fission fragment parameters are measured, have been acquired. The efficiency and energy calibration was performed with standard  $\gamma$ -ray sources. Calibration data and the respective calibration curves are shown in Fig. 3. The necessary corrections for ionization chamber signals have been applied to the raw data and preliminary preneutron fragment masses and TKE's have been calculated. The yield of  $\gamma$ -rays for different fission fragment mass windows has been calculated too, which exhibits indeed an enhanced  $\gamma$ -ray yield for masses around  $A \approx 132$  and  $\gamma$ -ray energies from 2 to 6 MeV, Fig. 4. In this Figure the yield is shown as a function of the  $\gamma$ -ray energy for the fragment masses  $A \geq 136$  and  $126 \leq A < 136$ .

Furthermore, the  $\gamma$ -ray spectra have been analyzed for individual masses too. In

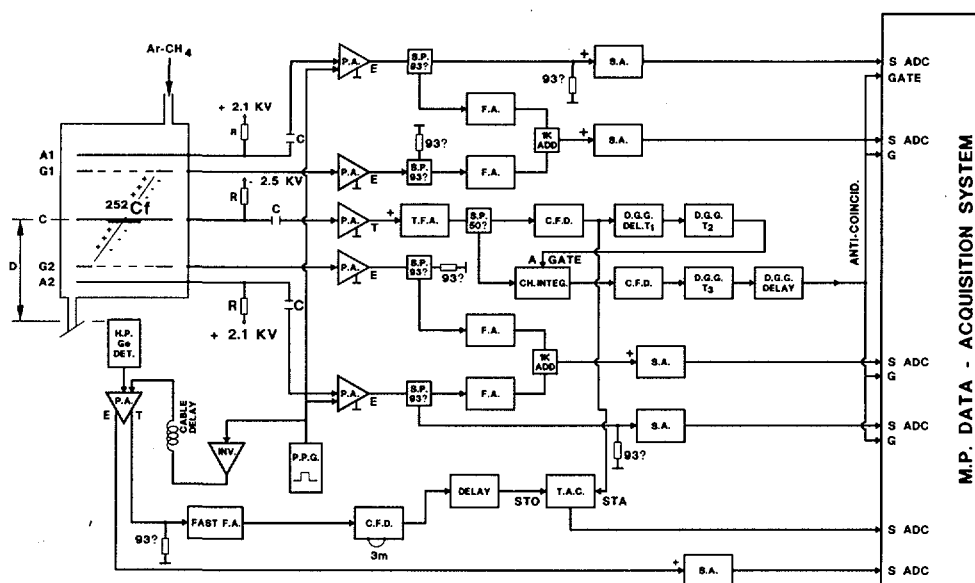
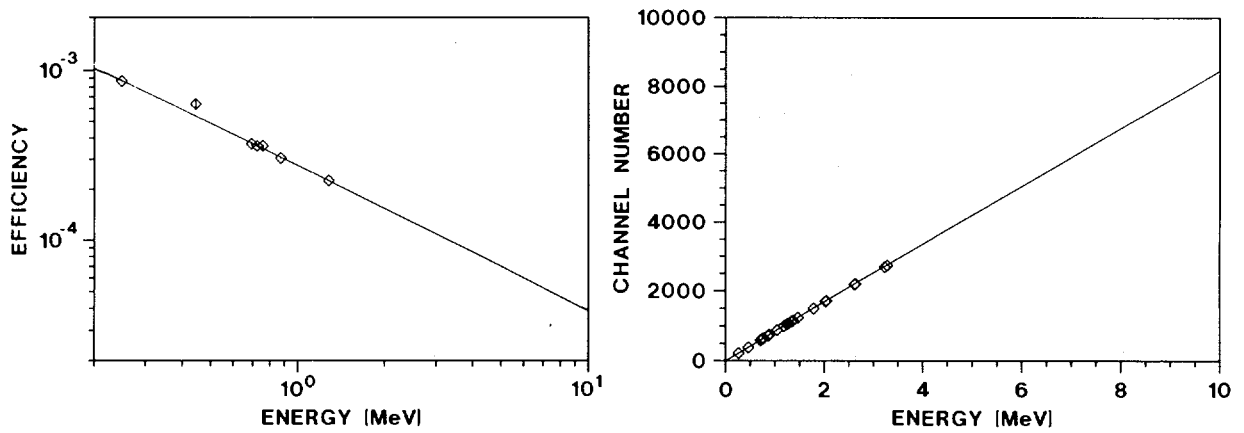


Fig. 2. The schematical block diagram of the experiment

- (1) P. Glaessel et al. Nucl. Phys. **A502**, (1989) 315c
- (2) A. Wiswesser, Diploma Thesis, MPI für Kernphysik, Heidelberg (1992)
- (3) P. Singer et al., Jahresbericht MPI für Kernphysik, Heidelberg (1993)



**Fig. 3.** Efficiency and energy calibration for the used HPGe detector. The solid lines show the fitted calibration curves and their extrapolation up to 10 MeV

Fig. 5 the preliminary data for two complementary masses ( $A = 107$  and  $A = 145$ ) are plotted. Evidently several  $\gamma$ -ray peaks are visible at different location for the light and the heavy fragment mass. However, the peak width is rather broad compared to the resolution of the HPGe detector, which is on one hand due to the Doppler broadening, but also due to slight shifts in the  $\gamma$ -ray energy spectra over the measurement period, which have to be corrected before the HPGe detector signals can be considered in the calibration of the ionization chamber.

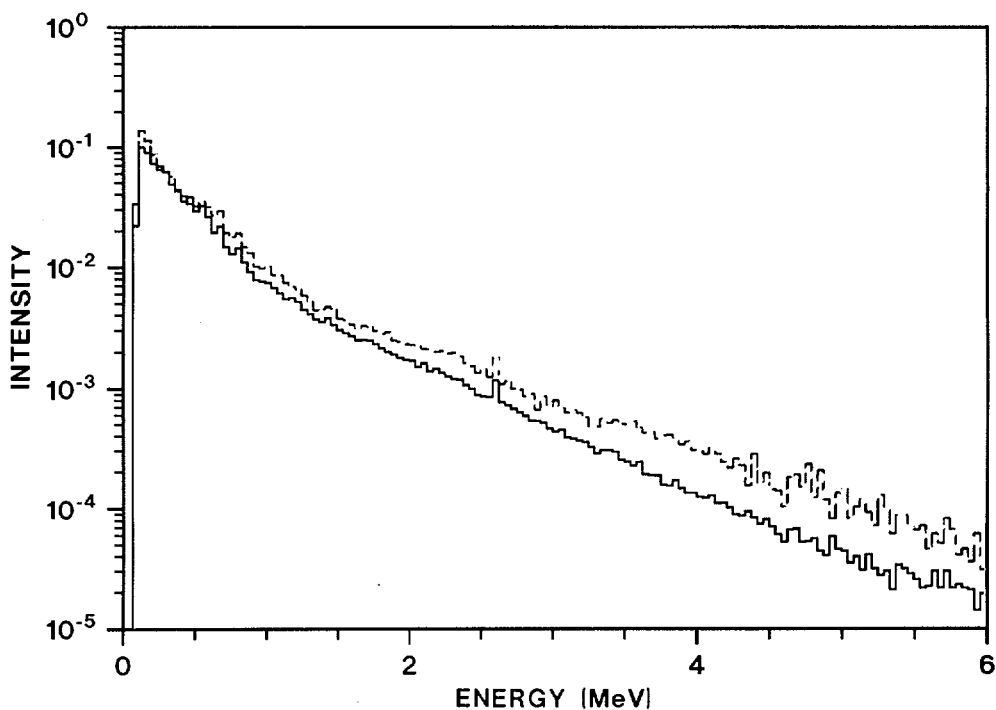


**Fig. 4.** The yield of  $\gamma$ -rays for different fission fragment mass windows,  $A > 136$  (full line) and  $126 \leq A \leq 136$  (dashed dotted line)

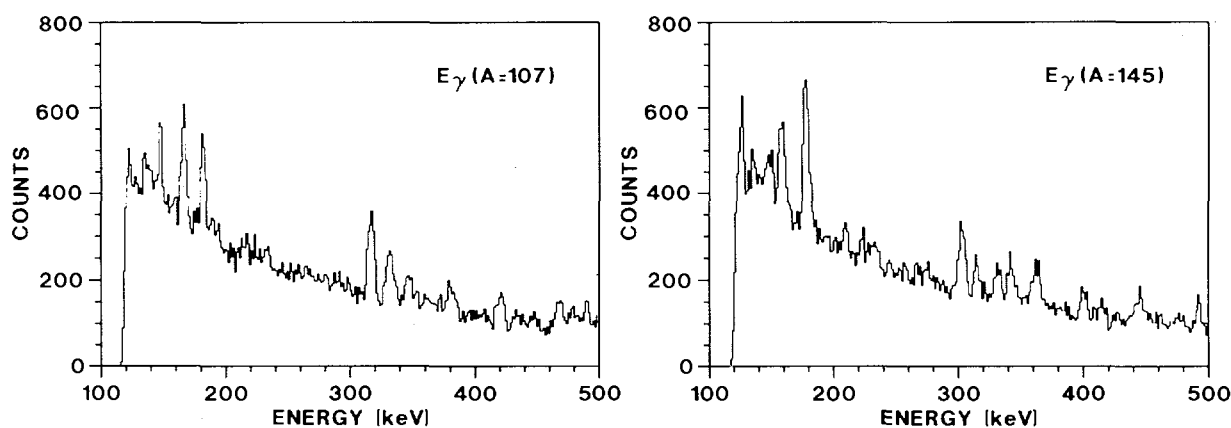


**Fig. 5.** The yield of  $\gamma$ -rays for different fission fragment masses,  $A = 107$  (left Figure) and  $A = 145$  (right figure)

**The Total Neutron Cross Section of  $^{10}\text{B}$  from 80 eV to 100 keV and from 1.5 to 18 MeV**

A.Brusegan, A.Crametz, E.Macavero, W.Schubert, C.Van der Vorst, E.Wattecamps

The  $^{10}\text{B}(n,\alpha)$  neutron cross section standard is of broad interest to the community of cross section measurers, evaluators and users because of both its importance and its relatively poor data base, which caused problems to the evaluators of the ENDF/B-VI files. In the framework of the NEANSC International Inter-Laboratory Collaboration on the  $^{10}\text{B}(n,\alpha)$  Standard Cross Section, the total cross section of  $^{10}\text{B}$  was measured at IRMM with two pulsed neutron sources, i.e. the 100 MeV GELINA and the 7MV Van de Graaff. The total cross sections of carbon and of  $^{11}\text{B}$  were determined, both as a test of the accuracy of the measurements and in order to determine the contribution of the  $^{11}\text{B}$  cross section. The GELINA measurements for  $^{10}\text{B}_4\text{C}$  and  $^{11}\text{B}_4\text{C}$  samples were analysed simultaneously with a least square fitting code and using for C the averaged total cross section values from ENDF/B-VI file. The resulting  $^{10}\text{B}$  total cross section values below 10keV agree to within  $\pm 0.5\%$  with ENDF/B-VI, but between 10 and 100 keV deviations up to 7% are observed. The  $^{10}\text{B}$  total cross section in the energy range from 1.5 to 18 MeV was measured at the Van de Graaff. Good agreement between experimental results and the ENDF/B-VI data is observed below 5 MeV.

Details on the measurement procedure are given in a paper presented at the International Conference on Nuclear Data for Science and Technology, Gatlinburg, USA in May 1994.

### **Neutron Fluence Measurement with Bonner Spheres**

C.Goddio\*, E.Wattecamps

In 1988 the CBNM (IRMM) participated in an international comparison of monoenergetic neutron fields of 2.5 and 14.7 MeV using the two-spheres technique<sup>(1)</sup>.

The participants BIPM, PTB and NPL made two independent background determinations: shadow cone and J. B. Hunt method. In 1991 the Bureau International des Poids et Mesures evaluated<sup>(2)</sup> 28 results of the four participating laboratories. The accuracy of the single measurements is 1.5 to 4.0 % and the deviation of the single measurements from the weighted mean is consistent with the statistical expectations, however one single result of CBNM (small sphere at 14.7 MeV) is 33 % higher than the mean value. To investigate this discrepancy, measurements with three Bonner spheres available at IRMM (5, 12.5 and 27.5 cm) were made recently at 14.7 MeV with the emphasis on a comparison of the J. B. Hunt procedure with the shadow cone method. Data analysis is in progress, as well as similar measurements at 2.5 MeV.

## **NUCLEAR DATA FOR FISSION TECHNOLOGY**

The objective of the work on nuclear data for fission technology is to reach a more accurate knowledge of data requested in fission research and in fission technology. Measurements cover actinide fission cross section data as well as structural material neutron interaction data. Research topics are taken to fulfil European demands collected in the NEA High Priority Request List.

### **Neutron data of Actinides**

#### **Revised Fission Mode Calculation for $^{252}\text{Cf}$**

J. van Aarle\*\*, F.-J. Hamsch

The calculation on fission modes in  $^{252}\text{Cf}$  (sf) using the multi-modal random neck-rupture model of Brosa, Grossmann and Müller<sup>(3)</sup> have been finished in the present reporting period. As the main result, the six expected fission modes were

---

\* EC Fellow from University of Torino, Italy  
\*\* EC Fellow from the University of Marburg, Germany  
(1) H. Liskien et al., CBNM Internal Report GE/R/VG/57/88  
(2) E.J. Axton, CCEMRI (III)91-4  
(3) U.Brosa, S.Grossmann and A. Müller, Physics Reports 197/4 (1990)

verified. The calculations have been executed on the SUN-SPARC computers of the Van de Graaff facilities as well as on the IBM RS-6000 computer of the LINAC facilities at IRMM. The program package has been described in an internal report<sup>(1)</sup>. The result of this code is an eight parameter data file containing the deformation energy ( $E_{\text{def}}$ ) as a function of five deformation parameters and the mass split. Since the visualization of an eight parameter data-set is impossible, Fig.6 shows two-dimensional plots in which the ordinate is always the semi-length  $l$  and the abscissa is one of the other parameters. In Fig. 6 (a), the energy  $E_{\text{gs}}-E_{\text{def}}$  is plotted as a function of the semi-length  $l$ . In this plane, the super-asymmetric fission mode (long-dashed line), the super-long mode (dotted dashed line), and the gross standard mode (solid, dotted, and short-dashed lines) are separated. The super-short fission mode (three-dotted dashed line) is also visible. Fig.6 (b) shows the neck-radius  $r$  as a function of the semi-length  $l$ . In this plane, the separation of the super-short channel (three-dotted dashed line) is clearly established. The bifurcation points for the super-asymmetric and the super-long mode are found to be in the ground state (gs) and in the second minimum, respectively. This is contrary to the earlier results<sup>(1)</sup> for  $^{252}\text{Cf}$ , who found the bifurcation point of the super-long mode behind the second minimum. In Fig. 11 (c), the asymmetry  $z$  is displayed as a function of the semi-length  $l$ . For the first time, this plane shows the three-partitioning of the standard fission mode into a standard I (solid line), a standard II (dotted line), and a standard III mode (short-dashed line). As a consequence of the asymmetry, the display of the heavy fragment mass  $A_{\text{H}}$  as a function of the semi-length  $l$  given in Fig. 6 (f) also shows the separation very distinct. The results from these calculations verified the existence of three separated standard channels. The two remaining Fig. 6 (d) and (e) show the curvature  $c$  and the center of gravity  $s$ , respectively as a function of the semi-length  $l$ . Again, the super-long, super-short and super-asymmetric modes are separately visible, whereas the three standard modes are more or less undiscernible. In all pictures of Fig.6, the pre-scission parameters can be obtained from the end-points of the given lines. The deformation parameters of the pre-scission shapes and the energy difference between the ground state  $E_{\text{gs}}$  and the scission point of each particular fission mode of  $^{252}\text{Cf}$  found in this calculation can be derived. Also, the parameters of the fission barriers of the standard fission mode, as well as the super-asymmetric, the super-long, and the super-short modes can be obtained. The parameters from this new calculation are in good agreement with earlier data<sup>(2)</sup>. For the first time, data for the standard III fission mode have been evaluated which enables a better explanation of experimental findings concerning the mass-yield and total kinetic energy distribution of  $^{252}\text{Cf}$ . The evaluation is still going on.

---

(1) P. Siegler, IRMM Internal Report GE/R/VG/84/94 (1994)

(2) IRMM Annual Progress Report on Nuclear Data (1993), EUR 15822 EN

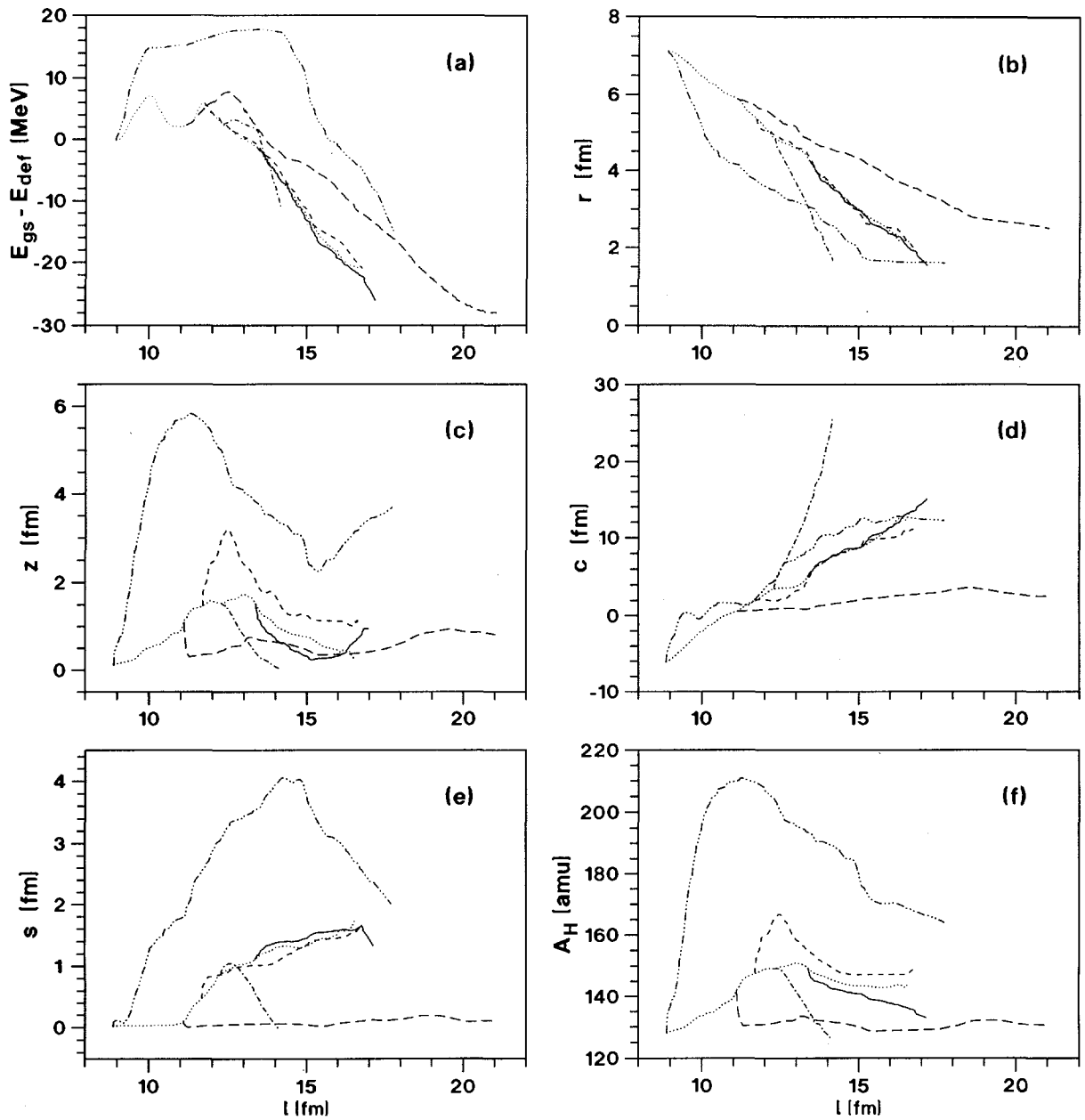


**Fig. 6.** Fission modes accompanying the spontaneous fission of  $^{252}\text{Cf}$ . For better visualization, the eight parameter data-set is displayed as a set of six two-dimensional graphs, namely (a) the energy difference  $E_{gs} - E_{def}$ , (b) the neck-radius  $r$ , (c) the asymmetry  $z$ , (d) the curvature  $c$ , (e) the center of gravity  $s$ , and (f) the heavy fragment mass  $A_H$ . Each parameter is plotted as a function of the semi-length  $l$  of the nucleus. The light fragment mass  $A_L$  is omitted since it represents just the same information as  $A_H$ . Each line given in the pictures represents a particular fission mode, namely the super-asymmetric mode (long-dashed line), the super-long mode (dotted dashed line), the super-short mode (three-dotted dashed line), the standard I mode (solid line), the standard II mode (dotted line), and the standard III mode (short-dashed line). The end-point of each particular fission mode represents the parameter set for the pre-scission configuration.

### Neutron Induced Fission of $^{237}\text{Np}$

P. Siegler\*, F.-J. Hambsch, R. Vogt

The analysis of fission fragment properties of the reaction  $^{237}\text{Np}(n,f)$  has been finished in the present reporting period.

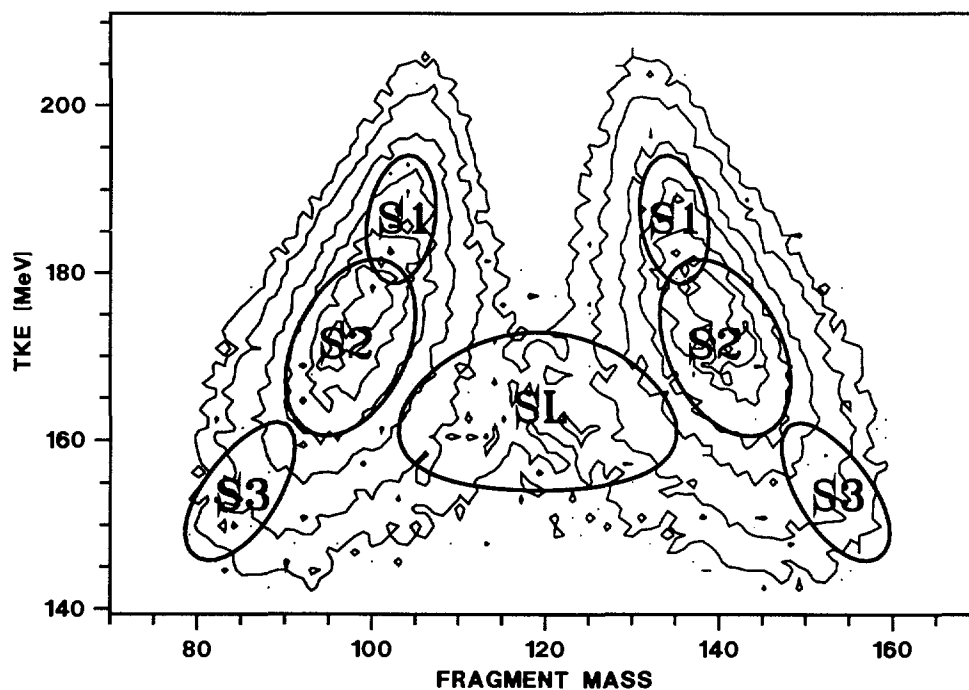
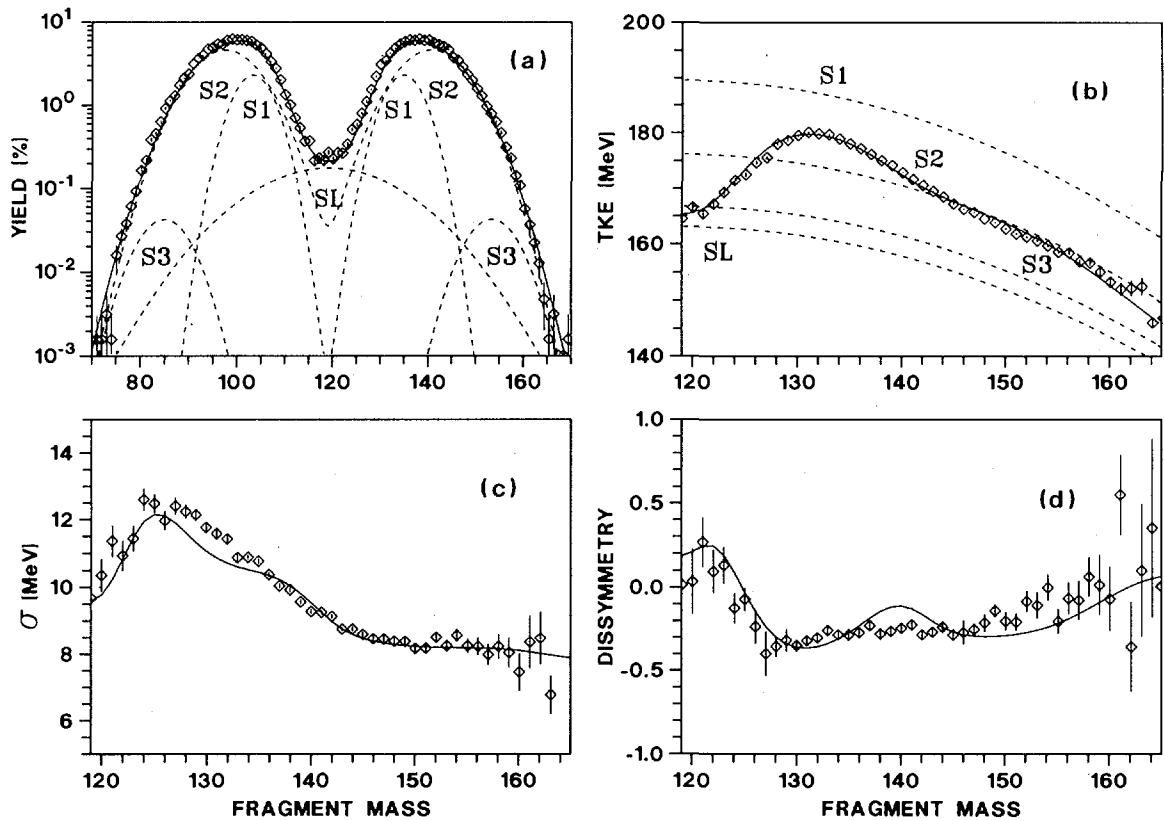


Fig. 7. Contour-plot of the mass-energy distribution for  $E_n=5.5$  MeV with the position of the four fission modes indicated by 50% contour lines

The crucial point was the understanding of the observed fluctuations in the mean total kinetic energy (TKE) of the fragments as a function of the incident neutron energy. The changes in the mass-yield and TKE(A) distribution could not be disentangled to explain the fluctuations found in TKE( $E_n$ ). However, including the achieved theoretical results from the multi-modal random-neck rupture calculations, performed<sup>(2)</sup> for the compound system  $^{238}\text{Np}$ , it was possible to describe and explain the TKE( $E_n$ ) fluctuations. The experimental yield distributions as a function of mass and TKE have been parameterized at each measured  $E_n$  by four two-dimensional Gaussian like functions, which are related to the four fission modes found by the theoretical calculations. The position and the FWHM of the four fission modes can be seen in the upper part of Fig. 7. In Fig. 8 the experimental data are compared to the fitted results for the mass-yield, the TKE(A),  $\sigma_{\text{TKE}}$  and the dissymmetry of the TKE(A) distribution. For the mass-yield and the TKE(A) the contributions of the fission modes are also indicated. It is obvious, that the fit reproduces the experimental data quite well and also the

\* EC Fellow from the Technical University of Darmstadt, Germany  
 (2) CBNM Annual Progress Report on Nuclear Data (1992), EUR 15155 EN



**Fig. 8.** Comparison of the fit with the data at  $E_n=5.5$  MeV for (a) the yield-distribution, (b) the TKE(A), (c)  $\sigma_{TKE}$  and (d) the dissymmetry. The full lines are the results of the fit, whereas in the upper part the fission mode contributions are given by dotted lines

existence of the standard III mode has been verified, resulting in a better chi-square if included.

Of interest is also the change of the population of the major fission modes standard I and II as a function of  $E_n$ . Starting from  $E_n=0.3$  MeV, the yield of standard I is decreasing continuously, whereas standard II shows an increasing yield. Also the TKE for each fission mode undergoes changes as a function of  $E_n$ . The TKE for standard I increases up to  $E_n \sim 2$  MeV which is slightly indicated also for standard II. Above  $E_n \sim 3$  MeV the TKE for each mode is nearly constant. With the observed changes in the mass-yield or the TKE of the individual fission modes the resulting changes in  $TKE(E_n)$  are calculated and presented in Fig. 9. It is evident that below the barrier the changes in TKE of the individual modes are the dominating factor, attenuated by the opposite behaviour of the fission modes in the mass-yield distribution. Above  $E_n \sim 0.7$  MeV, however, the individual TKE stays more or less constant and the decrease in  $TKE(E_n)$  is due to the change in the mass distribution.

This conduct can be explained assuming a transformation of the imparting neutron energy into pre-scission kinetic energy below the fission barrier, resulting in an increasing TKE of the fragments. On the other hand, the changing population of standard I and standard II above the barrier can not be understood from the model calculations because the bifurcation point is beyond the second

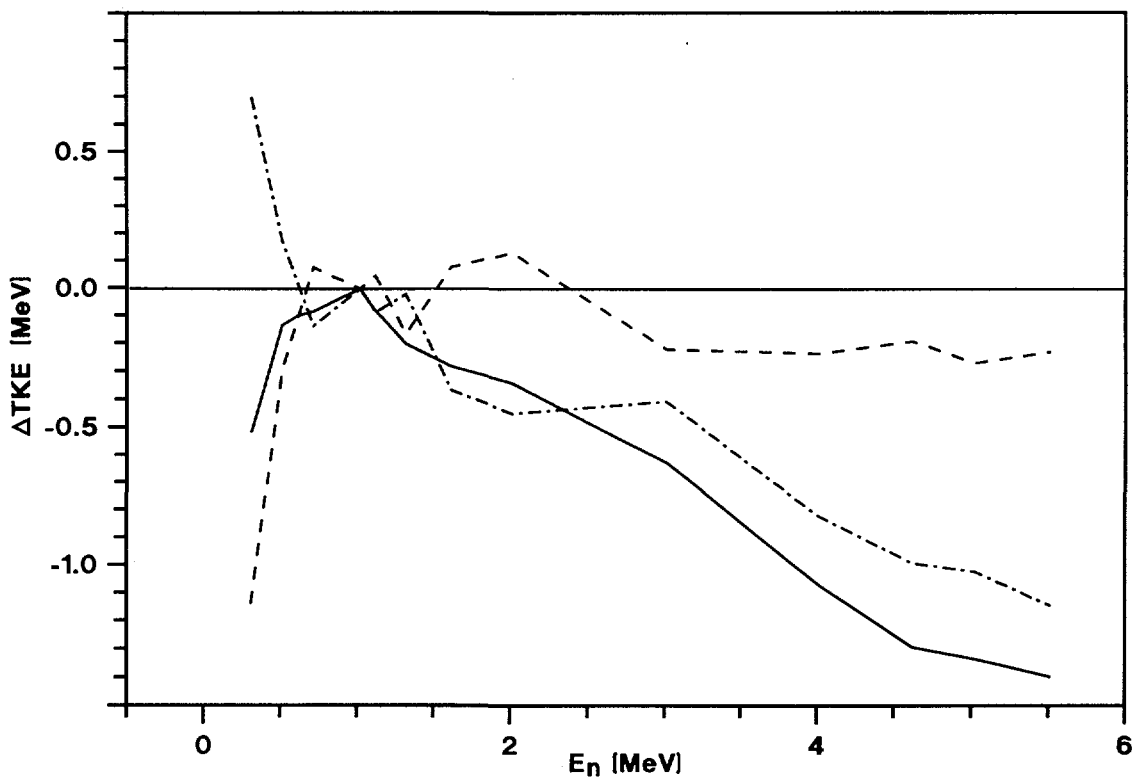


**Fig. 9.** *The fluctuation in TKE (relative to TKE at  $E_n=1.0$  MeV) (full line) and the partition in changes related to changes in TKE(A) (dashed line) and the mass distribution (dash-dotted line)*

barrier. An ansatz for this problem may be found in the temperature dependence of the potential energy at the scission point and its relation to the probability of forming different fission fragments. The nuclear temperature and an energy balance at scission has been included in a semiempirical model of Ruben et al.<sup>(3)</sup>. The calculated results from this model compared with the experimental TKE( $E_n$ ) show a reasonably good agreement. Also in the case of symmetric fission new results have been achieved, confirming the existence of an additional barrier. The partial cross section for this mode calculated from the yield and the absolute fission cross section is shown in Fig. 10 together with a Hill-Wheeler fit and the corresponding fit parameters. Evidence for a separate fission barrier is clearly shown for the super-long fission mode. The resulting barrier height of 10.3 MeV is in good agreement with the theoretical value of 10.9 MeV.

A complete description of the experiment and the results are available in form of a doctorate thesis.

(1) A. Ruben et al., Z. Phys. **A338** (1991) 67

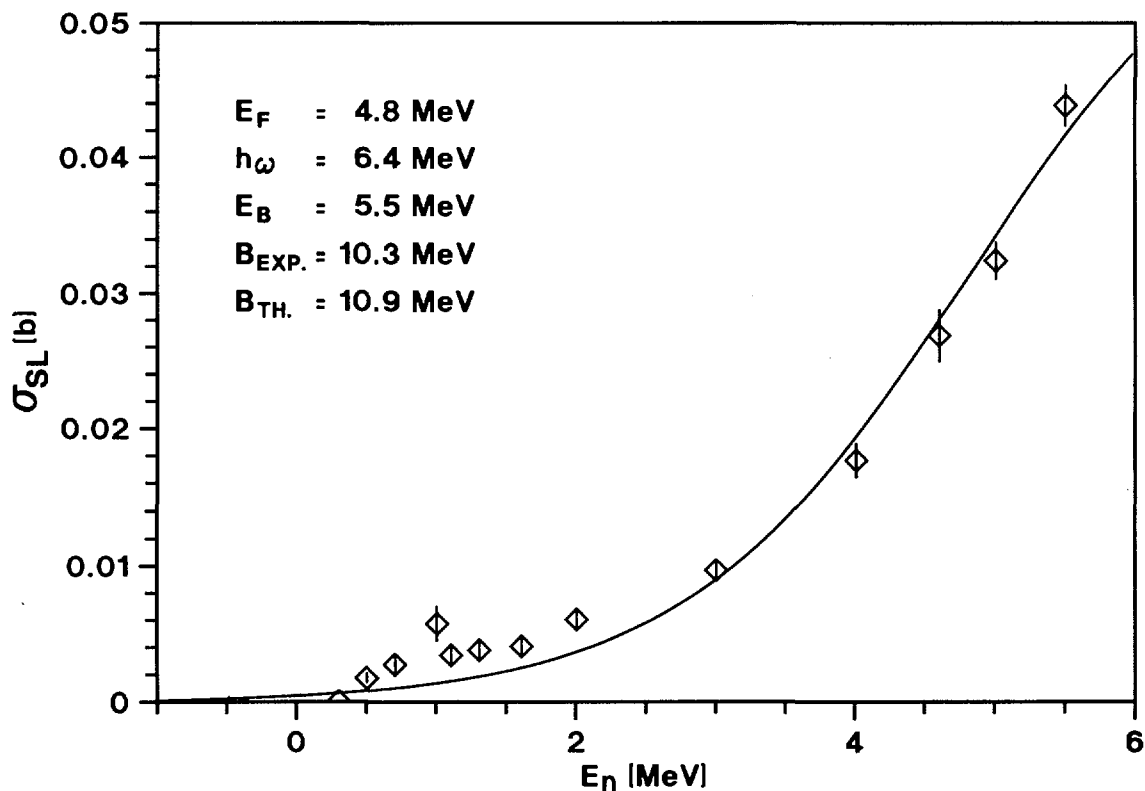


Fig. 10. The fission cross section of the super-long mode compared to a Hill-Wheeler fit (full line)

#### Fission-Mode Calculations for Nuclei with $90 \leq Z \leq 114$

S. Oberstedt\*, F. J. Hamsch

With the computer code RAYLSCAN<sup>(1,2)</sup> the energy landscape of about 50 isotopes between  $^{230}\text{Th}$  and  $^{292}114$  have been investigated between ground-state and scission. Initial data sets for fission-mode calculations in e.g.  $^{232,234,\dots,239}\text{U}$ ,  $^{238,\dots,243}\text{Am}$  and the even isotopes  $^{250,\dots,260}\text{Fm}$  are available now.

From 18 isotopes also fission-mode calculation of the standard as well as the super-long mode (super-short mode in cases of  $^{256,258}\text{Fm}$  and  $^{292}114$ ) have almost been completed. The calculated shape isomeric ground-state energy  $E_{II}$ , the heights of the inner and outer standard barriers,  $E_A$  and  $E_B$ , the superlong as well as the supershort barriers,  $E_{sl}$  and  $E_{ss}$ , are listed in Table 1.

\* SCK/CEN, Mol, Belgium

(1) S. Oberstedt, Internal Report IRMM GE/R/VG/77/93

(2) IRMM Annual Progress Report on Nuclear Data (1993) EUR 15822 EN

**Table 1.** Fission barrier heights  $E_A$ ,  $E_B$  and isomeric ground-state energies  $E_{II}$  obtained from fission-mode calculations.  $E_{sl}$  and  $E_{ss}$  denote the heights of the outer barriers related to the superlong and supershort fission-mode, respectively. All energies are in MeV

	$E_{II}$	$E_A$	$E_B$	$E_{sl}$	$E_{ss}$
$^{230}\text{Th}$	2.3	4.7	8.8	-	-
$^{233}\text{Th}$	1.8	5.5	8.5	12.2	-
$^{236}\text{U}$	2.4	6.3	9.5	10.9	-
$^{238}\text{U}$	2.6	6.2	10.1	11.2	-
$^{239}\text{U}$	2.4	6.8	9.9	-	-
$^{237}\text{Np}$	2.7	5.2	7.2	11.0	-
$^{238}\text{Np}$	2.9	5.6	7.5	11.0	-
$^{240}\text{Pu}$	2.5	6.7	8.7	10.3	-
$^{241}\text{Pu}$	2.3	6.9	9.1	-	-
$^{241}\text{Am}$	2.7	6.4	8.1	-	-
$^{242}\text{Am}$	2.8	6.9	8.4	-	-
$^{243}\text{Am}$	2.9	6.8	8.1	10.1	-
$^{244}\text{Cm}$	2.2	6.1	7.7	-	-
$^{246}\text{Cf}$	2.0	6.2	6.0	7.0	-
$^{252}\text{Cf}$	1.9	7.0	6.3	7.7	-
$^{256}\text{Fm}$	1.4	7.4	4.6	-	(3.2)
$^{258}\text{Fm}$	1.2	7.1	(4.1)	-	(3.4)
$^{292}114$	-	-	12.4	12.0	12.1

### **Investigations on the Fission Barrier Penetrability**

S. Oberstedt\*

On the basis of results from fission-mode calculations (see preceding section) the penetrability of the double-humped fission barrier has systematically been investigated.

Although several attempts were already made<sup>(1-4)</sup>, the extrapolation to hitherto unknown shape isomers, e.g. in  $^{239}\text{U}$  and  $^{238}\text{Np}$ , still appears as an open problem.

---

\* SCK/CEN, Mol, Belgium

- (1) H. Weigmann and J. P. Theobald, Nucl. Phys. A187 (1972) 305
- (2) V. Metag, Nucleonica, 20 (1975) 789
- (3) P. Möller, J. R. Nix and W. J. Swiatecki, Nucl. Phys. A469 (1987) 1
- (4) P. Möller, J. R. Nix and W. J. Swiatecki, Nucl. Phys. A492 (1989) 349

In this approach the penetrability of the fission barrier at excitation energy  $E$  has been calculated in WKB-approximation

$$P(E) = \left\{ 1 + \exp \left[ 2 \int_{D_1}^{D_2} (2B(D)/\hbar^2 [V(D) - E])^{1/2} dD \right] \right\}^{-1} \quad (1)$$

where  $V(D)$  is the energy of the fission barrier at deformation  $D$ . The integration limits  $D_1$  and  $D_2$  are determined by  $V(D_1) = V(D_2) = E$ .

For the effective inertia  $B(D)$  a slightly modified approximation has been used<sup>(3)</sup>:

$$B(D) = \mu(D) \left\{ 1 + 18.13 ((D_{sc} - D)/(D_{sc} - 0.75))^m \exp[-2.51(D - 0.75)] \right\}$$

which reduces to  $B(D) = \mu(D)$  for  $D > D_{sc}$ , the respective deformation at scission<sup>(3,4)</sup>. Instead of considering only  $m = 2$  or  $m = 4$  the parameter  $m$  is now individually adjusted in order to reproduce experimental half lives. Additionally, the reduced mass  $\mu$  depends now on  $D$  according to the calculated mass-asymmetry along the respective fission-mode. Only the standard-mode has been considered being the most important mode in low-energy fission.

A series of calculations based on various approximations have been performed. Details of the successive approaches have been described in some papers prepared for publication during the reporting period.

In order to prepare the next investigations, the calculations have been extended to estimate the shape isomeric half lives in  $^{233}\text{Th}$ ,  $^{239}\text{U}$  and  $^{238}\text{Np}$ . The shape isomer in both nuclei should decay predominantly via  $\gamma$ -ray emission back to the groundstate with a half life  $T_{1/2} \approx 200$  ns and  $T_{1/2} \approx 20$   $\mu\text{s}$ , respectively, consistent with recently obtained experimental results. The estimated half life for the shape isomer in  $^{238}\text{Np}$  ( $\approx 0.5$   $\mu\text{s}$ ) suggests the need for a new  $(n, \gamma)$ -experiment at subthreshold energies.

### ***Gamma Spectroscopy above the Shape Isomeric Groundstate of $^{239}\text{U}$***

S. Oberstedt\*, F. Gunsing\*\*

Gamma rays from resonance neutron capture in  $^{238}\text{U}$  s-wave resonances at neutron energies  $E_n$  between 20 eV and 800 eV have been investigated. Several hitherto unknown gamma transitions could be observed<sup>(1)</sup> in the  $\gamma$ -ray spectrum of the subthreshold fission resonance at  $E_n = 721.6$  eV, which was supposed to be the first observation for  $\gamma$ -decay of a quasi class-II state within the second potential well of  $^{239}\text{U}$ . These transitions are also visible to much weaker extent in

---

\* SCK/CEN, Mol, Belgium

\*\* EC Fellow from the University of Delft, The Netherlands

(1) CBNM Annual Report 1992, EUR 15029 EN

the  $\gamma$ -ray spectra of the other fission resonances belonging to the same intermediate structure around  $E_n = 720$  eV. Possible  $\gamma$ -transitions from the deexcitation of a class-II state were found at  $E_\gamma = 1299.2, 1339.2, 1344.6, 1475.8$  and  $1479.6$  keV.

In a quantitative analysis the relative peak area  $I_\gamma$  of all presumable class-II transitions obtained from the four strongest neutron resonances, accounting for almost 100 % of the fission intensity of the intermediate structure, were compared to theoretical values  $I_\gamma^{\text{theor}}$  estimated from the class-II fraction and the decay widths of the respective neutron resonance<sup>(1)</sup>. It turned out that the observed relative peak areas are strongly correlated with their expected values  $I_\gamma^{\text{theor}}$ . Several well-known transitions of the  $\gamma$ -cascade to the groundstate ( $E_\gamma = 629.7, 638.5, 787.2$  and  $794.1$  keV) show a strong anti-correlation, which is due to the small fraction  $(1 - c_{II})$  within the first potential well. Additionally the deexcitation of the shape isomeric ground-state may proceed through different  $\gamma$ -decay branches within the first potential well.

From both results and the fact that these transitions could not be found in any of the other s-wave neutron resonances between 20 eV and 700 eV, the possibility of having observed capture  $\gamma$ -rays from the cascade toward the ground-state may be excluded. Also the alternative interpretation as being  $\gamma$ -quanta from fission fragments seems to be very unlikely, because they are not observed in  $\gamma$ -ray spectra of any other s-wave fission resonance below  $E_n = 700$  eV in  $^{238}\text{U}$  being all of class-I type.

### ***Investigation of the Fission Fragments' Mass and Energy Distributions for Several Plutonium Isotopes***

L. Dematté\*, C. Wagemans\*\*, P. D'hondt\*\*\*, S. Pommé\*\*\*, A. Deruytter, R. Barthélémy, J. Van Gils

In the frame of a systematic study of the mass and energy distributions (and their correlations) of the spontaneously fissioning plutonium isotopes, about 32000  $^{242}\text{Pu}(\text{SF})$  and 18000  $^{244}\text{Pu}(\text{SF})$  events have been recorded. The measurements were performed with the double energy detection method and relative to the well known  $^{239}\text{Pu}(n_{\text{th}},f)$  reaction, for which purpose a thermal neutron beam of the BR1 reactor (SCK/CEN, Mol, B) was used.

As explained in the previous annual report, the neutron emission data of Wahl<sup>(2)</sup> for the reaction  $^{239}\text{Pu}(n_{\text{th}},f)$  were used for the neutron emission correction of the

---

\* EC fellow from the University of Padova, Italy

\*\* University of Gent, Belgium

\*\*\* SCK/CEN Mol, Belgium

(1) S. Oberstedt and F. Gunsing, Internal Report IRMM GE/R/ND/01/94

(2) A.C. Wahl, Atom. Data and Nucl. Data Tables 39 (1988) 1

$^{242}\text{Pu}(\text{SF})$  and  $^{244}\text{Pu}(\text{SF})^{(1)}$  measurements, after normalizing them to the average number of neutrons emitted in  $^{242}\text{Pu}(\text{SF})$  and  $^{244}\text{Pu}(\text{SF})$ , respectively. The pre-neutron emission mass distributions obtained in this way are shown in Fig. 11 and compared with similar results previously obtained for  $^{236}\text{Pu}(\text{SF})$ ,  $^{238}\text{Pu}(\text{SF})$  and  $^{240}\text{Pu}(\text{SF})^{(1)}$ , re-analysed with the same neutron correction method presently used for the sake of consistency. It is apparent that  $^{242}\text{Pu}$  acts as a kind of "turning point": up to  $A = 242$  the mass yield around  $m_h \approx 135$  increases with increasing values of  $A$ , whilst the mass yield around  $m_h \approx 142$  correspondingly decreases. For  $A = 244$  however, the mass yield around  $m_h \approx 135$  decreases as compared to  $A = 242$ , whilst the mass yield around  $m_h \approx 142$  stabilizes. This behaviour can be understood by the interplay of the standard I and standard II fission modes (or the corresponding shells) together with the conservation of the  $N/Z$  ratio of the fissioning nucleus during the fission process. A quantitative analysis of this hypothesis is currently under investigation.

Furthermore, a method of analysis of the so-called cold fission (i.e. fission without emission of neutrons) was developed, based on the calculation of the nuclear masses by Möller et al.<sup>(2)</sup> and applied to the five spontaneously fissioning plutonium isotopes and to the  $^{239}\text{Pu}(n_{\text{th}},f)$  data as well.

In fact, without a direct measurement of the neutron emission, the only way to analyze the cold fission consists in selecting the events having too little internal energy to emit a neutron, i.e. having a very high total kinetic energy. Very often this is achieved by putting a window on the light fragment energy. A better way is to calculate the maximum  $Q$ -value for the fission process with one neutron emission: above this limit, only cold fission events can exist. As can be seen from Fig. 12 the two methods give quite different results for symmetric and very asymmetric mass splitting.

### ***Fission Modes and Ternary Fission : Is there a Correlation with the Fission Modes?***

S. Pommé\*, C. Wagemans\*\*, R. Barthélémy, J. Van Gils

The objective of this investigation is the question whether there exists a correlation between 'fission modes' and the probability for ternary fission of a heavy nucleus.

Charged particle emission is a fast phenomenon that takes place in the final stage of the fission process. The energy required to release these particles, being a large fraction of the available energy, needs to be stored in a readily available form.

---

\* SCK/CEN, Mol, Belgium

\*\* University of Gent, Belgium

(1) C. Wagemans et al., Nucl. Phys. A502 (1989) 287c

(2) P. Möller, J.R. Nix, W.D. Myers, and W.J. Swiatecki, to be published in Atom. Data and Nucl. Data Tables

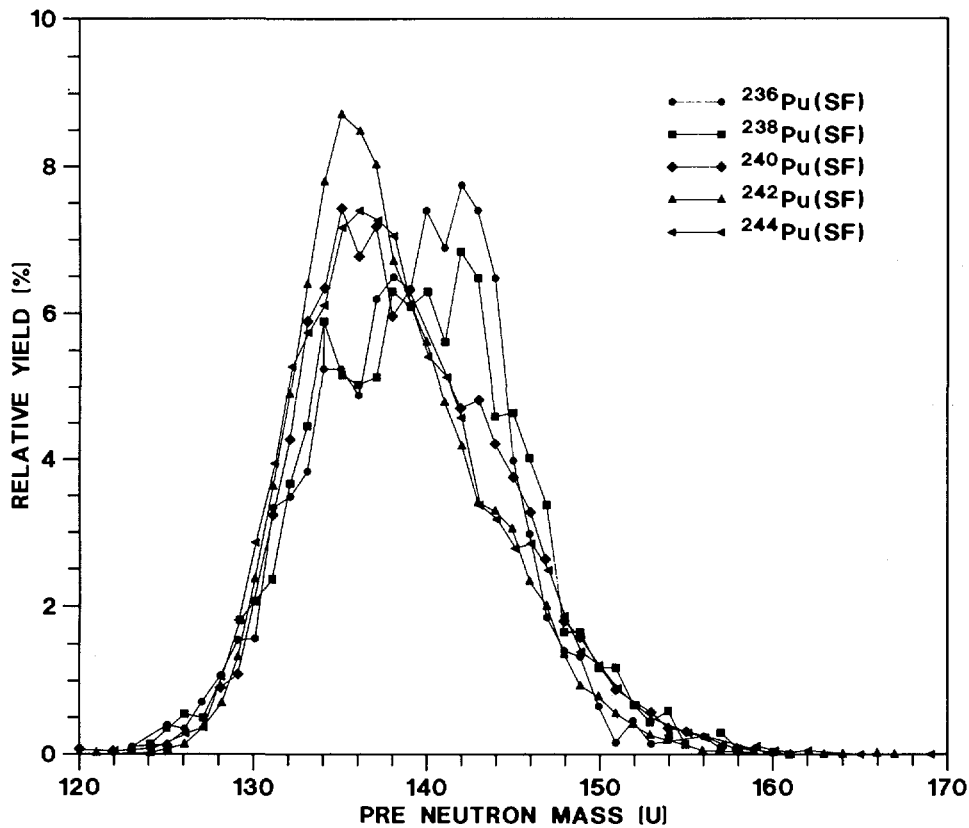


Fig. 11. Pre-neutron emission mass distributions for  $^{236,238,240,242,244}\text{Pu}$  (SF)

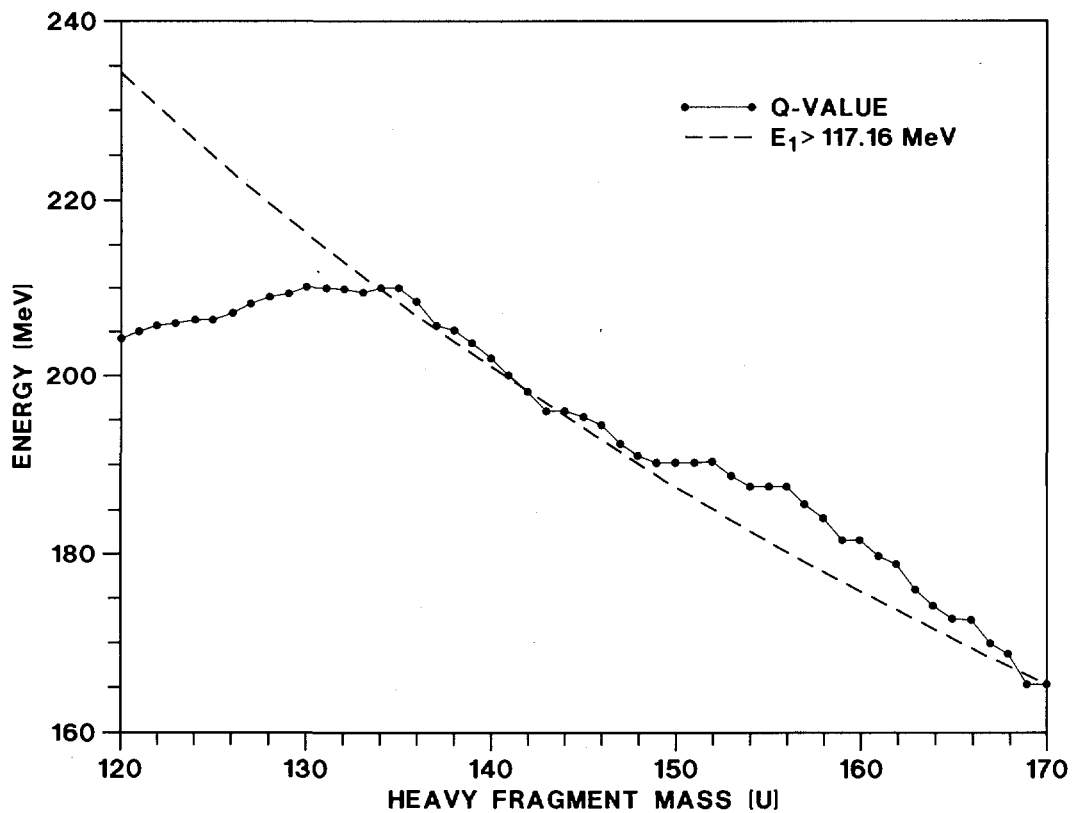


Fig. 12. Selection of cold fission events using a window on  $E_1$  and via a calculation of the maximum Q-value for the fission process with one neutron emission

Both conditions are fulfilled by the deformation energy of the nascent fragments, hence a correlation of the ternary particles emission probabilities with the deformation energy of the fissioning system is likely to exist. Besides that, it has become common practice to analyse fission data through the concept of fission modes.

Binary (B) and Long-Range-Alpha (LRA) accompanied fission counting rates have been measured for a series of resonances. In the case of the 12.4 eV resonance area e.g., the statistical accuracy was 0.7% and 1.9% respectively. The LRA-to-binary fission ratio for selected resonances has been calculated and normalized to 1  $[(LRA/B)_{rel}]$  for the average of a few of the strongest resonances between 1.14 eV and 2.5 Kev.

In Fig. 13 the measured  $(LRA/B)_{rel}$ -data are plotted as a function of  $W_I/W_{II}$ , the yield ratio of the standard I and standard II fission modes in the corresponding resonances. It seems that the  $(LRA/B)_{rel}$ -values remain close to 1, indicating that the ternary fission yield does not change dramatically among the different resonances. It is assumed that ternary fission proceeds through the same modes as binary fission.

In order to facilitate the intercomparison of fissioning systems and to identify the impact of the various fission modes, it is imperative to reduce the number of parameters involved. Most favourable in this respect are the even-even spontaneously fissioning isotopes, since here fission takes place at constant (zero) excitation energy and at the same spin and parity, namely  $J^\pi = 0^+$ . A promising set of nuclei are the  $^{236,238,240,242,244}\text{Pu}$  isotopes, since a systematic study of the binary fragment characteristics has already revealed an evolution in the relative contribution of the two main fission modes, i.e. standard I and standard II.

As a starting exercise the influence of fission modes on neutron induced ternary fission of  $^{235}\text{U}$  has been studied. The contribution of the standard I and II fission modes differs significantly amongst the different low-energy fission resonances<sup>(1)</sup>, which has also an effect on the average fragment kinetic energy. A qualitative explanation for this phenomenon was recently given by Furman and Kliman<sup>(2)</sup>. The resolved resonances correspond to well-defined levels  $J^\pi = 3^-$  or  $4^-$  (which can nevertheless originate from different transition states) at an almost constant excitation energy of 6.55 MeV.

The attention has been concentrated on ternary  $\alpha$ -particles and tritons, since they represent the majority of the ternary fission events. The experimental work was carried out at an 8 m flight path of the GELINA. A double  $\Delta E$ -E detection set-up was used to measure the yield and energy characteristics of the ternary particles, together with the energy (time-of-flight) of the neutrons that induced the fission

---

(1) F.-J. Hamsch, H.-H. Knitter and C. Budtz-Jørgensen, Nucl. Phys. A491 (1989) 56-90

(2) V. Furman, J. Kliman, Proc. Int. Workshop on Dynamical Aspects of Nuclear Fission, (Smolenice, Slovakia, 1993), ed. J. Kristiak and B.I. Pustyl'nik (1994) p. 305

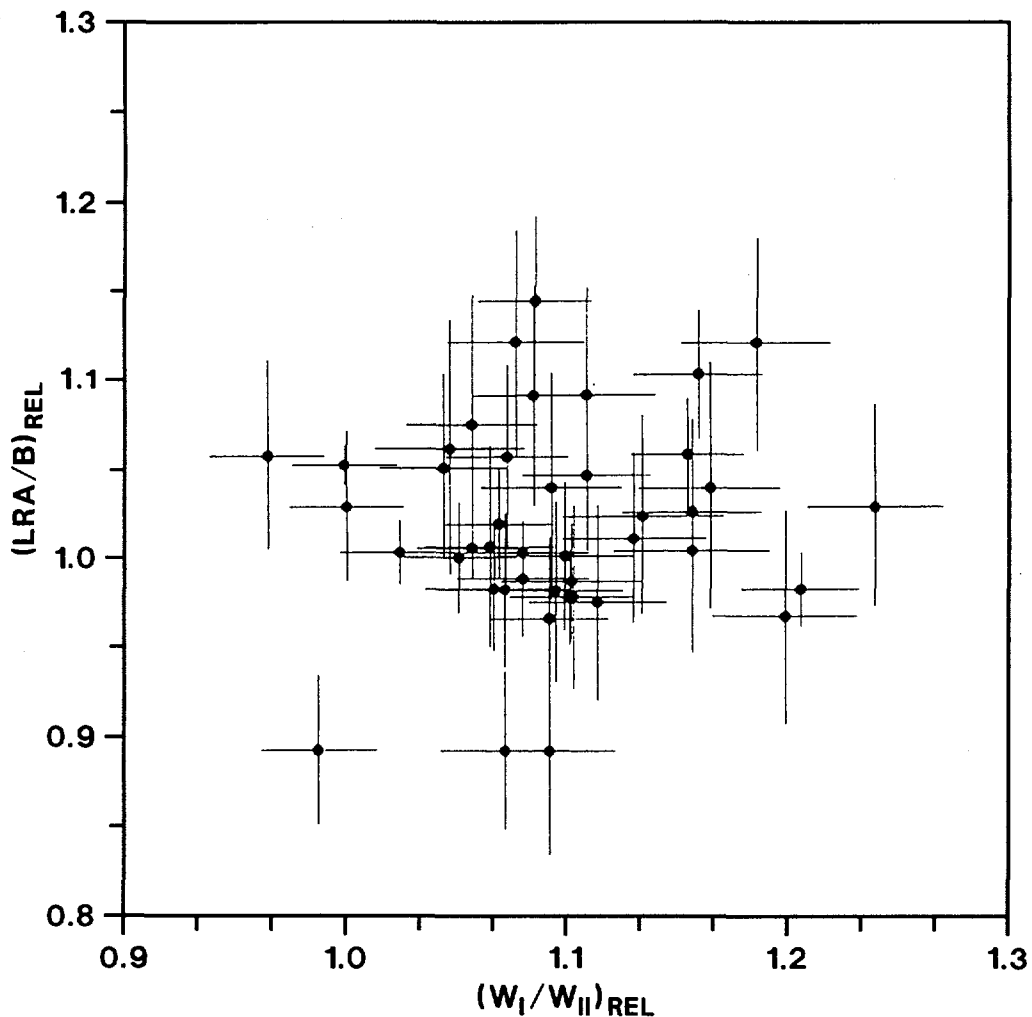


**Fig. 13.** *Correlation between the (relative) ratio of the weights  $W_I/W_{II}$  of the fission modes which describe the mass asymmetric part of the mass distribution and the (relative) ratio LRA-accompanied ternary fission to binary neutron induced fission of  $^{235}\text{U}$  for the corresponding resonance*

process. Also binary fragments could be detected under identical geometrical conditions. The experimental results have been compared with a computer simulation of the expected energy signals for the applied configurations. A detailed description of the set-up and analysis methods are being published. The same has been said about the ternary triton-to LRA yield ratio. Moreover, the absolute triton/LRA yields up to 2.5 keV neutron energies are consistent with the thermal value of 0.063 evaluated by Wagemans<sup>(1)</sup>.

It is clear that the increase by more than a factor of two, reported by Fluss et al.<sup>(2)</sup>, above 200 keV neutron energies is not confirmed at lower energies.

(1) C. Wagemans, "The nuclear fission process", CRC Press, Boca Raton (USA), 1992  
 (2) M. Fluss, N. Dudev and R. Malewicki, Phys. Rev. C6 (1972) 2252

Within the boundaries of the statistical accuracies realised, no significant correlation between  $(LRA/B)_{rel}$  and  $W_I/W_{II}$  has been found. A substantially better statistical accuracy is mandatory to continue the search for a possible relationship between both variables.

Nevertheless it can already be concluded that the probability for ternary fission is non-zero for standard I as well as for standard II fission, and that both probabilities are of the same order of magnitude. Only systems with large differences in the relative weights of the standard I and standard II fission modes seem suitable for establishing the possible link between fission modes and ternary fission probabilities.

In the margin of the present investigation,  $LRA/B$  has been calculated as a function of the resonance spins. Considering only resonances which are sufficiently well resolved,  $\langle (LRA/B)_{rel}(J^\pi=3^-) \rangle = 1.009 \pm 0.012$  and  $\langle (LRA/B)_{rel}(J^\pi=4^-) \rangle = 1.030 \pm 0.015$  have been obtained. This confirms the conclusion of Wagemans<sup>(1)</sup>. (based on measurements on several fissioning systems) that *"the influence of the spin J on ternary alpha emission is very weak, if existing at all"*.

## Neutron Data of Structural Materials

### **Very High Resolution Transmission Measurements and Resonance Parameters of $^{58}\text{Ni}$ and $^{60}\text{Ni}$**

A. Brusegan, G. Rohr, R. Shelley, E. Macavero, C. Van der Vorst, F. Poortmans\*, L. Mewissen\*, G. Vanpraet\*\*

High resolution neutron transmission measurements on samples of enriched  $^{58}\text{Ni}$  and  $^{60}\text{Ni}$  were carried out at IRMM in the energy ranges 14 eV up to 7.5 MeV and 40 eV up to 30 MeV respectively with the time-of-flight technique. The total cross section data from 3 sample thicknesses per isotope have been analysed up to 831 and 801 keV, respectively with 2 different R-Matrix codes.

New resolution function distributions for the moderated and unmoderated neutron beam have been calculated for the present configuration of the (U + Be) canned water moderator assembly.

The 1 ns electron burst width of GELINA and its unmoderated neutron spectrum are well suited for very high resolution cross section measurements. Average resonance parameters have been deduced from the analysis of 356 levels observed for  $^{58}\text{Ni}$  and of 348 for  $^{60}\text{Ni}$ .

---

\* SCK/CEN - B 2440 Mol, Belgium

\*\* RUCA, Antwerpen, Belgium

(1) C. Wagemans, "The nuclear fission process", CRC Press, Boca Raton (USA), 1992(

Details of the measurements were described in a contribution to the International Conference on Nuclear Data for Science and Technology, Gatlinburg, USA, May 1994.

### *Resonance Neutron Capture in $^{58}\text{Ni}$*

F. Corvi, M.C. Moxon\*, K. Athanassopoulos

High resolution neutron capture measurements covering the range (1 - 700) keV were performed at GELINA at a flight distance of 58.6 m using a nickel disc of 8 cm diameter and a thickness of  $N = 0.0084$  at/b, enriched to 99.93 %  $^{58}\text{Ni}$ . Normalization was carried out with a thinner sample by comparing capture in  $^{58}\text{Ni}$  in the 6 to 16 keV region to capture in the  $E_0 = 1.15$  keV resonance of  $^{56}\text{Fe}$ . To avoid any  $\gamma$ -ray self-shielding effect, the  $^{56}\text{Fe}$  sample thickness was chosen to match that of  $^{58}\text{Ni}$ . The R-matrix code REFIT was used to determine the normalization constant for the main data set in simultaneous fit with two transmission runs performed at GELINA. The aim was to derive the parameters of the levels at 6.906, 13.317, 13.636 and 15.397 keV as well as the energy and neutron width of the first negative energy resonance. The values of the capture areas of the three lowest energy resonances are in the average 12.5 % lower than the corresponding ORNL values.

For the main run the capture yield was analysed with the REFIT code over the neutron energy range (15 - 264) keV and the parameters of 142 resonances were determined. All data were corrected for prompt neutron sensitivity effects which are particularly important for s-waves. Where possible both, the neutron width  $\Gamma_n$  and the radiation width  $\Gamma_\gamma$ , were determined for an assumed value of the spin and parity. The values of  $\Gamma_n$  derived in this way were usually found in reasonable agreement with those obtained from transmission data. This fact proves that the resolution parameters used in REFIT and their neutron energy dependence describe the observed data down to a level of  $\sim 1$  % of the peak amplitude. When  $\Gamma_n$  was too small to be fitted, it was taken equal to a constant value in agreement with the available transmission data, and  $\Gamma_\gamma$  was fitted. Finally, for resonances not observed in transmission, a fix value  $\Gamma_\gamma = 0.68$  eV was assumed and  $\Gamma_n$  only was determined in the fit.

The mean radiation widths and their standard deviations obtained in the present work are compared in Table 2 to those measured at ORELA<sup>(1)</sup>. The ratio  $r = 0.87$  between the mean p-wave widths of GELINA and ORELA reflects the fact that the present normalization is in the average 12.5 % lower than that one of Oak Ridge. A possible explanation of this discrepancy is the wrong weighting function

---

\* Visiting Scientist from AEE, Harwell, United Kingdom

(1) C.M. Perey et al., Phys. Rev. C47 (1993) 1143

used in Oak Ridge at the time. In the case of s-waves, the mean width is almost a factor of two lower than the ORELA one in agreement with the trend observed in most structural material isotopes. This is currently ascribed to the insufficient correction for prompt neutron background due to the larger neutron sensitivity of the  $C_6F_6$  scintillators used in Oak Ridge relative to the  $C_6D_6$  detectors used in Geel. At the Gatlinburg Conference, where this subject was presented, there was also a contribution of E. Fort<sup>(1)</sup> dealing with the validation of the JEF 2.2 file using a large integral data base. One of the conclusions of this exercise was that  $\sigma_\gamma$  of  $^{58}Ni$  should decrease over the entire energy range by about  $(15 \pm 8) \%$ . Since the JEF 2 file for this isotope is mainly based on the Oak Ridge data, this finding is an important confirmation of the present results obtained at IRMM.

**Table 2.** Average values of the capture widths and standard deviations of their distributions for s- and p-waves of  $^{58}Ni(n,\gamma)$  measured at GELINA and ORELA, respectively.

$l$	GELINA		ORELA		$\frac{\langle \Gamma_\gamma \rangle_{GEL}}{\langle \Gamma_\gamma \rangle_{ORE}}$
	Nb. of resonances	$\langle \Gamma_\gamma \rangle$ [eV]	Nb. of resonances	$\langle \Gamma_\gamma \rangle$ [eV]	
0	14	$1.25 \pm 0.31$	27	$2.3 \pm 1.7$	0.543
1	17	$0.67 \pm 0.13$	39	$0.77 \pm 0.33$	0.870

## NUCLEAR DATA FOR FUSION TECHNOLOGY

The objective of the work on nuclear data for fusion technology is to contribute to an improved knowledge of data for neutron transport calculation in the blanket and for an estimate of the gas production. Measurements are presently done in two areas (1) high resolution total cross section measurements and (2) double differential charged particle emission cross sections.

### *High Resolution Total Cross Section of Natural Iron*

K. Berthold\*, C. Nazareth, G. Rohr, H. Weigmann

The experimental work was described in the previous progress report<sup>(2)</sup>. The measured cross section still shows rather strong fluctuations up to several MeV

\* EC Fellow from the Technische Hochschule Darmstadt, Germany

(1) E. Fort in Nuclear Data for Science and Technology, J.K. Dickens (ed.), A.N.S., La Grange Park, 1994, p. 768

(2) IRMM Annual Report 93, EUR 15659 EN

neutron energy. As an example, in the upper half of Fig. 14, the measured total cross section in the region between 3.7 and 4.2 MeV is compared to the cross section for  $^{56}\text{Fe}$  given in ENDF/B-VI. In the lower half of the figure the corresponding transmission curves through 40 cm of iron are shown; although the average cross sections are practically identical in this energy region, the stronger fluctuations of the measured cross section result in an increased transmission by about 25 %.

The measured high resolution total cross section data are presently being used at ECN, Petten and ENEA, Frascati for shielding benchmark calculations.

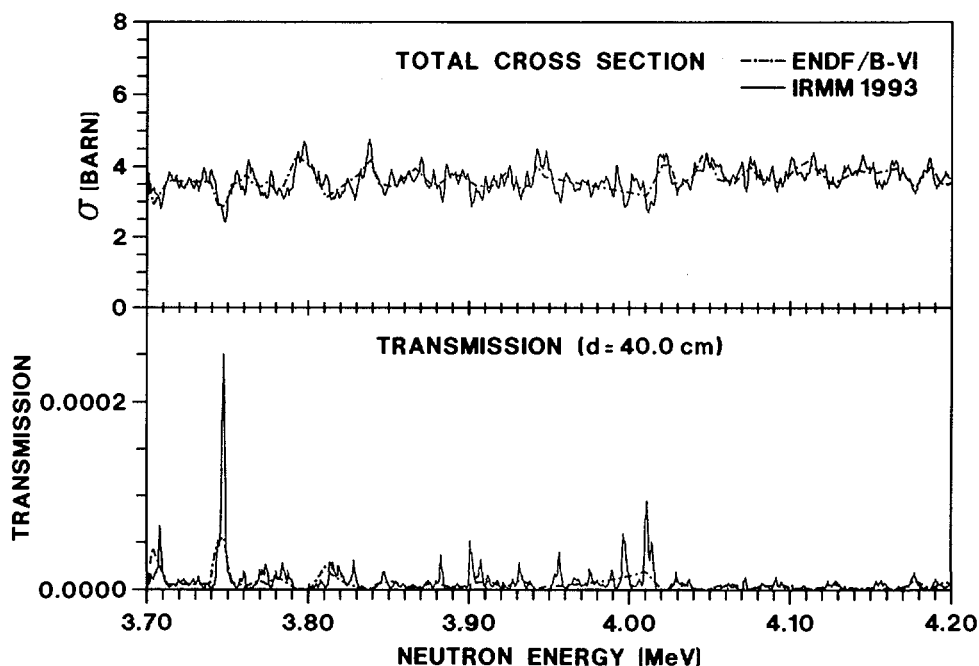


**Fig. 14.** Total cross section of iron between 3.7 and 4.2 MeV compared to ENDF/B-VI and corresponding transmission through 40 cm of iron

### Total Neutron Cross Section Measurement of $^{27}\text{Al}$ at High Energy

R. Shelley, G. Rohr, C. Nazareth, M. Moxon\*

The experimental part of this project was extensively covered in the previous report<sup>(1)</sup>. In the meantime the resonance analysis has been extended up to the inelastic threshold at 844 keV. The results of this work were presented at the International Conference on Nuclear Data for Science and Technology, Gatlinburg, May 1994. The cross section data in the energy range 200 keV to 20 MeV has been sent to the NEA data bank for incorporation into the file.

\* Visiting Scientist from AEE, Harwell, United Kingdom

(1) IRMM Annual Report 93, EUR 15659 EN

### **Vanadium Neutron Total Cross Section**

R. Shelley, G. Rohr, C. Nazareth, A. Brusegan

Vanadium is a candidate for the blanket material in fusion reactors and is presently being considered by the Engineering Design Activities (EDA) of the International Thermonuclear Experimental Reactor (ITER). A thorough study of the total neutron cross section has been initiated at GELINA and first measurements with natural vanadium of 99.8 % purity have been performed. Time of flight neutron transmission through two samples (28 mm and 14 mm thick) was recorded in the neutron energy range (0.175 - 25) MeV, utilising the highest resolution at GELINA (400 m flightpath, 1ns pulsewidth and 800Hz). The data were stored in 64k 1ns energy channels and have been corrected for background and deadtime effects. Part of the resulting neutron cross section is shown in Fig. 15 and compared with the most recent ENDF/B-VI evaluation. In the lower energy resonance region the advantage of such high resolution measurements is clearly seen. The discrepancy between the two sets of data at higher energies will be the subject of further investigation. One further measurement at even lower neutron energies (80 eV - 1 MeV) has been performed with a 2 mm transmission sample.

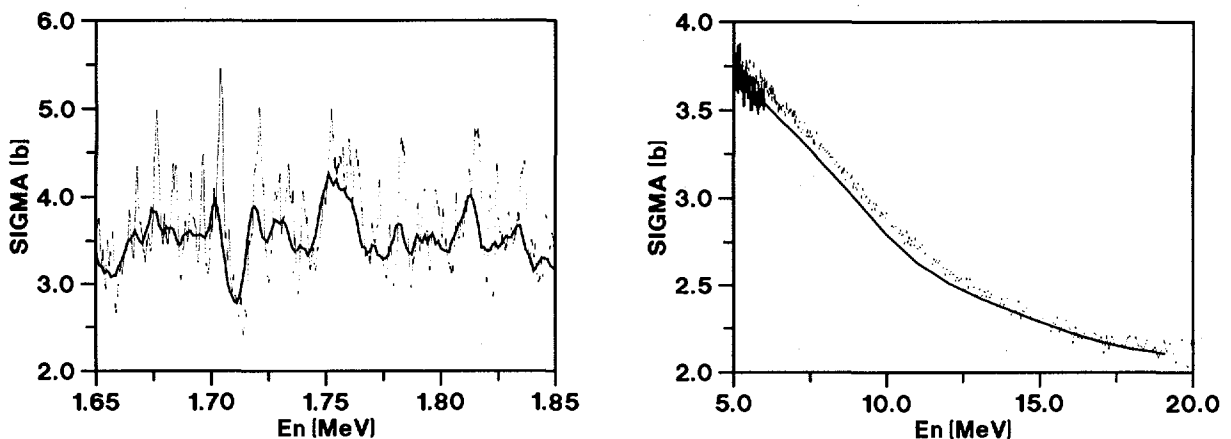


**Fig. 15. Vanadium neutron total cross section measured in the resonance region and at higher energies and compared with ENDF/B-VI evaluation**

### **Total Neutron Cross Section Measurements of $^{232}\text{Th}$ from 1.5 to 18 MeV**

A.Crametz, W.Schubert, E.Wattecamps

Total neutron cross section data of  $^{232}\text{Th}$  have been determined in the energy

range from 1.5 to 18 MeV (Fig 16. continuous curve). Recommended values of the ENDF/B-VI file are also shown as dotted curve in the same figure. In a previous analysis, it was demonstrated that the measured neutron total cross section of  $^{12}\text{C}$ , made simultaneously, under identical conditions and with the same correction procedures for dead time, background and sample positioning, agreed with the ENDF/B-V values to within 3% or better, all over the neutron energy range from 1.5 to 18 MeV. The measured values for  $^{232}\text{Th}$ , on the other hand, are larger than the ENDF/B-VI by 6.5 % in the neutron energy range from 3 to 5 MeV, and coincide well with the ENDF/B-VI values above 6 MeV. The accuracy of the measured neutron total cross section value, achieved in 70 minutes runs, in zones of smooth shape and in energy bins of 10% width, is 1.7, 1.0, 2.1 and 3.8 % at energies of 2, 4, 8 and 16 MeV, respectively. The available  $^{232}\text{Th}$  sample was thin (0.068 atoms of  $^{232}\text{Th}$  per barn) and to achieve more accurate values a thicker sample would be needed. Details of the study were presented to the International Conference on Nuclear Data for Science and Technology, Gatlinburg, USA, May 1994.

***Measured and Calculated Differential and Total Yield Cross Section data of  $^{58}\text{Ni}(n,\alpha)$  and  $^{63}\text{Cu}(n,xp)$  in the Neutron Energy Range from 2.0 to 15.6 MeV***

C.Tsabarlis \*, E.Wattecamp, G.Rollin, C.T.Papadopoulos\*\*

Double differential (n,xp) and (n,x $\alpha$ ) cross section ratio measurements are performed at the 7 MV Van de Graaff accelerator for neutron energies between 2.0 and 15.6 MeV. The following reaction rate ratios are measured:  $^{58}\text{Ni}(n,\alpha)$  to  $^{27}\text{Al}(n,\alpha)$ ,  $^{58}\text{Ni}(n,\alpha)$  to  $^{58}\text{Ni}(n,p)$ ,  $^{63}\text{Cu}(n,xp)$  to  $^{27}\text{Al}(n,\alpha)$  and  $^{63}\text{Cu}(n,xp)$  to  $^{58}\text{Ni}(n,p)$ . Protons or alpha-particles are detected by  $\Delta E$ - $\Delta E$ -E telescopes under 14, 51, 79, 109 and 141 degree. The energy spectrum of the emitted particles and the angular yield distribution are measured. First measurements provide double differential cross section data for  $^{27}\text{Al}(n,\alpha)$  and  $^{58}\text{Ni}(n,p)$  by normalisation to the known total yield reference cross section values. Subsequently, the reaction rate ratios of  $^{58}\text{Ni}(n,\alpha)$  and  $^{63}\text{Cu}(n,xp)$  to  $^{27}\text{Al}(n,\alpha)$  or  $^{58}\text{Ni}(n,p)$  provide double differential cross sections of  $^{58}\text{Ni}(n,\alpha)$  and  $^{63}\text{Cu}(n,xp)$  in barn/(MeV·sr). The measured double differential cross section data, the particle energy spectra, the angular distributions and the total yield cross section data are compared with measured data from literature and with nuclear reaction model calculations performed at IRMM with the computer codes STAPRE-H and EXIFON. As an example the total yield cross section of  $^{58}\text{Ni}(n,\alpha)$  is shown in Fig.17.

---

\* EC Fellow from the University of Athens, Greece

\*\* National Technical University, Athens, Greece

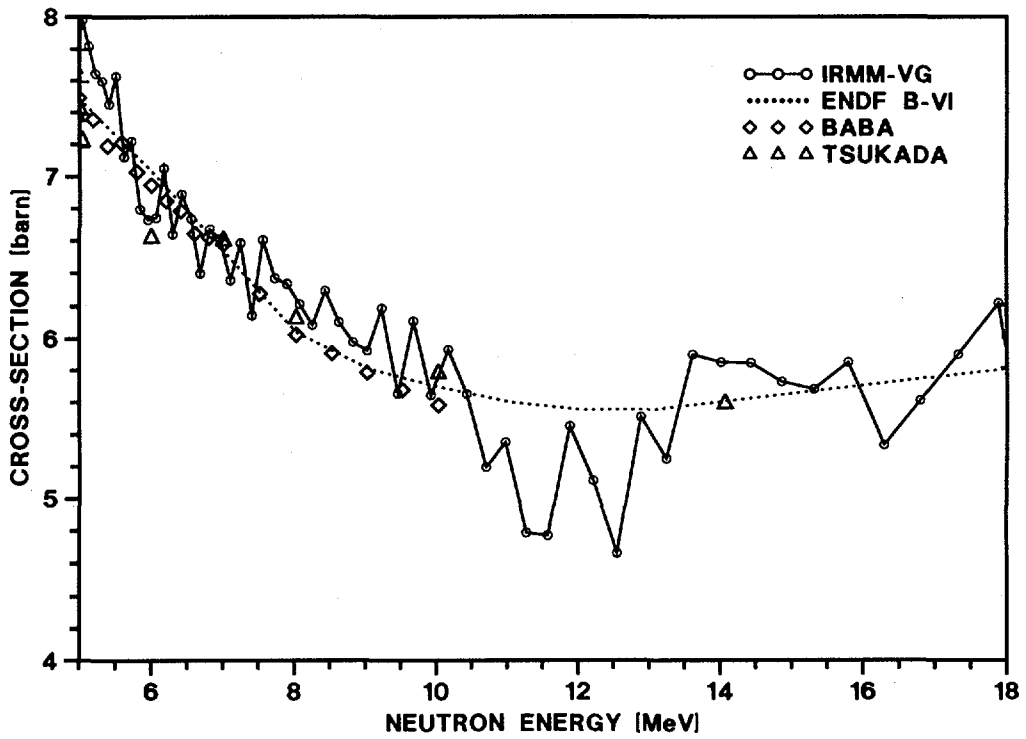
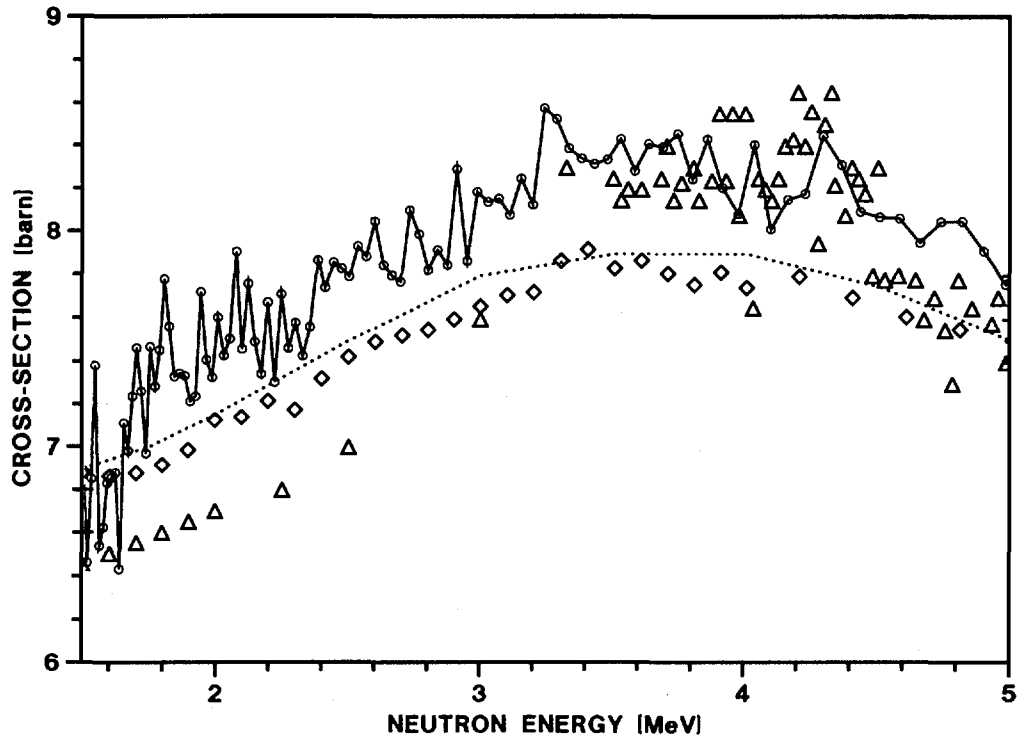
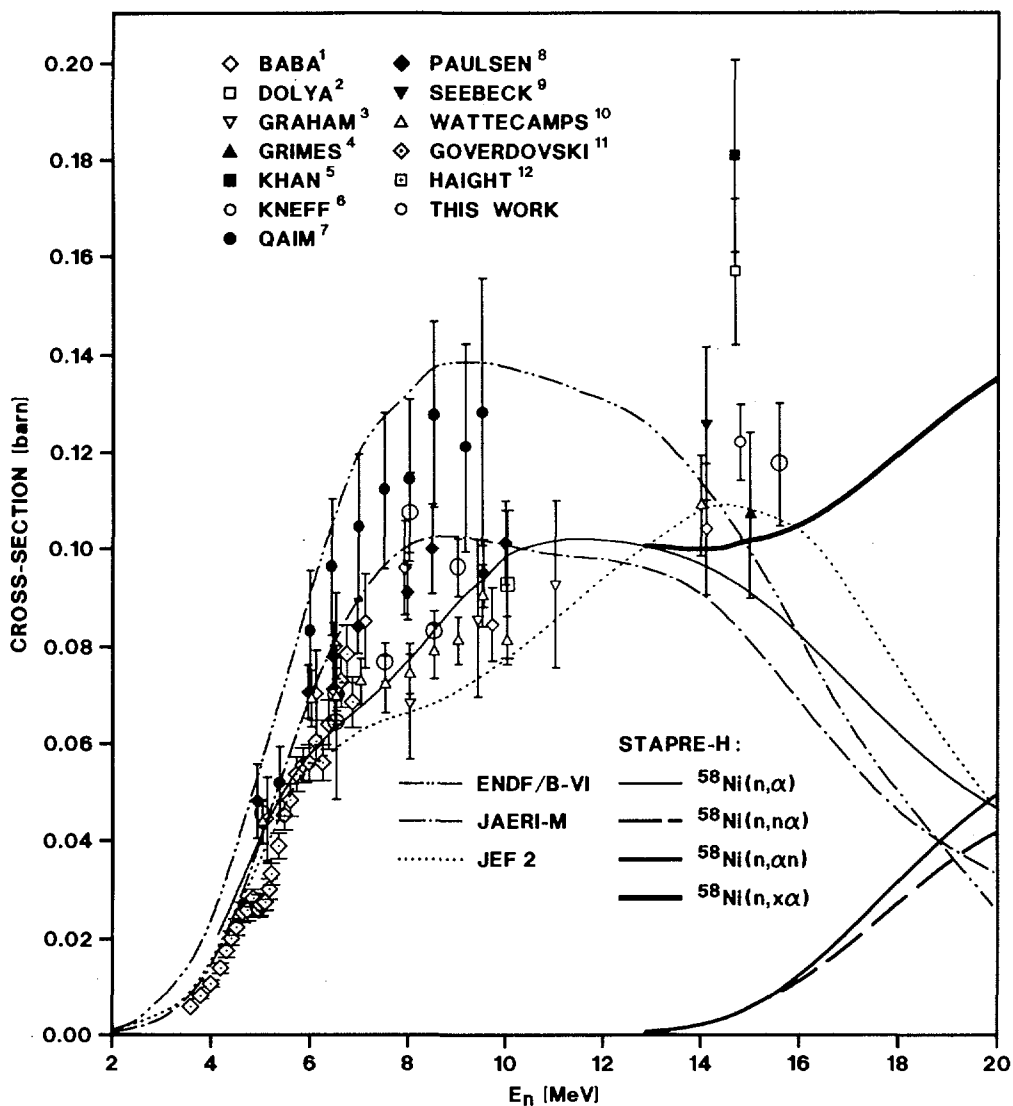


Fig.16. The measured total neutron cross section of  $^{232}\text{Th}$  compared with some other measurements and with the recommended data of ENDF/B-VI (dotted line)



**Fig.17. Measured, evaluated and calculated total yield cross section data of  $^{58}\text{Ni}(n,xa)$  reactions.**

1. M.Baba et al., J.Nucl.Sci.Tech. 31, 745 (1994) and Proc.Int.Conf. Nucl.Data.Sci. Tech., Gatlinburg, USA, May (1994)
2. G.P.Dolya et al., Proc. 3rd All Union Conf. Kiev, USSR, Atominform, p.173 CIII (1973)
3. S.L.Graham et al., Nucl.Sci.Eng. 95, 60 (1987)
4. S.M.Grimes et al., Phys. Rev. C,19, 2197 (1979)
5. N.A.Khan et al., Nucl.Phys. A202, 123 (1973)
6. D.W.Kneff et al., Rep. INDC(NDS)-179/6 (1986)
7. S.M.Qaim et al., Nucl.Sci.Eng. 88, 143 (1984)
8. A.Paulsen et al., Nucl.Sci.Eng. 78, 3337 (1981)
9. U.Seebeck et al., Nucl.Phys. 68, 387 (1965)
10. E.Wattecamps, Proc. Int. Conf. Nucl.Data. Sci. Tech., Julich, Germany, p.310 (1991)
11. A.Goverdovski et al., Proc.Int.Conf.Nucl.Data.Sci.Tech., Gatlinburg, USA, May (1994)
12. R.Haight et al., Proc.Int.Conf.Nucl.Data.Sci.Tech., Gatlinburg, USA, May (1994)

It has been concluded that:

- the  $^{58}\text{Ni}(n,\alpha)$  cross section data of this experiment globally confirm the lower data available in literature. The accuracy of this and other recent measurements by Baba et al. and by Goverdovski et al. may suggest the need to update evaluations;
- the  $^{63}\text{Cu}(n,p)$  cross section data below 9 MeV are presently unique and agree with the current ENDF-B/VI values;
- the comparison of measured data with calculated cross section data obtained with the STAPRE-H and EXIFON codes is satisfactory and such test cases for detailed comparison of theory and experiment remain essential.

Details of the study were reported at the International Conference on Nuclear Data of Science and Technology, Gatlinburg, USA, May 1994 and in a paper submitted for publication in Nucl.Sci.Engineering.

## SPECIAL STUDIES

A series of special measurements linked to the data programme has been performed. These research topics concerned PhD work as well as extended international collaboration making use of the unique features of GELINA as a high energy-resolution machine for neutron measurements.

### *The $^{35}\text{Cl}(n,p)^{35}\text{S}$ , $^{36}\text{Cl}(n,p)^{36}\text{S}$ and $^{36}\text{Cl}(n,\alpha)^{38}\text{P}$ Reactions and their Astrophysical Implications*

S. Druyts\*, C. Wagemans\*, R. Barthélémy, J. Van Gils

Final results for the  $^{35}\text{Cl}(n,p)^{35}\text{S}$  reaction up to 100 keV neutron energy have been published.

For the measurements on  $^{36}\text{Cl}$ , two samples with an enrichment of 41.65 % in  $^{36}\text{Cl}$  were prepared by evaporating AgCl on a 20  $\mu\text{m}$  thick aluminium backing foil coated with 400  $\mu\text{g}/\text{cm}^2$  of platinum. In this way, two homogeneous and stable layers were obtained with thicknesses of 68 and 174  $\mu\text{g AgCl}/\text{cm}^2$ , respectively.

Fig. 18 shows the results of a high resolution measurement with the thickest sample on a 30 m flight path. Due to the energy loss in the sample, the 2.2 MeV  $^{36}\text{Cl}(n,\alpha)$ -particles were not fully separated from the 1.9 MeV  $^{36}\text{Cl}(n,p)$ -particles.

---

\* University of Gent, Belgium

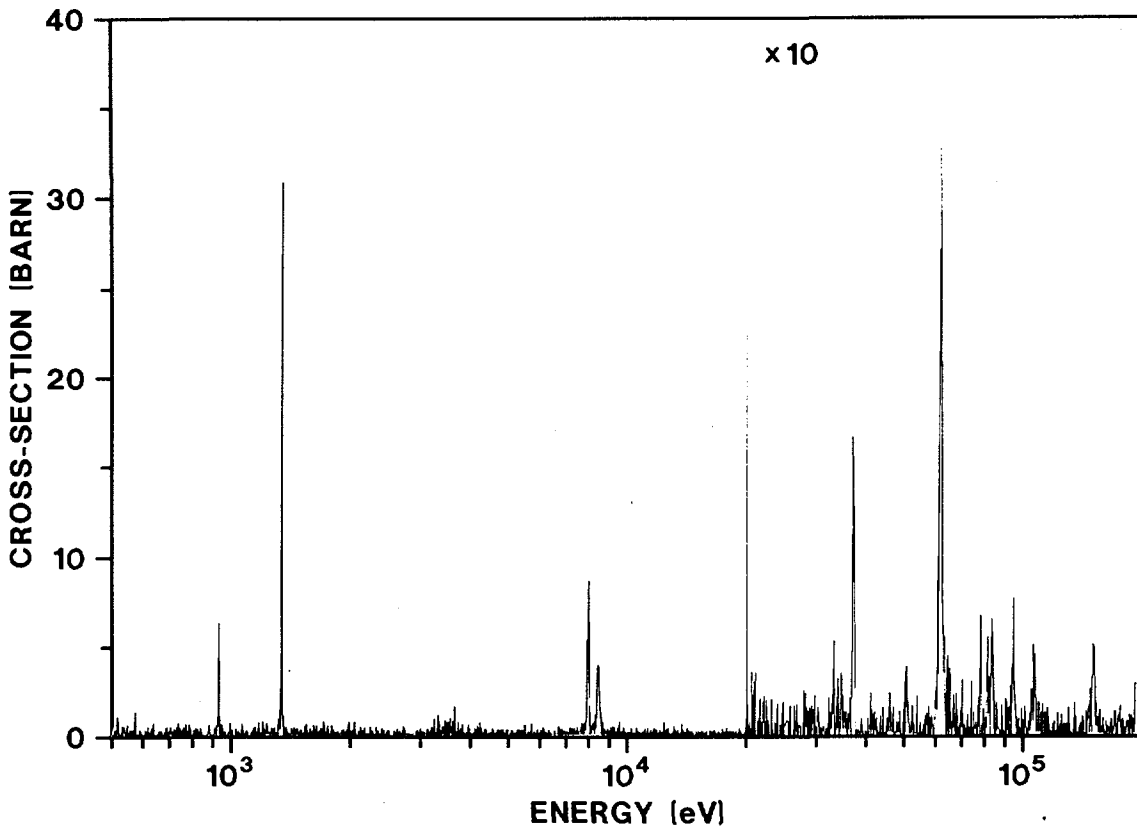


Fig. 18.  $^{36}\text{Cl}(n,p) + ^{36}\text{Cl}(n,\alpha)$  cross-section versus neutron energy

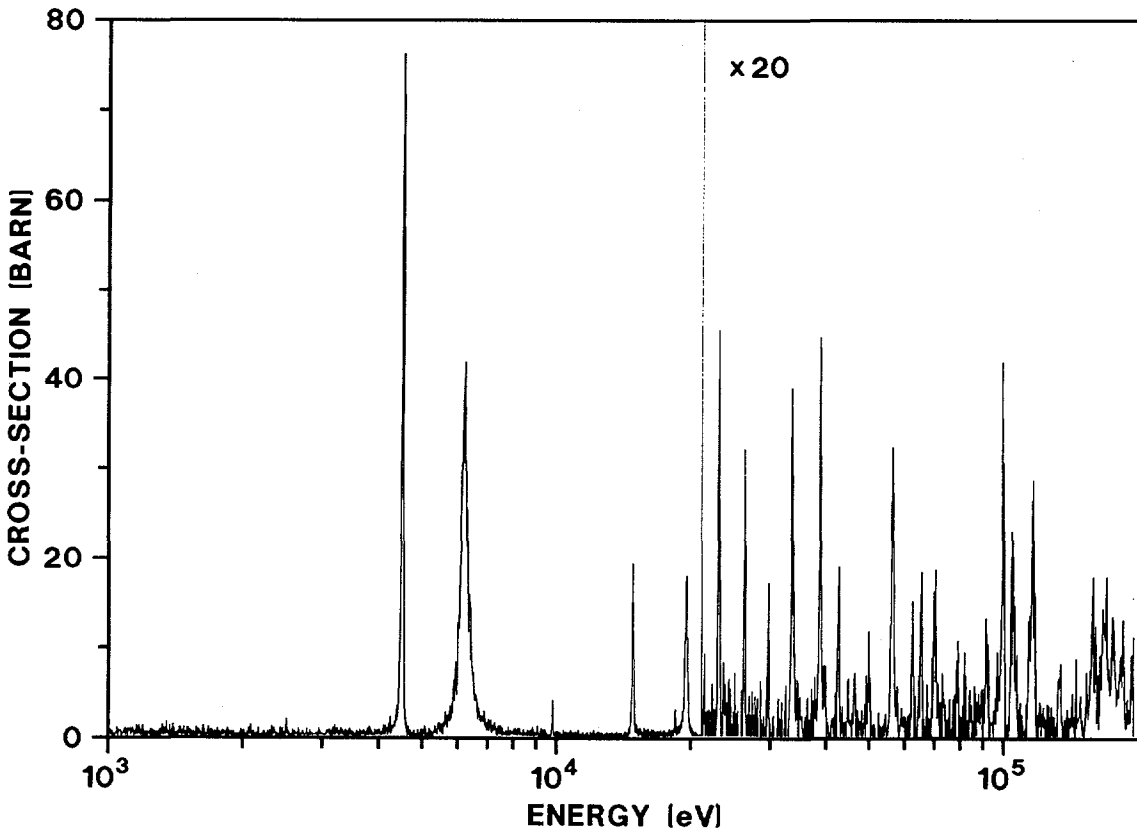


Fig. 19.  $^{41}\text{Ca}(n,\alpha_0)^{38}\text{Ar}$  cross-section versus neutron energy

The data shown in Fig. 18 correspond to the sum of both reaction cross-sections. Except for the resonance at 930 eV, the  $^{36}\text{Cl}(n,p)$ -reaction is by far dominating. Additional measurements will be performed with the thinner sample in order to achieve an unambiguous separation of both processes. Further treatment of the data shown in Fig. 18, e.g. being transformed into Maxwellian averaged cross-sections as a function of the stellar temperature  $kT$ , is still going on.

### **Study of the $^{41}\text{Ca}(n, \alpha)$ Reactions**

C. Wagemans\*, S. Druyts\*, H. Weigmann, R. Barthélémy, J. Van Gils

After capture of an s-wave neutron in  $^{41}\text{Ca}$ , the excited compound nucleus  $^{42}\text{Ca}$  can decay via several channels, e.g.  $^{41}\text{Ca}(n,\alpha_0)^{38}\text{Ar}$ ,  $^{41}\text{Ca}(n,\alpha_1)^{38}\text{Ar}$ ,  $^{41}\text{Ca}(n,\gamma\alpha)^{38}\text{Ar}$ ,  $^{41}\text{Ca}(n,p)^{41}\text{K}$ . A detailed investigation of all these reactions is being performed up to 500 keV neutron energy, using different detectors and samples.

Fig. 19 shows the (dominant)  $^{41}\text{Ca}(n,\alpha_0)^{38}\text{Ar}$  cross-section determined at a 30 m long flight-path with an ionization chamber.

### **Spin Assignment of s- and p-Wave Neutron Resonances in $^{113}\text{Cd}$**

F. Gunsing\*\*, F. Corvi, K. Athanassopoulos, H. Postma\*\*\*, Yu. Popov•, E.I. Sharapov•, F. Becvar••

The TRIPLE collaboration has successfully observed parity non-conservation (PNC) in p-wave neutron resonances of  $^{238}\text{U}$  and  $^{232}\text{Th}$  and has derived estimates of the root-mean-square value  $M$  of the PNC matrix elements for these nuclei. In order to investigate a possible dependence of  $M$  on the atomic mass number  $A$ , these studies have been extended to nuclei situated in the 3p-maximum of the neutron strength function, i.e. around  $A = 100$ . In particular the isotope  $^{113}\text{Cd}$  was studied at Los Alamos in late 1993. In order to interpret these data, a spin assignment experiment on  $^{113}\text{Cd}$  was carried out at IRMM in collaboration with Delft University and JINR, Dubna, using a cadmium metal disc of 91 g weight enriched to 93.35 %  $^{113}\text{Cd}$ , on loan from the Russian Isotope Pool.

The low-level population method of spin assignment was used, consisting of measuring in individual resonances the intensity ratio of two low-energy capture

---

\* University of Gent, Belgium

\*\* EC Fellow from the Technical University of Delft, The Netherlands

\*\*\* Visiting scientist from the Technical University of Delft, The Netherlands

• Visiting scientist from the Joint Institute for Nuclear Research, Dubna, Russia

•• Charles University, Prague, Czech Republic

$\gamma$ -rays. When such  $\gamma$ -rays are conveniently chosen, this ratio depends significantly on the resonance spin  $J$ . Particularly useful for assigning the spin was the intensity ratio between the 725 keV transition de-exciting a  $4^+$  level and the 558 keV line de-populating the  $2^+$  first excited state. Values of this ratio are plotted in Fig. 20 for  $l=0$  and  $l=1$  resonances, respectively. The ratios split into two groups for s-waves and three for p-waves, each group being associated with the quoted spin.

These results has been validated by simulating the  $\gamma$ -ray decay with the Monte Carlo program DICEBOX; the population ratios derived are shown as shaded bands in Fig. 20. They are in good agreement with the experimental points. In such a way the spins for 23 s-waves and 21 p-waves have been determined. Using the PNC asymmetries found in Los Alamos in combination with the IRMM spin values, the following estimate of  $M$  has been deduced:

$$M = 2.00 \begin{matrix} +1.5 \\ -0.9 \end{matrix} \text{ meV}$$

A paper on the subject has been submitted for publication in Physical Review.

***Resonance Parameters of  $^{138}\text{Ba}+n$  from High Resolution Transmission Measurements***

A. Brusegan, E. Macavero, C. Van der Vorst

The isotope  $^{138}\text{Ba}$  with magic neutron number plays an important role in s-process nucleosynthesis. In order to complement the capture data obtained at IRMM in previous years, transmission measurements were performed at GELINA at a flight distance of 49 m and with 1 ns burst width. The sample consisted of 109 g of  $\text{BaCO}_3$  enriched to 99.2 %  $^{138}\text{Ba}$ , on loan from the Russian Isotope Pool. A total of 40 resonances were observed in the range between 0.1 and 200 keV and analysed with the R-matrix code REFIT in order to derive their neutron width and, when possible, the spin and parity. Those resonances showing the typical interference pattern with the potential scattering could be easily identified as s-waves while for all the others an orbital momentum  $l = 1$  was assumed. Amongst these, a spin  $J = 3/2$  was assigned to those resonances exhibiting a large peak cross section which could not be fitted with  $J = 1/2$ .

The average resonance parameters for s- and p-wave levels are quoted with their errors in Table 3. The level spacing for s-wave levels is more than twice the value quoted earlier<sup>(1, 2)</sup>.

---

(1) A.R.de Musgrove, B.J.Allen, J.W.Boldeman and R.L.Macklin, Nuclear Physics A252(1975) 301-314  
 (2) A.R.Musgrove, B.J.Allen and R.L.Macklin, Aust.J.Phys.,32(1979), 213

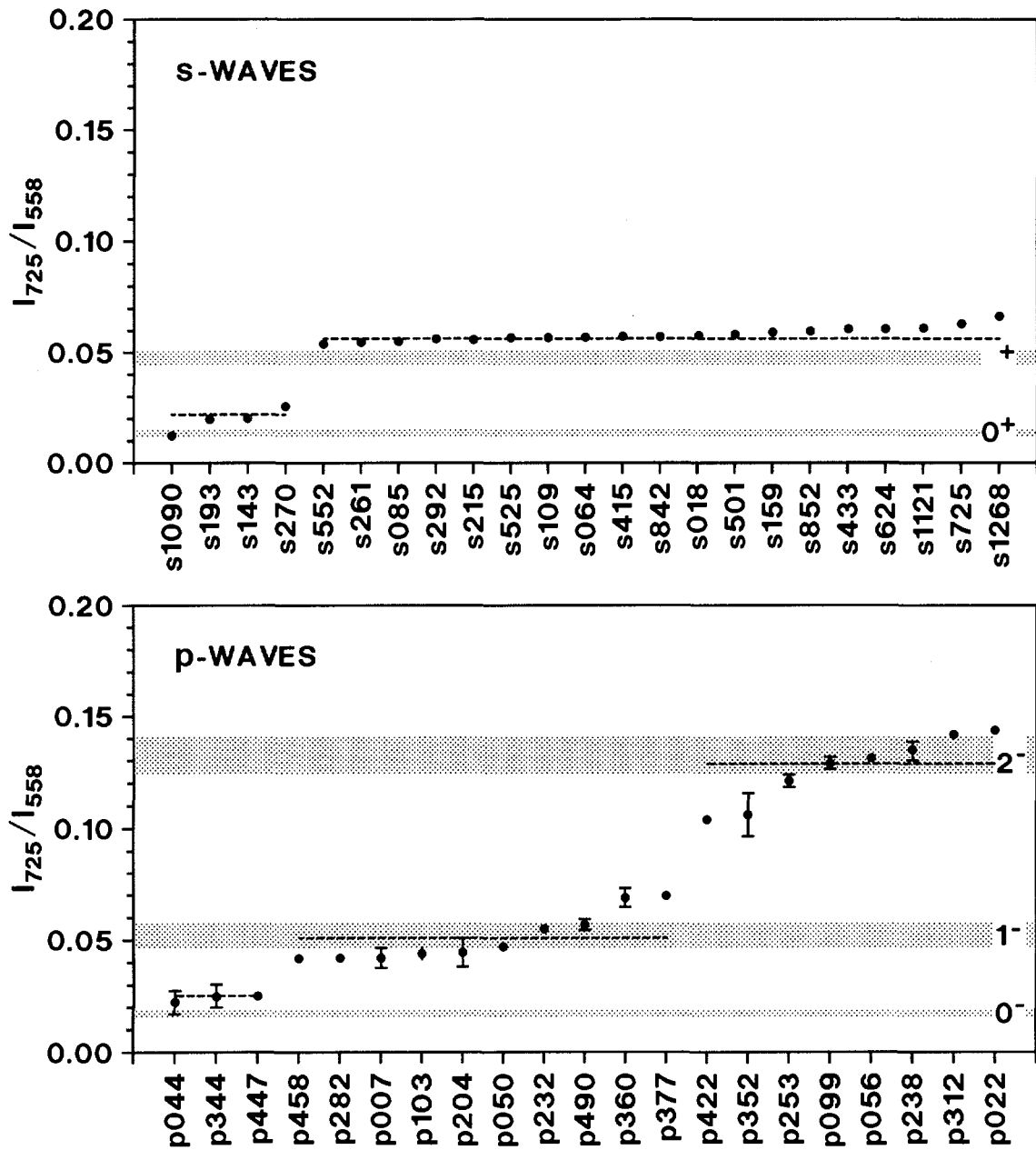


Fig. 20. The ratio of the intensities of the 725 keV and the 558 keV gamma-rays, for both s- and p-waves in increasing order. The dotted lines indicate the weighted mean of each spin group. The gray regions represent the results of the numerical simulations

The s-wave strength function is much lower than the value  $S_0 = 1.5 \cdot 10^{-4}$  given by E.G.Bilpuch et al.<sup>(1)</sup>, but it agrees within the errors with the value of A.R.de Musgrove et al.<sup>(1)</sup>. The ratio of the s-wave to the p-wave spacing is of the order of three, according to the  $(2l + 1)$  dependence of the level density.

(1) E.G. Bilpuch, K.K. Seth, C.D.Bowman, R.H. Tabony, R.C. Smith and H.W.Newson, *Annals of Physics*, 14, p. 387-418 (1961)

**Table 3. Average resonance parameters of  $^{138}\text{Ba}$** 

Energy range		647eV- 200 keV
Number of s-wave res.		11
Number of p-wave res.		29
Spacing [keV]	$l=0$	$18.7 \pm 2.9$
Spacing [keV]	$l=1$	$6.76 \pm 0.67$
Strength function $\times 10^4$	$l=0$	$0.66 \pm 0.28$
Strength function $\times 10^4$	$l=1$	$0.67 \pm 0.18$

**Cross Sections of the  $(n,n'\gamma)$  Reaction for Low-lying Levels of Palladium Isotopes**

A.Meister \*, G.Rollin, W.Schubert, E.Wattecamps

The  $(n,n'\gamma)$  excitation functions for low-lying levels of palladium isotopes are measured for neutron energies from 0.2 to 3.3 MeV. The measurement was carried out at the 7 MV Van de Graaff accelerator at IRMM with a "white" neutron source utilising the  $^7\text{Li}(p,n)$  reaction with a thick target. The neutron spectroscopy is done by time-of-flight technique with a 4 m flight path. For detection of the gamma rays from inelastic scattering a HPGe detector is used covering a broad angle at  $90^\circ$  scattering angle. The 478 keV gamma ray from a boron sample enriched in  $^{10}\text{B}$  is registered simultaneously as a reference reaction.

The measurements and the data analysis of up to fourteen excitation functions are described in detail elsewhere<sup>(1)</sup>.

The data acquisition of time-of-flight and  $\gamma$ -ray pulse height is done in two-dimensional acquisition of 1024 by 1024 channels. The samples of palladium and the  $^{10}\text{B}$  are two disks of approximately the same size in back to back geometry. The  $\gamma$ -ray lines of palladium and  $^{10}\text{B}$  are detected simultaneously. The  $\gamma$ -ray emission in both cases was assumed to be isotropic.

The neutron time-of-flight distribution is obtained after subtraction of the continuum  $\gamma$ -ray background and subsequent subtraction of the epithermal time-of-flight background distribution. The palladium to  $^{10}\text{B}$  time-of-flight reaction rate ratios provide the  $\text{Pd}(n,n'\gamma)$  reaction cross section in barn by using the  $^{10}\text{B}(n,\alpha\gamma)$  reference cross section. Five corrections were applied: background subtraction 30 to 80 %, count loss 1 to 20 % due to chosen window width, neutron beam attenuation in the samples 1 to 7 %, multiple neutron scattering up to 10 % and  $\gamma$ -ray attenuation in the samples 3 to 20 %.

The excitation functions of fourteen palladium lines are shown on Fig. 21. The excitation functions of  $\gamma$ -ray emission from the first, and some from the second, 2+ levels of even palladium isotopes are shown on top of Fig. 21. Some levels of

---

\* Visiting Scientist from the Technical University of Dresden, Germany  
(1) A. Meister and E. Wattecamps IRMM Internal Report GE/R/VG/83/94

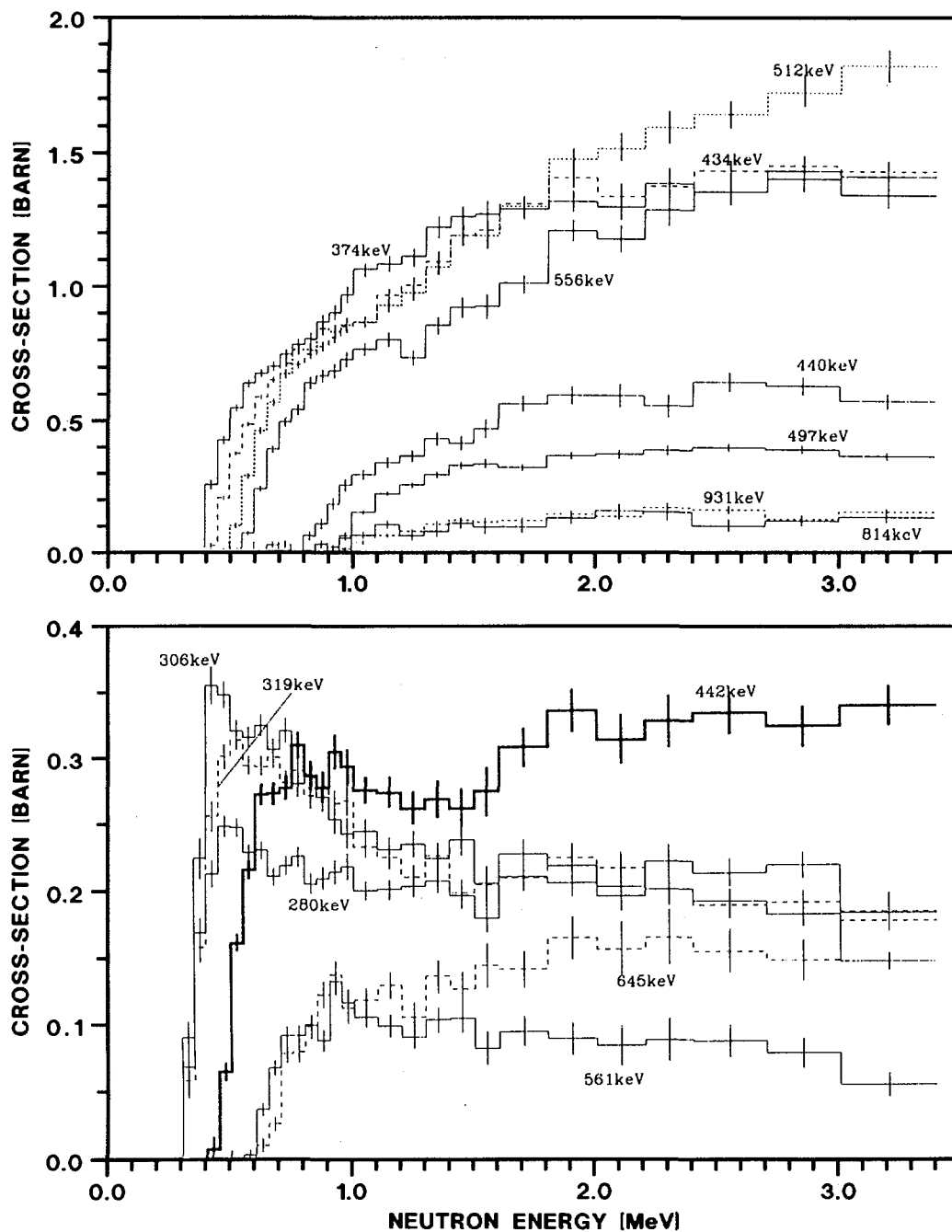


**Fig. 21.** top : Excitation functions for the  $\gamma$ -ray emission of even palladium isotopes.  
 - First or second  $2+$  levels to ground state  $0+$ : 556 keV of  $^{104}\text{Pd}$ , 512 keV of  $^{106}\text{Pd}$ , 434 and 931 keV of  $^{108}\text{Pd}$ , 374 and 814 of  $^{110}\text{Pd}$ .  
 - Second  $2+$  level to first  $2+$  level transition: 497 keV of  $^{108}\text{Pd}$  and 440 keV of  $^{110}\text{Pd}$   
 bottom : Excitation functions for the  $\gamma$ -ray emission of the odd palladium isotope  $^{105}\text{Pd}$   
 - Levels 280 keV  $3/2+$ , 306 keV  $7/2+$ , 319 keV  $5/2+$ , 442 keV  $5/2+$ , 561 keV  $5/2+$  and 644 keV  $7/2-$  to ground state  $5/2+$

the odd mass palladium isotopes are shown in the lower part of Fig 21. Above the thresholds of the second excited levels these curves include contributions due to feeding of the respective states by  $\gamma$ -ray cascades. The accuracy of the measured cross section of  $\text{Pd}(n,n'\gamma)$  is 4 to 9 % per energy bin for the stronger  $\gamma$ -ray lines. Half of this uncertainty is due to the 2 to 6% uncertainty of the  $^{10}\text{B}(n,\alpha\gamma)$  reference cross section value.

The interpretation of the measured excitation functions by nuclear model calculation is done at ECN Petten, Netherlands<sup>(1,2)</sup>. The analysis for the 374  $\gamma$ -ray lines of  $^{110}\text{Pd}$  shows that a fair description by the "coupled channel CC-, two-phonon vibrational-model", code ECIS88, is possible and that the cross section value is high compared to previous ENDF/B-V and VI evaluations.

Calculations of the angular distribution of some first level 2+ ground state transitions<sup>(3)</sup>, show that the anisotropy is substantial above threshold and tends to isotropy with raising neutron energy. The anisotropy correction factor for the measurements made at 90° is less than 10 % for energies larger than double threshold energy.

A paper on the topic was presented at the International Conference on Nuclear Data for Science and Technology, Gatlinburg, USA, May 1994.

### ***Measurement of (n,n'γ) Cross Sections for Low-lying Levels of Molybdenum Isotopes***

I.-G. Birn\*, E. Wattecamps

In the pursuit of the determination of (n,n'γ) cross sections of low-lying levels of palladium isotopes similar experiments are performed for the molybdenum isotopes. These measurements are carried out at the 7 MV Van de Graaff accelerator with a 1.5ns wide pulsed proton beam of 5.5 MeV. A thick lithium target provides a white neutron source relying on the  $^7\text{Li}(p,n)^7\text{Be}$  reaction. Irradiations are done simultaneously with the molybdenum and the  $^{10}\text{B}$  sample in back to back geometry, thus measuring the (n,n'γ) cross sections relatively to the cross section of the  $^{10}\text{B}(n,\alpha\gamma)$  reaction. The neutron flight path length is 4.03 m. The  $\gamma$ -rays are detected with a HPGe detector under 90°. A two-dimensional "γ-ray pulse height - neutron time of flight" spectrum is taken in listmode and analysed off-line. The white neutron source allows the measurement of the excitation functions for the different  $\gamma$ -ray lines in a single run from threshold up to 2 MeV. Fig. 22 shows a measured  $\gamma$ -ray spectrum from a first test run, integrated over all neutron flight times (ca. 20 hours of acquisition time).

---

\* EC Fellow from the Technical University Dresden, Germany

(1) H.Gruppelaar and H.Hogenbrik, Rep. ECN-RX-92-040,

(2) H.Hogenbrik, Rep. JEF/DOC March 1994

(3) A. Meister, ECN Activity Report 1994

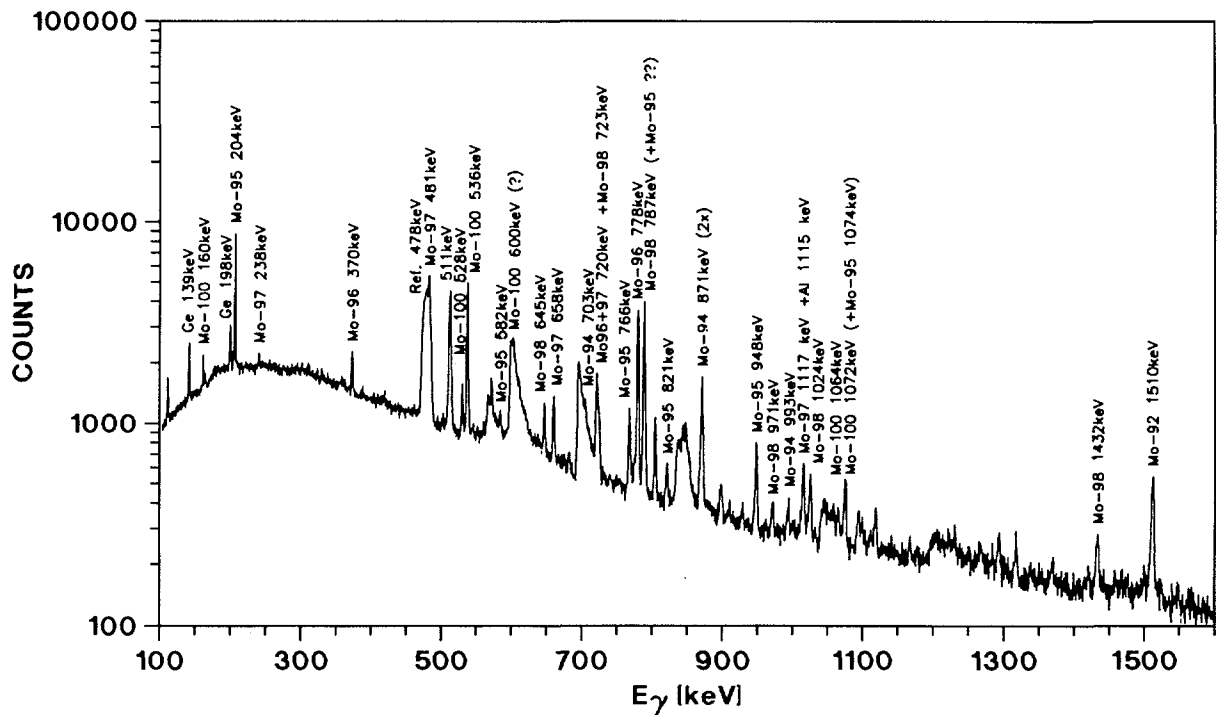


Fig. 22.  $^{nat}\text{Mo}(n,n'\gamma)$  - Measured  $\gamma$ -ray spectrum, integrated over all neutron flight times

Natural molybdenum consists of 7 stable isotopes. Many  $\gamma$ -lines are observed and some of them overlap. The analyses the  $\gamma$ -ray spectra on a PC the program GAMMAW V15.10 are still in progress.

On top of the 478 keV reference line from the  $^{10}\text{B}(n,\alpha\gamma)$ , which is Doppler broadened, there is a  $\gamma$ -line from the inelastic scattering of neutrons on  $^{97}\text{Mo}$  (481 keV). These peaks may properly be analyzed by the commercially available PEAKFIT program.

#### ***Influence of Lattice Vibrations on the Doppler Broadening of the 0.18 eV Cadmium Neutron Resonance Cross Section***

A.Meister\*

The capture cross section in the vicinity of the 0.18 eV neutron resonance is calculated for a metallic cadmium sample. The description of Doppler broadening starts from the lattice vibration spectrum of cadmium. The result shows only a tiny difference if compared with the free gas approximation for the Doppler broadening. This justifies the application of the free gas approximation in the case of this low energy resonance and the weakly bound cadmium lattice. Moreover, for cases of strong lattice binding it can be concluded that the Doppler broadened shape of neutron resonances can be determined with high precision if

\* Visiting Scientist from the Technical University of Dresden, Germany

a realistic model is used which includes lattice dynamics.

The results of the study were presented at the International Conference on Nuclear Data for Science and Technology, Gatlinburg, USA, May 1994.

***Measurement of the Doppler Broadening Effect of Neutron Resonances in  $^{238}\text{U}$  Metal,  $\text{UO}_2$  and  $\text{Hg}_2\text{Cl}_2$***

H. Tagziria\*, A. Royer\*\*, A. Brusegan, M. Moxon\*\*\*

First test transmission measurements have been carried out on natural uranium samples (u metal and  $\text{UO}_2$ ) and on a single crystal sample of  $\text{Hg}_2\text{Cl}_2$  in order to determine the spectra of vibrational excitations in these solids by investigating precisely the shape of the Doppler-broadened neutron resonances for temperatures between 25 and 300 °K. The  $\text{Hg}_2\text{Cl}_2$  sample is used to calibrate the sensitivity of the experimental set-up as this crystal presents a structural phase transition at 185 °K already well studied by Raman spectroscopy and inelastic neutron scattering. A powerful pulsed neutron source with good energy resolution is provided by GELINA in connection with time of flight techniques. A multi-level R-matrix code, REFIT, is used for the data analysis. Instead of the free gas model approximation, it is planned to use a more detailed model which is adequate at low neutron energies<sup>(1)</sup>.

Fig. 23 a) and b) show examples of the fit to the 6 eV resonance in  $^{238}\text{U}$  and to the 23 eV resonance in  $^{198}\text{Hg}$ , respectively. The shape of the residuals for the 6 eV resonance may be related to the inaccuracy of the gas model approximation.

The data analysis revealed that the background level is still too high (6 %) and that the detection resolution needs to be improved.

***The Stellar Capture Rate of  $^{208}\text{Pb}$***

F. Corvi, P. Mutti\*, K. Athanassopulos, H. Beer\*\*

It is well known that the s-process of stellar nucleosynthesis terminates at the isotopes of lead and bismuth since all further neutron captures produce  $\alpha$ -unstable nuclei which are then cycled back to the main lead isotopes. In order to explain the abundances of these isotopes, a so-called strong s-process component was introduced. To study its characteristics, the capture cross sections of all concerned isotopes, and in particular of  $^{208}\text{Pb}$ , is needed. Being double magic, this nucleus

---

\* EC Fellow from the University of Sussex, United Kingdom

\*\* EC Fellow from the University of Grenoble, France

\*\*\* Scientific Visitor from AEE, Harwell, United Kingdom

• EC Fellow from the University of Torino, Italy

•• Visiting Scientist from KfK, Karlsruhe, Germany

(1) A. Meister, IRMM Internal Report GE/R/VG/78/94

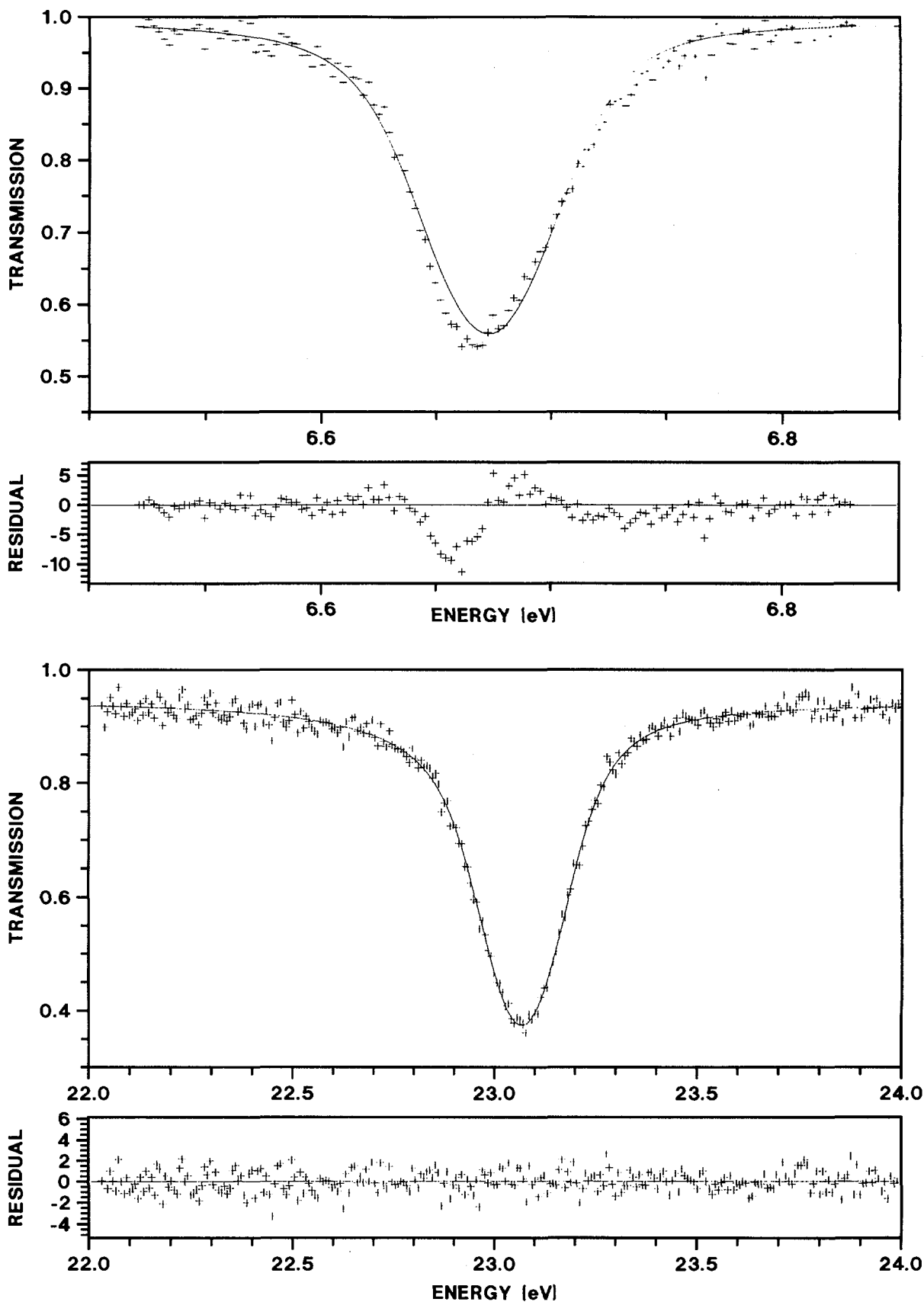
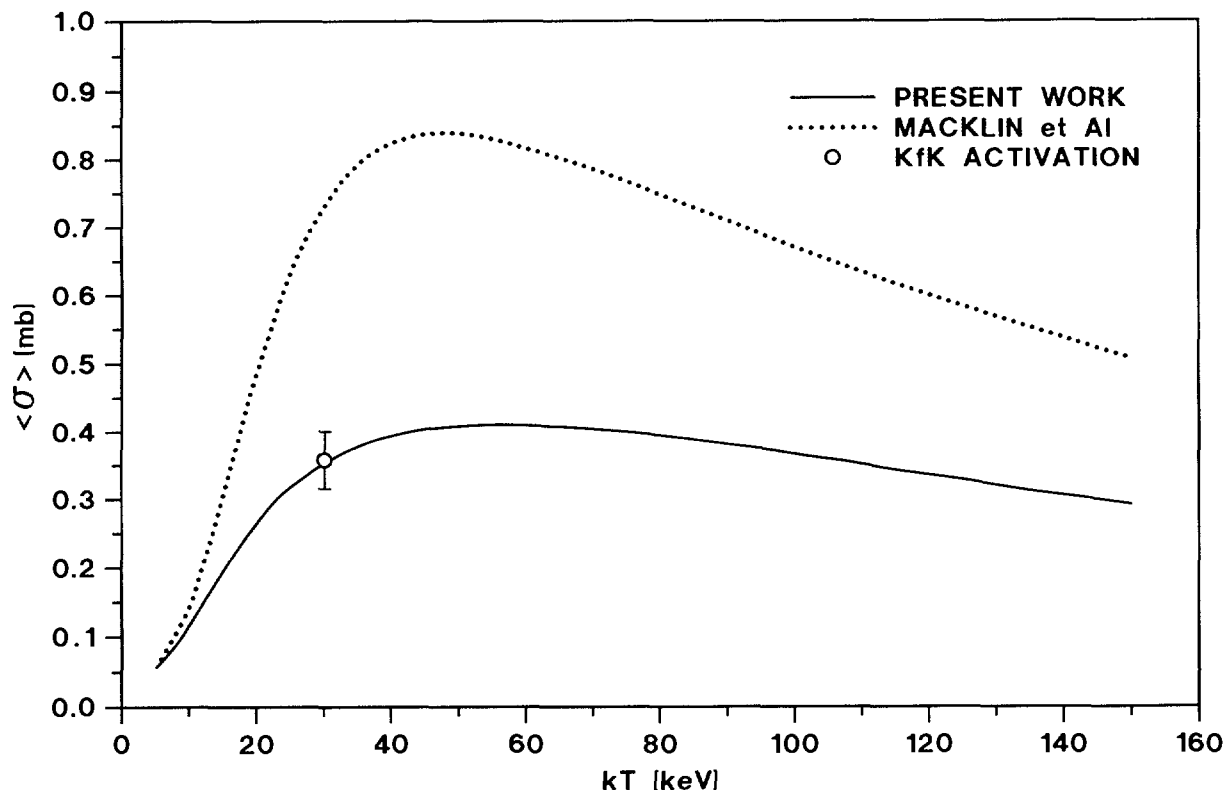


Fig. 23. Fit to experimental results for (a) the 6.67 eV resonance in  $^{238}\text{U}$  at 25°K, and (b) the 23 eV resonance in  $^{198}\text{Hg}$  at 185° K

has the smallest Maxwellian-averaged capture (MAC) cross section  $\langle\sigma\rangle$  of all the heavier elements and as such it introduces the most stringent limitations for the s-process flow at the termination of the synthesis.

Unfortunately a great uncertainty exists about the value of  $\langle\sigma\rangle$  at 30 keV since the one derived at ORELA from neutron capture in resolved resonances<sup>(1)</sup> is a factor of two larger than the results of activation measurements from the same laboratory<sup>(2)</sup> and more recently from Karlsruhe<sup>(3)</sup>. In order to solve this discrepancy, the cross section of  $^{208}\text{Pb}(n,\gamma)$  was remeasured with high resolution at GELINA in the energy range (1 - 900) keV using a lead disc of 102 g weight enriched to 99.75 %  $^{208}\text{Pb}$ , on loan from ORNL. Preliminary results reveal twelve resonances observed below 400 keV and their capture areas were obtained by normalizing to  $^{109}\text{Ag}(n,\gamma)$  at 5.2 eV. The MAC cross section derived from these data is plotted as a function of the stellar temperature  $kT$  in Fig. 24 after adding the direct capture contribution obtained from calculations. The results are in excellent agreement with the KfK activation value  $\langle\sigma\rangle = (0.36 \pm 0.03)$  mb at 30 keV but are a factor of 2 lower than the ORELA data. This discrepancy may be ascribed to an insufficient correction for the prompt neutron scattering of the ORELA data, in particular concerning the value of  $\Gamma_\gamma$  for the broad resonance at 77.8 keV.



**Fig. 24.** The MAC cross section  $\langle\sigma\rangle$  for  $^{208}\text{Pb}(n,\gamma)$  as a function of the stellar temperature  $kT$

- 
- (1) R.L. Macklin, J. Halperin and R.R. Winters, *Ap. J.* **217** (1977), 222
  - (2) R.L. Macklin and J.H. Gibbons, *Phys. Rev.* **181** (1969), 1639-1642
  - (3) U. Ratzel, KfK Karlsruhe, Private Communication (1988)

### **Spin Assignment of $^{238}\text{U}$ Neutron p-Wave Resonances**

F. Gunsing\*, F. Corvi, K. Athanasopoulos, H. Postma\*\*

The aim of this experiment is to contribute to parity-non-conservation (PNC) studies performed at Los Alamos in the frame of the TRIPLE collaboration. Reasons for and preliminary results of this long-lasting measurement were already presented earlier<sup>(1)</sup>.

The 12 gigabyte of listmode data from the  $^{238}\text{U}(n,\gamma)$  reaction were sorted out into gamma-ray spectra corresponding to about 80 time-of-flight intervals, associated with s-wave, p-wave and background regions. In order to obtain the pure capture yield of a given resonance, the gamma-spectrum corresponding to nearby background regions was subtracted from the raw data after proper normalization. A limited energy region of two of these spectra for p-waves having different spin is shown in Fig. 20. The ratio of the areas of the peaks around 539 and 553 keV is quite different. The values of this ratio, plotted versus the resonance energy in Fig. 21, appear to split into two groups corresponding to spin and parity  $J^\pi = 3/2^-$  and  $1/2^-$ , respectively.

High-energy gamma-ray spectra were also investigated in p-waves and several primary transitions leading to  $J^\pi = 5/2^+$  states, were observed in some of them. If these transitions are visible, they are assumed to be E1 and therefore the resonance has  $J^\pi = 3/2^-$ . If a transition to a  $J^\pi = 5/2^+$  state does not occur, nothing can be said about the spin because of Porter-Thomas fluctuations.

The spin assignments derived from the ratio of the low-energy gamma rays and from the observation of primary gamma rays are summarized in Table 3 for a total of 19 p-wave resonances. The two sets are consistent and by combining them a set of adopted spin values can be obtained.

### **The Parameters of the Bethe Level Density Expression and their Energy Dependence Tested with Experimental Neutron Resonance Data**

G. Rohr

A prediction of the Bethe level density parameters for nuclei far off the stable region is proposed. The base line method applied to the level density is used which provides a systematics of the nuclear temperature as a function of the atomic number. The temperature is determined using the ground state shift at neutron separation energy, due to correlations between nucleons. The level density parameters are temperature dependent and the level density as a function of energy includes a phase transition at the critical temperature. Beside pairing of

---

\* EC Fellow from Technical University of Delft, The Netherlands

\*\* Visiting Scientist from Technical University of Delft, The Netherlands

(1) CBNM Annual Report 91, EUR 14374 EN; CBNM Annual Report 92, EUR 15029 EN

nucleons there are also larger nucleon cluster correlations for excited nuclei near magic neutron numbers, indicated by a ground state shift which corresponds to a gap larger than that for pairing. These correlations are due to additional attractive forces applied in the BCS-Theory. The additional attractive forces between nucleons reduce the level density. However for odd-odd nuclei at  $A = 150$  ( $N = 90$ ) and  $A = 230$  ( $Z = 90$ ) the level density is increased indicating negative ground state shifts, which can be interpreted with additional repulsive forces between nucleons. The different phases of nucleons in nuclei are responsible for the complicated structure of the level density systematics at neutron separation energy.

A contribution of this topic was presented at the International Conference on Nuclear Data for Science and Technology, Gatlinburg, USA, May 1994.

## NUCLEAR METROLOGY

### RADIONUCLIDE METROLOGY

The objective of the work on radionuclide metrology is to advance the experimental know-how in the field of radioactivity. This is done in four major areas: the determination of decay-scheme data, the improvement and development of measurement techniques, the preparation of particular standard and reference samples and the participation in international comparisons and evaluations.

#### *Standardization of a $^{56}\text{Co}$ Solution*

T. Altitzoglou, D.F.G. Reher, G. Sibbens, G. Grosse

A standard solution of  $^{56}\text{Co}$ , prepared and certified by the SCK/CEN was used to prepare an extended area source for the calibration of a detector system at GELINA. To check the certified activity value the solution was re-standardized at IRMM using three different methods, i.e.  $\gamma$ -ray spectrometry,  $4\pi\gamma$ -counting, and  $4\pi\beta$ - $\gamma$ -coincidence measurement.

The accuracy of the weighted average of the three standardizations was 1.1 % at the level of one standard deviation. The activity concentration measured was 8.4 % below the certified value of the SCK/CEN. The  $^{57}\text{Co}$  and  $^{58}\text{Co}$  impurities were 1.8 % and 0.58 % of the  $^{56}\text{Co}$  activity, respectively.

#### *Standardization of Two Extended Area Sources of $^{41}\text{Ca}$*

D.F.G. Reher, B. Denecke

Two rectangular  $^{41}\text{Ca}$  sources were standardized employing a medium solid angle proportional counting system. Spectra of the 3.6 keV KX-rays were taken and small corrections for fluorescence of the Al-backing and for the low energy tails of the KX-ray peaks were applied. The auto-transmission of the sources was calculated to be  $> 0.99$ . The source chamber was under vacuum, hence no attenuation of the KX-rays occurred. The transmission of the KX-rays through the Be-window of the detector was calculated to be  $0.931 \pm 0.009$  and the counting gas efficiency was  $> 0.999$ . The geometry factor was about  $4 \cdot 10^{-4}$  of  $4\pi$  sr.

For the determination of the activity of the sources, the electron capture probability,  $P_K = 0.896 \pm 0.004$  was calculated and the fluorescence yield

$\omega_K = 0.144 \pm 0.004^{(1)}$  were used. Additionally, the half life of  $^{41}\text{Ca}$ , necessary for the calculation of its mass in the sources,  $T_{1/2} = (1.06 \pm 0.10) \cdot 10^5$  a, has been evaluated from literature. The mass of  $^{41}\text{Ca}$  in the sources was found to be  $(281 \pm 36) \mu\text{g}$  and  $(22 \pm 3) \mu\text{g}$ , respectively. The large uncertainty is mainly due to the uncertain half life, the inhomogeneity of the sources, and their non-flatness. In order to improve the accuracy of the determination of  $^{41}\text{Ca}$  in these sources (e.g.  $\pm 5\%$ ), mass spectrometry should be used to determine the  $^{41}\text{Ca}$  in the mother solution.

### ***Standardization of an Extended Area Source of $^{37}\text{Ar}$***

D.F.G. Reher, B. Denecke

A rectangular  $^{37}\text{Ar}$  source was standardized employing a low solid angle proportional counting system. Spectra of the 2.6 keV X-rays were taken and small corrections for fluorescence of the Al-backing and for the low energy tails of the KX-ray peaks were applied. The auto-transmission of the sources was calculated to be  $0.9927 \pm 0.0004$ , for an implantation depth of 240 Å. The source chamber was under vacuum, hence no attenuation of the KX-rays occurred. The transmission of the KX-rays through the Be-window was calculated to be  $0.862 \pm 0.012$  and the counting gas efficiency was  $> 0.999$ . The geometry factor was about  $4 \cdot 10^{-4}$  of  $4\pi$  sr.

For the determination of the activity of the sources, the electron capture probability,  $P_K = 0.920 \pm 0.004$  was calculated and the fluorescence yield  $\omega_K = 0.094 \pm 0.005^{(2)}$  was used. The half life of  $^{37}\text{Ar}$ , necessary for the calculation of its mass in the sources,  $T_{1/2} = (35.04 \pm 0.04)\text{d}$ , has been taken elsewhere<sup>(3)</sup>.

The mass of  $^{37}\text{Ar}$  in the source was found to be  $(0.155 \pm 0.010)$  ng, which corresponds to  $2.5 \cdot 10^{12}$  atoms. The reference date was 01.10.1994 at 0h MET.

### ***Traceability of Activity Measurements to the SIR of BIPM***

D.F.G. Reher

The SIR (International Reference System) establishes the SI unit Bq at the BIPM for a rather large set of  $\gamma$ -ray emitting radionuclides. It consists of two ionization chambers (type IG11 of Centronic Ltd., Croydon, UK) and a set of five  $^{226}\text{Ra}$  reference sources. Primary standards laboratories produce input to the system by

- 
- (1) A. Solé, Nucl. Instr. and Meth. in Phys. Res. A329 (1993) 418.
  - (2) W. Bambynek, B. Crasemann, R.W. Fink, H.U. Freund, H. Mark, C.D. Swift, R.E. Price and P. Venugopala Rao, Revs. Mod. Phys. 44, (1972) 716.
  - (3) E. Browne and R.B. Firestone, V.S. Shirley, (ed.), Table of Radioactive Isotopes, John Wiley & Sons, New York, 1986.

sending standardized solutions of  $\gamma$ -ray emitting radionuclides in standard ampoules to the BIPM. These are measured against the  $^{226}\text{Ra}$  reference sources and a value  $A_e$ , which is the equivalent activity of the strongest reference source, is determined. By this the results from different laboratories can be compared without the necessity of exchanging solutions<sup>(1)</sup>.

The standard ionization chamber of IRMM is of a similar type as that of BIPM. It is an IG12 chamber loaded with 2 MPa of Ar. It has been calibrated for a few radionuclides with own standards and some obtained from NIST in 1986. For a small number of radionuclides IRMM has produced input to SIR. This allows us to compare our results with those of other primary standards laboratories - but furthermore, the feasibility of deriving secondary calibrations can be assessed. Fig. 25 shows a preliminary graph of IRMM calibration figures as a function of  $1/A_e$  of SIR. A linear fit gives a slope with a low uncertainty of  $\pm 1.3\%$ . A consequence of this is the possibility of obtaining secondary standards of other radionuclides from this relationship, provided there exists a calibration at SIR.

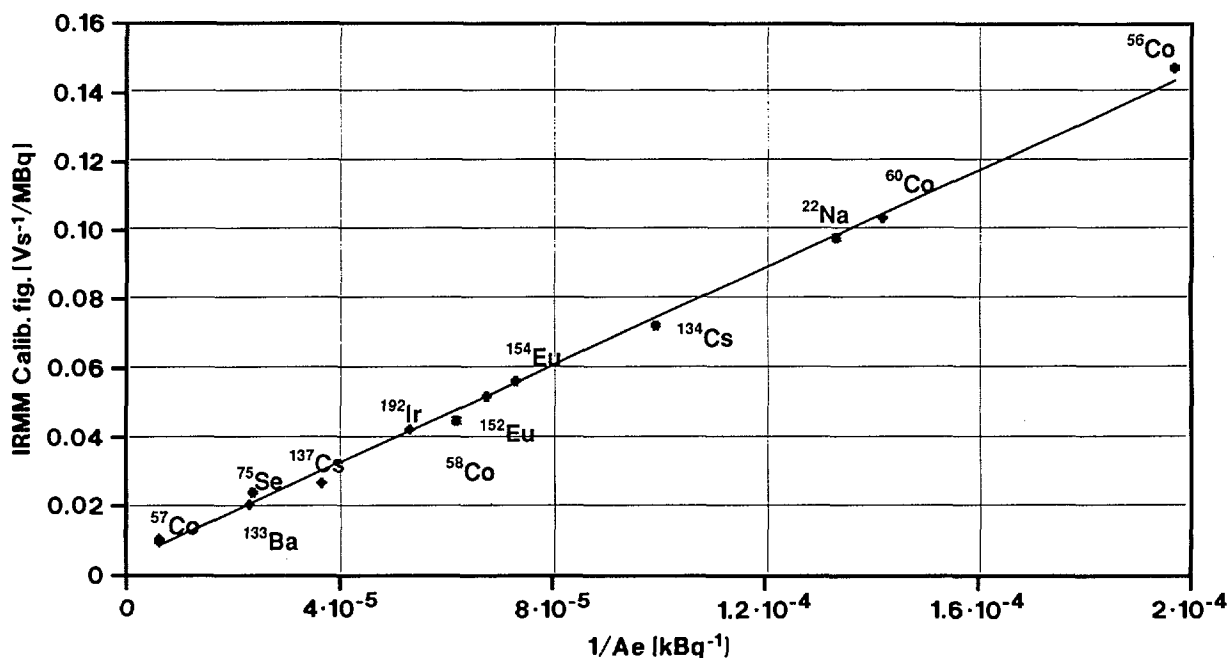


Fig. 25. Plot of the IRMM calibration figures against the reciprocal equivalent activity values of SIR

#### Preparation of a $^{60}\text{Co}$ Standard Solution

G. Sibbens, D.F.G. Reher

A 5 year old  $^{60}\text{Co}$  material from Amersham was used to prepare a  $^{60}\text{Co}$  standard solution.

After homogenization the  $^{60}\text{Co}$  solution was subdivided into ten IRMM and four

(1) A. Rytz, Int. J. Appl. Radiat. Isot. 34(1983) 1047

SIR/NIST standard ampoules. These ampoules were measured with the IRMM standard ionization chamber (IG12 loaded with 2MPa of Ar). The standard deviation of the ionization chamber's response divided by the mass of the solution was 0.04 %.

Preliminary  $4\pi\beta\text{-}\gamma$ -coincidence measurements of sources made from the solution of one ampoule gave results which differ 0.4 % from the calibration figure of the ionization chamber for  $^{60}\text{Co}$ .

Procedures have been written for the preparation of the  $^{60}\text{Co}$  standard solution, the subdivision of the solution into ampoules and the source preparation.

### ***Standardization of a $^{63}\text{Ni}$ Solution by Liquid Scintillation Counting***

T. Altitzoglou

The standardization of a  $^{63}\text{Ni}$  solution was done in the framework of the EUROMET 297 action using the Liquid Scintillation Counting (LSC) technique. The aim was the comparison of various activity measurement methods in LSC, and the exchange of models and ideas on the topic. In the exercise 9 laboratories participated, worldwide.

$^{63}\text{Ni}$  is a pure  $\beta$  emitter with an endpoint energy of 66 keV and LSC is an appropriate method for its standardization. The  $^{63}\text{Ni}$  solution was provided by the Laboratoire Primaire des Rayonnement Ionisants (LPRI, Gif-sur-Yvette, France), together with five ready-to-be-measured samples and a standard  $^3\text{H}$  solution.

$^{63}\text{Ni}$  measurements of the supplied samples and other samples prepared gravimetrically were performed, using a two-phototube liquid scintillation counter. In total 33 samples of  $^{63}\text{Ni}$ , with varying degrees of chemical quenching, were measured more than 10 times each. In addition  $^3\text{H}$  samples prepared from the provided solution, and an existing  $^3\text{H}$  standard solution were measured.

The analysis of the data was done by both the CIEMAT/NIST method<sup>(1)</sup> and the Efficiency Tracing method<sup>(2)</sup>. The results of the activity concentration of the  $^{63}\text{Ni}$  solution from the two methods used agree very well. In addition, the results of the activity measurements of the LPRI  $^3\text{H}$  standard solution are in agreement with those of the IRMM  $^3\text{H}$  standard solution.

### ***ZIRCAN 259-01 Reactor Neutron Dosimetry***

T. Altitzoglou and C. Bastian

Eleven neutron fluence monitor sets, containing wires of Ni-Co, iron, titanium

---

(1) E. Garcia-Toraño and A. Grau Malonda, *Comp. Phys. Comm.* **36** (1985) 307

(2) H. Ishikawa, M. Takiue and T. Aburai, *Int. J. Appl. Radiat. Isot.* **35** (1984) 463.2

and niobium metals, have been irradiated in the High Flux Reactor (HFR) of JRC Petten during 10 reactor cycles (between October 23, 1992 and August 11, 1993). After the end of irradiation, the fluence-monitor sets in their original stainless steel minitubes were transferred to IRMM. The monitors were recovered by dissolving the stainless steel minitubes. Because of the high activity, the work was performed in a hot cell at the SCK/CEN. Unfortunately the monitors sets were recuperated only partially.

The activity of eight radionuclides, namely  $^{58}\text{Co}$ ,  $^{60}\text{Co}$ ,  $^{59}\text{Fe}$ ,  $^{54}\text{Mn}$ ,  $^{46}\text{Sc}$ ,  $^{93\text{m}}\text{Nb}$ ,  $^{94}\text{Nb}$  and  $^{95}\text{Nb}$ , produced by nuclear reactions was measured with coaxial HPGe detector and a planar HPGe detector (for  $^{93\text{m}}\text{Nb}$ ). The detectors were connected with standard electronics to a 8192 channel Pulse Height Analyser (PHA). The activities of the monitors at the reference time were calculated from the counting results corrected for dead time, geometry variations and self attenuation.

The activities of the fluence monitor sets were analysed with the code GERDA (GEel Reactor Dosimetry Analysis) designed for this purpose. It was only possible to obtain results for 8 sets.

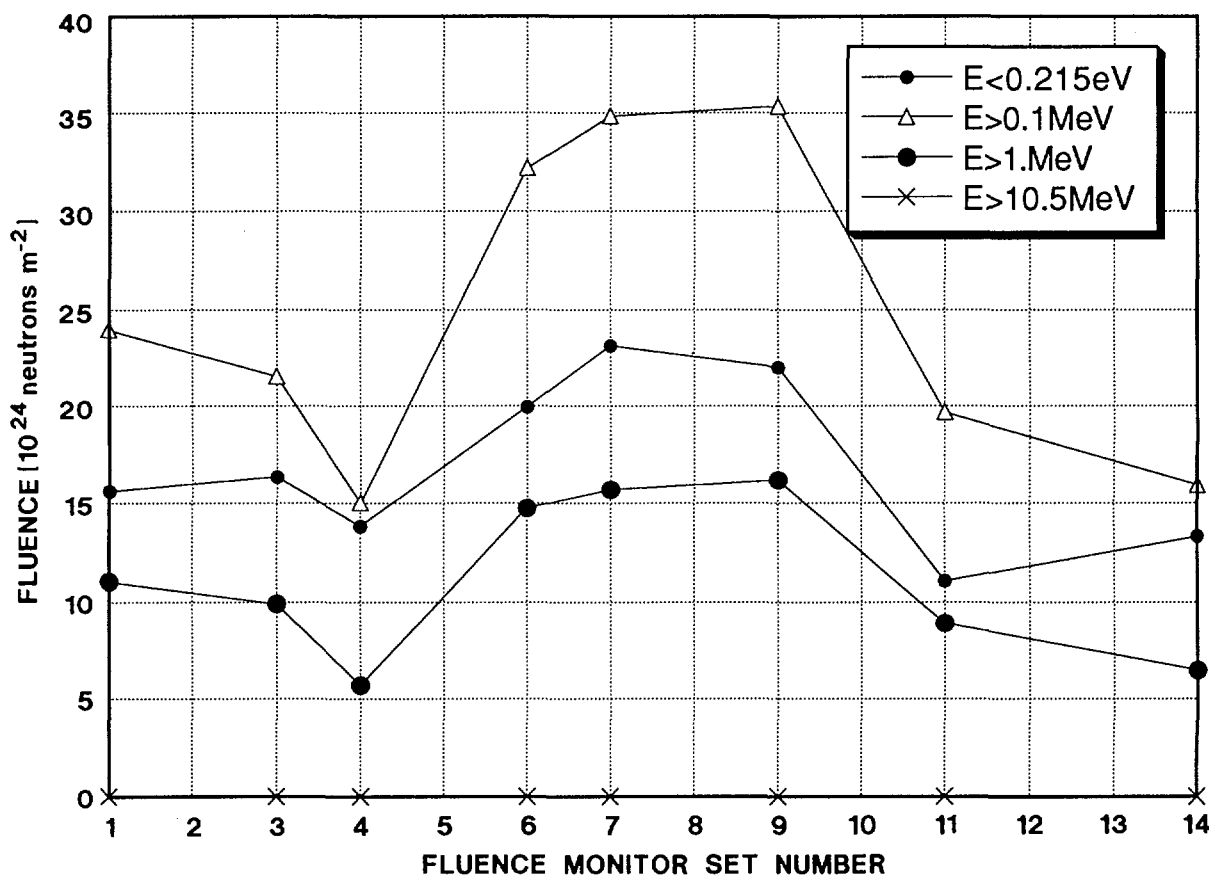


Fig. 26. Fluence by domains of energy, in units of  $10^{24}$  neutrons/ $\text{m}^2$

From the measured activity of a given monitor, the activation per atom has been calculated. This is a measure of the integral of the activation cross-section times the fluence over the neutron energy range. The neutron spectrum could be fitted by a least-squares procedure to a linear combination of three weakly overlapping

components: a Maxwellian, a  $1/v$ -distribution, somewhat tilted and clipped with half Gaussians and a representation of the superposition of two Watt-type functions. For the calculations of the neutron spectrum of the HFR core, the group cross-section library DOSCROS<sup>(1)</sup> was used. Fig. 26 shows the fluence components in four energy bins for all monitor sets.

### ***Neutron Fluence Distribution Measurements using Gold Monitors***

D.F.G. Reher, P. Robouch, G. Sibbens

The neutron fluence distribution at the neutron activation set-up at BR1 reactor of SCK/CEN, was measured. For this purpose gold monitors of cylindrical shape were used: series A of 2 mm diameter and 5 mm length, series B of 2 mm diameter and  $\sim 4$  mm length. During irradiation in the BR-1 the monitors were positioned in an aluminium holder perpendicular to the direction of the neutron flux. Both sets were irradiated in the same beam position, however, set A was irradiated with an additional boron ionization chamber positioned in front of the monitors, and set B was without. The  $\gamma$ -ray emission rate of the  $^{198}\text{Au}$  was measured using a 6" x 6" NaI(Tl) well crystal, the well being of 50 mm diameter and 100 mm depth. The pulses from the detector were amplified and counted above a threshold, and additionally spectra were taken. The latter mainly served for stability checks. Furthermore, a  $^{137}\text{Cs}$  source was measured at regular intervals to check the stability of the system.

Fig. 27 shows a three-dimensional plot of the  $^{198}\text{Au}$  count rate from the set A monitors, which is proportional to the neutron fluence, as a function of the monitor position in the neutron beam. It was found that the neutron fluence is not very uniform within the beam, and that the centre of the aluminium holder is out of position by  $X = -2$  mm.

### ***Low-Energy X-ray Measurements and Standards***

B. Denecke, G. Grosse

Two sets of KX-ray fluorescence sources were standardized for their X-ray emission rate by measuring the emitted X-rays at a defined low solid angle of  $2.5 \cdot 10^{-4}$  sr. These sources will be used to calibrate X-ray detectors especially the windowless Si(Li) spectrometer. A third source with a mixed fluorescer was prepared to be used for energy calibrations and resolution tests of low energy X-ray detectors.

---

(1) W.L. Zijp, H.J. Nolthenius and G.C.H.M. Verhaag, 1984, ECN Report 160

$^{55}\text{Fe}$  layers with an activity of 3 to 15 MBq sealed in a housing form the excitation source for the exchangeable fluorescence layers (Fig. 28). The source No. XRF11 was used to standardize fluorescence layers of magnesium, aluminium, silicon, phosphorous, chlorine, calcium, titanium and vanadium yielding X-ray emission rates between 300 and 14000  $\text{s}^{-1}$ . The source No. XFF12 was standardized with aluminium, silicon, phosphorous and chlorine fluoescers with emission rates between 500 and 2300  $\text{s}^{-1}$ . Accuracies between 1 and 3 % were reached (Table 11). Additional layers of sulphur are ready to be shaped and standardized. Excitation source No. XRF13 is to be used with an aluminium ring foil and calcium carbonate as fluoescers. No standardization was made, only the distribution of the different emitted X-rays was optimised for energy calibrations.

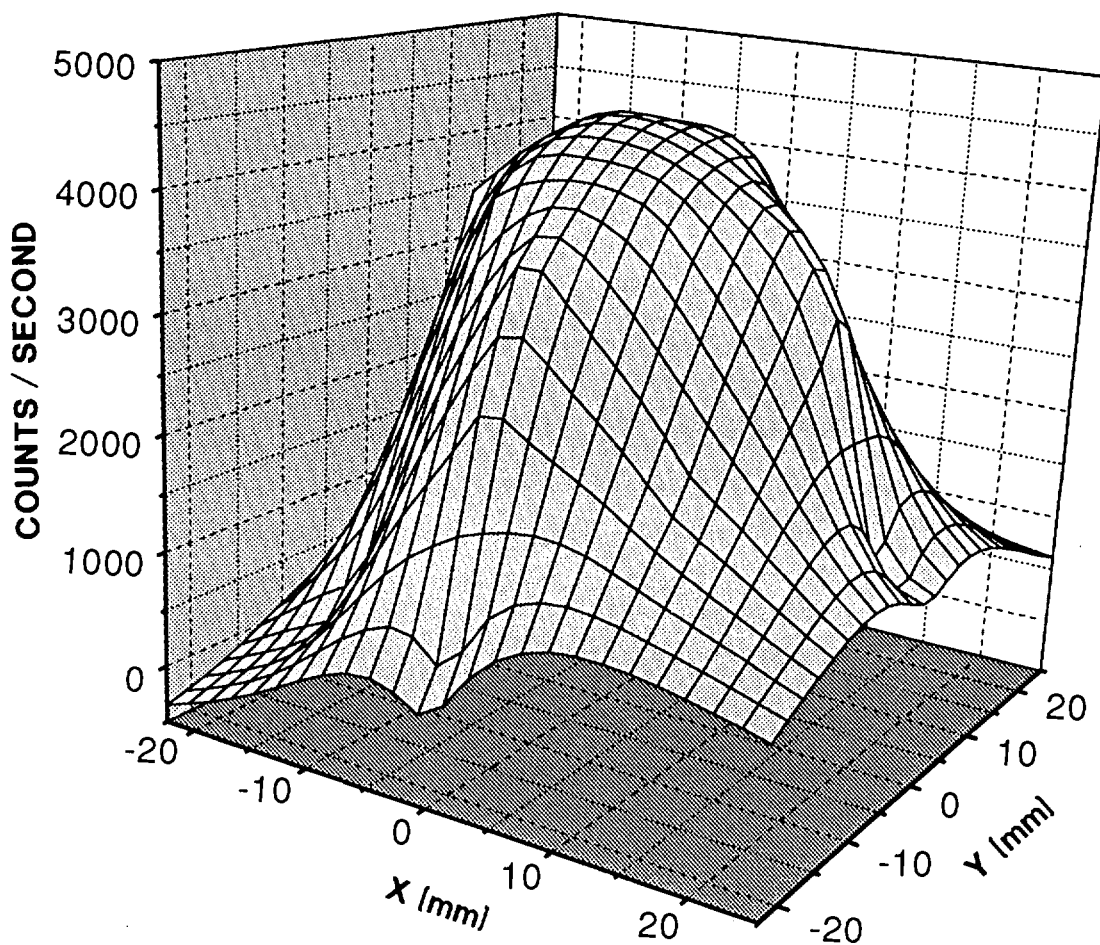


**Fig. 27.** *Three-dimensional plot of the count rates of the monitors of series A as a function of their position in the aluminium holder*

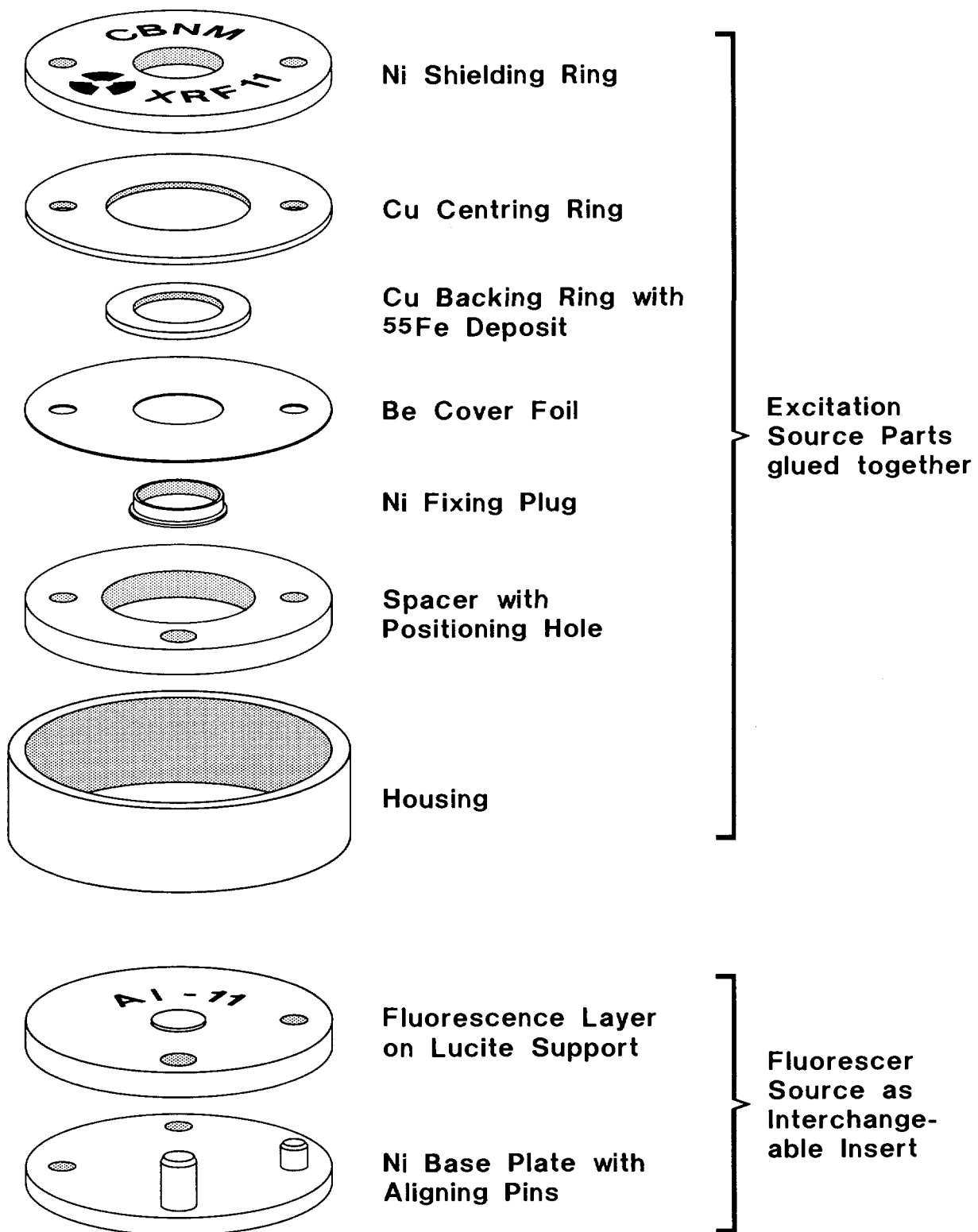


**Fig. 28.** *Low energy X-ray reference source set*

**Table 4. Emission Rates of the KX-ray fluorescence sources [ $s^{-1}$  for  $4\pi sr$ ]**

Fluorescer	Excitation Source	
	XRF12	XRF11
Magnesium	300 (12)	
Aluminium	863 (18)	515 (5)
Silicon	1447 (10)	866 (8)
Phosphorous	1636 (10)	986 (8)
Chlorine	3688 (84)	2304 (15)
Calcium	5904 (69)	ongoing
Titanium	11940 (100)	ongoing
Vanadium	13920 (100)	

**Analysis of Low-Statistic Alpha-Particle Spectra**

G. Bortels, C. Hurtgen\*, D. Santry\*\*

In low-level alpha spectrometry, weak sources are measured using a large detector (e.g. 300 mm<sup>2</sup>) in a large solid angle (e.g. 15 % of  $4\pi sr$ ). The result is a spectrum of relatively poor peak resolution (more than 16 keV FWHM) that is deformed by coincidence summing of alpha particles, conversion electrons and Auger electrons, and in addition has poor statistic. In such a case deconvolution of multiplets is a problem.

Single-isotope sources of <sup>239</sup>Pu and <sup>240</sup>Pu were produced that have closely the same size and thickness as the mixed-isotope sources. Sources were measured using a 300 mm<sup>2</sup> ion-implanted silicon detector in a geometry of 13 % of  $4\pi sr$ . The spectra were fitted to obtain satisfactory residuals. The peaks and their positions used in the fit constitute an isotope-specific set that can be used to analyse the spectra of mixed isotopes. An energy scale of 0.84 keV/channel was chosen throughout.

A typical spectrum is shown in Fig. 29. Results for five activity ratios of <sup>239</sup>Pu/<sup>240</sup>Pu from R = 1.35 to 0.10 are shown in Table 5. Only two sets of pure-isotope sources were used. Results are very satisfactory, except for source #3 where the peak resolutions of pure-isotope sources (16.7 keV) and mixed-isotope source are definitely too different.

\* SCK/CEN, Mol, Belgium

\*\* NRCC, Ottawa, Canada

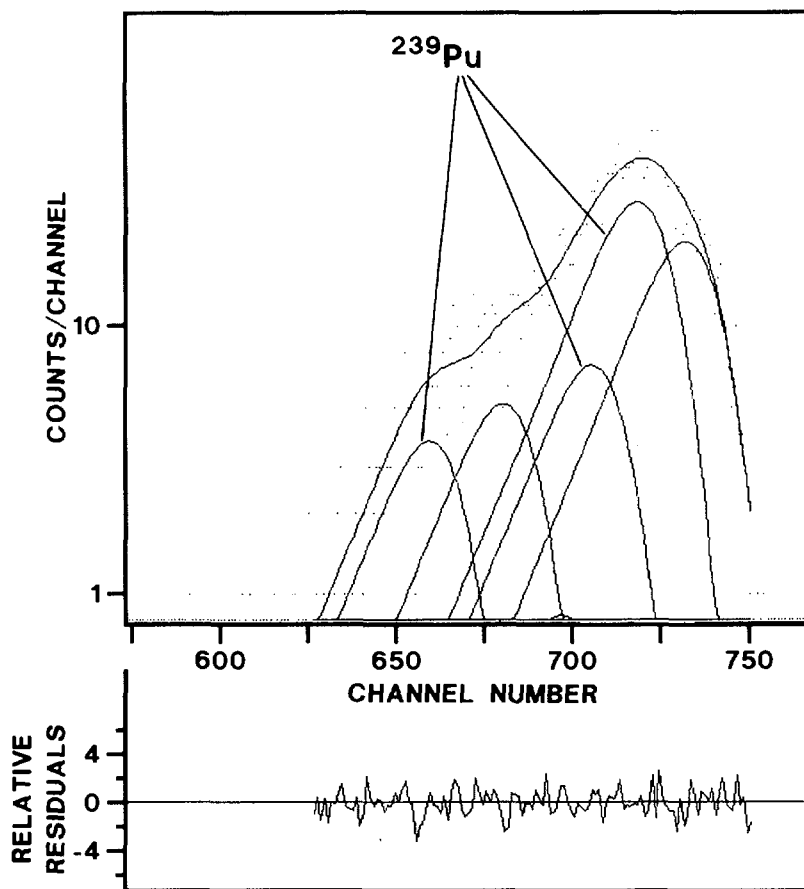


Fig. 29. Fitted spectrum and residuals of the mixed  $^{239}\text{Pu}$  and  $^{240}\text{Pu}$  source #4. Peak resolution is 22.5 keV FWHM

Table 5. Mean value of analysed activity ratios  $R=^{239}\text{Pu}/^{240}\text{Pu}$  in alpha spectra from different sources. The number of diverging fits is given in brackets after the number of measurements

Source	#4	#3	#2	#185C	#103	#104	#105
Measurements	10(1)	10(2)	10(1)	14(0)	16(0)	16(0)	24(0)
Counts	1923	1637	1514	2231	2234	2340	2226
$R_{\text{ref}}$	1.353(3)	1.353(3)	1.353(3)	0.670(2)	0.40(1)	0.233(6)	0.100(3)
$R_{\text{anal.}}(s)$	1.47(33)	0.96(34)	1.29(32)	0.61(5)	0.388(44)	0.232(42)	0.116(60)
$s_p$	0.06	0.07	0.07	0.03	0.02	0.012	0.07
$R_{\Sigma}(s')$	1.45(12)	0.96(19)	1.31(11)	0.61(2)	0.388(17)	0.231(13)	0.113(10)
FWHM [keV]	22.5	29.5	20.4	12.4	17.2	16.8	17.2

$R_{\text{ref}}$  is the reference value;  $R_{\text{anal.}}$  is the mean activity ratio from the analysed spectra; (s) is the standard deviation of that data distribution.  $s_p$  is the standard deviation of the activity ratio that corresponds to the Poisson counting statistics for a single spectrum.  $R_{\Sigma}$  is the result from the analysis of the sum spectrum; (s') is the standard deviation to  $R_{\Sigma}$ , taking into account covariances. FWHM is the resolution of the fitted peaks.

**Measurement of Radionuclide Concentrations ( $^{238}\text{U}$ ,  $^{232}\text{Th}$  and  $^{235}\text{U}$  Decay-series,  $^{40}\text{K}$ ) in a Manchester Clay Standard**

R. Wordel, D. Mouchel, U. Wagner\*

In collaboration with the Technical University of München, measurements of low-level radioactivity in a widely used Manchester clay standard were done, using two low-level HPGe  $\gamma$ -ray detection systems. One of these is operated in an underground laboratory (HADES) at a depth of 500 m w.e. (water equivalent) and has a 0.5 mm thick copper entrance window. This system is especially sensitive to energies above 200 keV. To measure the 63.3 keV  $\gamma$ -line of  $^{234}\text{Th}$  and the 46.5 keV line of  $^{210}\text{Pb}$  a second low-level low-energy detector with a 0.5 mm aluminium entrance window was used. It is operated at ground level and has a shielding of 15 cm thick old lead. The results are shown in Table 6.

**Table 6. The content of natural radionuclides in the Manchester clay standard**

Radionuclide	Disintegration rate [Bq·kg <sup>-1</sup> ]	Content [ $\mu\text{g}\cdot\text{g}^{-1}$ ]
$^{238}\text{U}$	34 ± 8	2.7 ± 0.7
$^{226}\text{Ra}$	45 ± 2*	(1.23 ± 0.06) · 10 <sup>-6</sup>
$^{210}\text{Pb}$	46 ± 5	(1.64 ± 0.16) · 10 <sup>-8</sup>
$^{232}\text{Th}$	54 ± 3	13.2 ± 0.7
$^{235}\text{U}$	0.010 ± 0.003	0.020 ± 0.005
$^{40}\text{K}$	419 ± 15	1.45 ± 0.05

\* The radium content was obtained using the  $\gamma$ -transitions of the radon daughters. For equilibrium conditions the sample was packed airtight and the measurements were started after some half lives of  $^{222}\text{Rn}$ .

**Background Characterization of the IRMM Low-Level HPGe Semiplanar Detector**

R. Wordel, D. Mouchel, G. Heusser\*\*

The detector's quality specifications with respect to background, were defined by two test runs. A 14 days background measurement was performed in the underground laboratory of the Max-Planck-Institute für Kernphysik, Heidelberg with the detector shielded by 15 cm of lead plus 2 cm of steel and an active anti-cosmic shield consisting of six gas proportional counter chambers covering the lead shield on the outside. In this measurement no internal contamination of the HPGe detector was observed.

\* Technical University of München, Germany

\*\* Max-Planck-Institute für Kernphysik, Heidelberg, Germany

Two other background measurements were performed with identical shielding: at ground level and underground at a depth of 500 m w.e. Fig. 30 shows the two spectra. The background reduction in the energy region from 5 to 3000 keV is about a factor 100. This background reduction improves the minimum detectable decay rate of some radionuclides by a factor of about 10. For  $^{210}\text{Pb}$  the lower limit of detection is now about 0.1 Bq/kg.

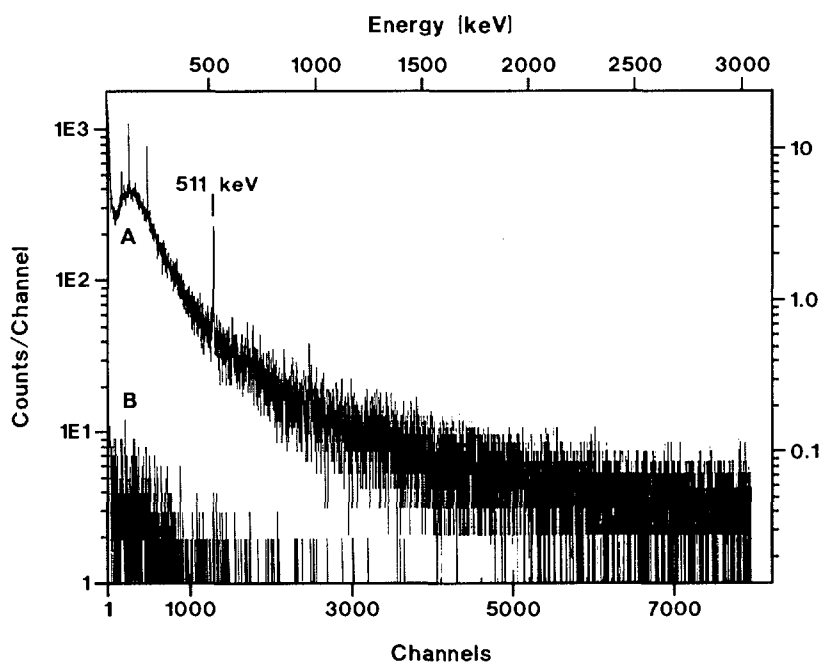


**Fig. 30.** Background count rate for a semi planar low-energy low-level HPGe detector with a shielding of 5 cm Boliden lead plus 10 cm old monument lead, and 6 cm of copper, A) at ground level and B) at -500 m w.e. Counting time for both spectra : 8 days

#### **Neutrons and Muons of Environmental Origin Investigated by Low Background Germanium Gamma-Ray Spectrometers**

R. Wordel, D. Mouchel and T. Altitzoglou, G. Heusser\*, B. Quintana Arnés\*\*, P. Meyendonckx\*\*\*

Two low-level HPGe detection systems have been used to measure the thermal and fast neutron fluxes, as well as the muon flux at different experimental sites at ground level, at -15 m w.e. and at -500 m w.e. underground. To improve sensitivity to cosmic events and weak radioactive samples, low-activity lead shields surrounded the detectors, reducing the count rate originating from the natural decay chains and  $^{40}\text{K}$  within the energy range 3 to 2800 keV, by a factor of  $\approx 10^4$ , for either detector. The remaining structure of the background spectra is due to cosmic interaction.

\* Max-Planck-Institute für Kernphysik, Heidelberg, Germany

\*\* Universidad de Salamanca, Spain

\*\*\* SCK/CEN, Mol, Belgium

The fast neutron flux ( $E > 691$  keV) varied in time between  $100 \text{ m}^{-2}\text{s}^{-1}$  and  $200 \text{ m}^{-2}\text{s}^{-1}$  at ground level. At  $-15$  m w.e. the flux was approximately  $10 \text{ m}^{-2}\text{s}^{-1}$  and at  $-500$  m w.e. it was smaller than  $2 \text{ m}^{-2}\text{s}^{-1}$ . The thermal neutron flux inside the shield is found to vary between  $10 \text{ m}^{-2}\text{s}^{-1}$  and  $40 \text{ m}^{-2}\text{s}^{-1}$ . The  $411$  keV gamma quanta following the reaction  $^{197}\text{Au}(n,\gamma)^{198}\text{Au}$  were used to estimate thermal neutron fluxes of environmental level outside the shield which were found to be about  $14 \text{ m}^{-2}\text{s}^{-1}$  at ground level. The muon flux is found to be  $< 0.2 \text{ m}^{-2}\text{s}^{-1}$  at  $-500$  m w.e., roughly 800 times lower than at ground level.

## TECHNICAL APPENDIX

### *Electron Linear Accelerator*

J.-M. Salomé, K. Cairns, R. Cools, F. Massardier, F. Melis, F. Menu, R. Van Bijlen, V. Van Reeth, J. Waelbers, C. Waller

GELINA was operated up to the end of July of 1994 and the electron beam was available during 1982 hours for the physics experiments.

Neutrons are produced in a rotary uranium target via  $(\gamma, n)$  and  $(\gamma, f)$  reactions. According to the requested neutron energies, various moderators are placed on both sides of the target. Twelve flight paths are equipped for neutron time-of-flight experiments. On the average, 9 neutron beams were used simultaneously when GELINA was operated at very short bursts and 5.7 of them when operated in other conditions.

On the  $0^\circ$  beam line, two Smith-Purcell experiments were carried out at various energies and at very low electron beam intensity to avoid damage of the optical gratings.

The refurbishment of the accelerator was ordered at the firm EuroMeV in 1993. It consists essentially of the replacement of the two long accelerating sections and all the focusing coils. After a time for reduction of the induced activity, the machine was completely dismantled in September 1994 and every component moved out of the gallery to ease the installation of the new accelerating sections. After acceptance tests in the factory for checking some parameters as phase velocity of the travelling waves, attenuation and filling time at low rf power, the sections were installed and accurately positioned. Also the focusing solenoids which present a radial field of less than 0.2% were adapted carefully to the vacuum vessels. Relatively large spaces are provided between the sections to place valves, current monitors, triplets of quadrupoles and in one position a double cross piece to allow beam parameter measurements and future alignments. At the end of 1994, the three sections were under vacuum and most of the electrical connections were done. The cooling circuits have been redesigned, specially to make easy a possible tuning of the sections by adjusting the water temperature. They will be connected in early 1995.

During this shut-down period, several other works were under realisation. The target-moderator system has been completely redesigned to be fitted with a remote-controlled mechanism of pipes, bellows and valves which will allow to get the electron beam on the neutron target or throughout the wall of the target room towards the new Radiation Physics laboratory. The programmable controller used to help operation of the Linac was modernised to facilitate the adjustments and to control several parameters of the accelerator.

The acceptance tests of the refurbished accelerator with long burst-low current and short burst-high current are foreseen to be achieved in February 1995. It is intended to make use of the optical transition radiation system to measure electron beam parameters as energy, divergence and probable emittance by the three gradient method.

### ***Radiation Physics Laboratory***

J.-M. Salomé, P. Rullhusen

The electron beam deviation allowing to change between the neutron production and the radiation physics modes of operation has been built and is being tested before installation. The remaining parts of the beamline including the safety beam shutters, vacuum chambers, beam dump magnet and beam catcher have been designed and ordered.

Extensive numerical simulations have been carried out for the design of the electron beamline and to predict the properties of the radiation produced by the different effects under consideration, i.e. Smith-Purcell effect, X-ray transition radiation, channeling radiation or parametric X-rays.

For the design of the electron beamline a new computer code based on the CERN computer code TRANSPORT was developed, which allows to optimize the elements in the beamline according to the experimental needs. It includes 2<sup>nd</sup> order corrections and a convenient graphical interface for visualization of the results.

For practical applications it would be desirable to use X-ray optics to enhance the photon flux on a target in the radiation physics laboratory. Therefore a new project has been started to design X-ray beam-lines taking into consideration both the finite electron beam emittance and the spectral and angular distribution of the different types of radiation.

### ***Radiation Physics***

R.Cools, O.Haeberlé\*, N.Maene\*\*, Th. Moreno\*\*\*, F.Poortmans\*\*, H.Riemenschneider, P.Rullhusen, J.-M.Salomé, F.Van Reeth

New experiments on Smith-Purcell (SP) radiation at optical wavelengths have been carried out using 20-110 MeV electrons and a grating ruled in SiC on a graphite backing with an aluminium coating. The experiments confirmed the

---

\* EC Fellow from the Université Louis Pasteur, Strasbourg, France

\*\* VITO, Mol, Belgium

\*\*\* EC Fellow from the University Paris VI, France

previous results obtained using glass gratings, but higher beam currents could be used and the radiation characteristics could be accurately measured also at large incidence angles of the electron beam relative to the grating. Measurements were carried out at incidence angles from  $0^\circ$  ( i.e. pure Smith-Purcell radiation ) to  $45^\circ$  and observation at specular reflection ( i.e. optical transition radiation (OTR) from a grating ). The spectral distribution at each incidence angle was measured using a set of optical filters of 10 nm bandwidth, and the degree of polarization was determined using a linear polarization filter. The radiation was observed at  $90^\circ$  to the beamline and the angle of incidence was changed by tilting the grating.

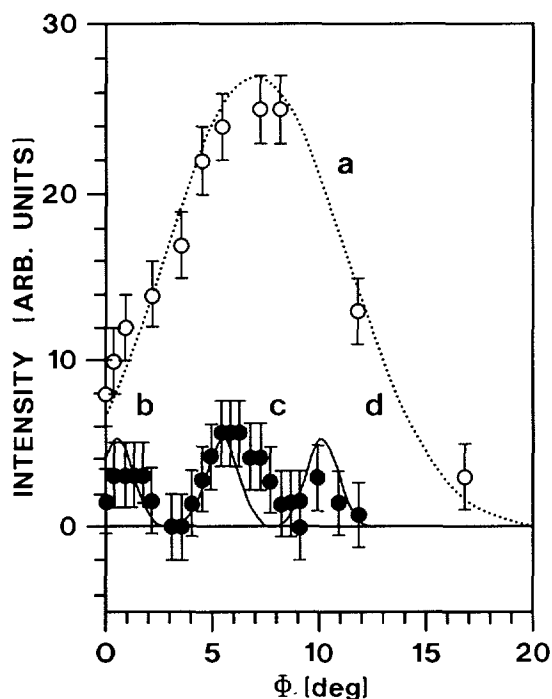


**Fig. 31.** a) Intensity as a function of incidence angle, observed with no filters. Dashed line: guide to the eyes. Lower part: using filters of b) 550 nm, c) 500 nm, d) 450 nm. Solid line: sum of Gaussians centered at the corresponding characteristic angles  $\Phi(\lambda)$  predicted by theory

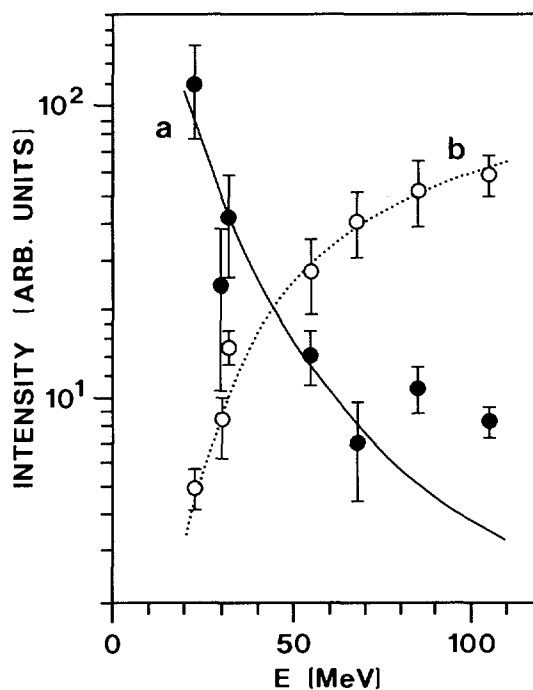


**Fig. 32.** Intensity as a function of electron energy. a) grazing incidence  $\Phi = 0^\circ - 6^\circ$ ; b)  $\Phi = 45^\circ$  and observation at specular reflection

Fig. 31 shows the intensity observed as a function of incidence angle  $\Phi$  and Fig.32 the energy dependence of the intensity observed for small angles of incidence and for  $\Phi = 45^\circ$  (specular reflection).

For small angles of incidence the radiation is H-polarized like pure SP radiation and quasi-monochromatic with a characteristic wavelength changing with incidence angle. The dependence on the electron energy  $E$  was found to be very similar to the  $E$ -dependence of SP radiation.

At an incidence angle of  $45^\circ$  and observing at specular reflection, the spectral distribution, polarization and E-dependence were found to be essentially the same as for OTR from flat surfaces. A new theoretical ansatz is under development which describes the process of radiation production by relativistic electrons interacting with gratings at arbitrary angles of incidence  $\Phi \cong 1/\gamma$  and predicts correctly the wave-lengths observed at small angles of incidence (curves b-d in Fig. 31).

### ***Van de Graaff Accelerators***

A. Crametz, P. Falque, J. Leonard, W. Schubert

The total working time of the two accelerators was 2908 hours. Both accelerators were operated simultaneously during 92 hours. For 78 % of the total time, the accelerators were used for applications.

For the neutron applications, it can be explained by the fact that the two students preparing their PhD have completed their experimental work in 1993 and were occupied with the analysis of the data and the redaction of their work. Three new students are planned for 1995.

The material applications on the CN concerned a) the first successful experiment using  $^{15}\text{N}^+$  ions as projectile at 6.4 MeV for hydrogen determination in polyimide foils and b) measurements of the electric field gradient at  $^{19}\text{F}$  impurity sites in crystalline silicon and highly oriented pyrolytic graphite. The materials applications on the KN were performed by analytical chemistry activities.

Between 5 and 7 MV, the accelerator tube of the CN should be conditioned and the small number of hours indicates that experiments with energetic ions have not been requested too much.

The maintenance consisted of replacements of the ion source (2 times on the CN) and of electronic repair on both accelerators.

Modifications on the CN dealt mainly with the complete disconnection of the former beam line at ground level, the replacement of the  $90^\circ$  analyzing magnet by a bigger one ( $(M \cdot E)/q^2 = 140$  instead of 24) in order to bend the  $^{15}\text{N}^+$  beam from vertical to horizontal plane and the installation of quadrupole lenses on the 31 m long beam tube (under a vacuum of around  $10^{-4}$  Pascal) through shielding walls and different areas to reach the target hall no. 2 for HI-ERDA experiments (Fig. 33).

In case of operating the KN at 3.5 MV instead of 2 MV, the radiation level in target hall no. 1 would become too high and the background not acceptable for experiments with the CN. To continue the operation of both accelerators simultaneously, the KN was shielded by a 5 mm thick lead plate. With this

modification, the radiation level had been reduced by a factor between 2 and 3 and is smaller than the admissible dose.

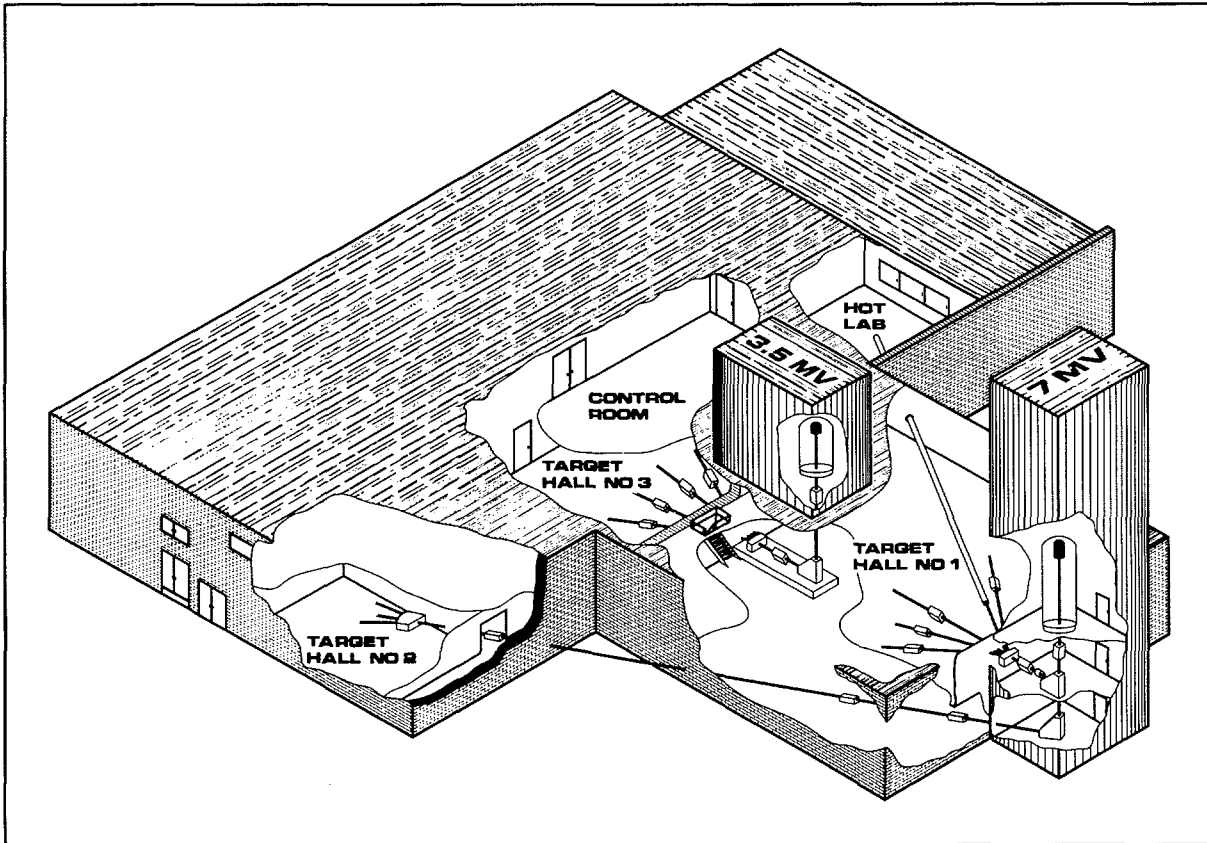


**Fig. 33.** *Situation of the three target halls and arrangement of the beam lines at the Van de Graaff facility*

***Hydrogen profiling at the 7 MV Van de Graaff accelerator.***

G. Giorginis, A. Crametz, M. Conti, S. Mathot\*, P. Courel\*\*, M. Hult\*\*\*

The materials analysis group of the 7 MV VG concentrated its activities on the installation of two hydrogen profiling techniques. The one, H-ERDA (Hydrogen Elastic Recoil Detection Analysis), uses elastic scattering of (2 - 3) MeV  $^4\text{He}^+$  ions on hydrogen atoms. From the energy spectrum of the recoiling hydrogen ions measured under forward angles the hydrogen concentration as function of the

---

\* EC Fellow from the University of Namur, Belgium  
\*\* EC Fellow from the University of Paris, France  
\*\*\* EC Fellow from the University of Lund, Sweden

sample depth (hydrogen profiling) is deduced. The other, H-NRRA (Hydrogen Nuclear Resonant Reaction Analysis), applies the resonant reaction  ${}^1\text{H}({}^{15}\text{N}, \alpha\gamma){}^{12}\text{C}$ . Varying the  ${}^{15}\text{N}^+$  ion energy from the resonance energy ( $E_R = 6.385$  MeV) upwards the hydrogen profiling is determined from the measured gamma ray yield ( $E_\gamma = 4.43$  MeV). While H-ERDA simultaneously analyses all hydrogen isotopes and has a high sensitivity, H-NRRA detects only  ${}^1\text{H}$  but is distinguished by the best depth resolution.

H-NRRA : A fully new versatile UHV-chamber was developed, equipped with a high efficiency BGO gamma ray detector, sample handling and cooling, as well as beam diagnosis systems. In addition a new beam line including a strong magnet for the deflection of the heavy  ${}^{15}\text{N}^+$  ions has been installed. The nearly completed system delivered very promising results in first test runs of hydrogen profiling in hydrogenated metallic samples. Fig. 34 shows a typical gamma ray spectrum measured at a scattering angle of  $0^\circ$  during irradiation of a hydrogenated tantalum sample with  ${}^{15}\text{N}^+$  ions of energy  $E = E_R$ .

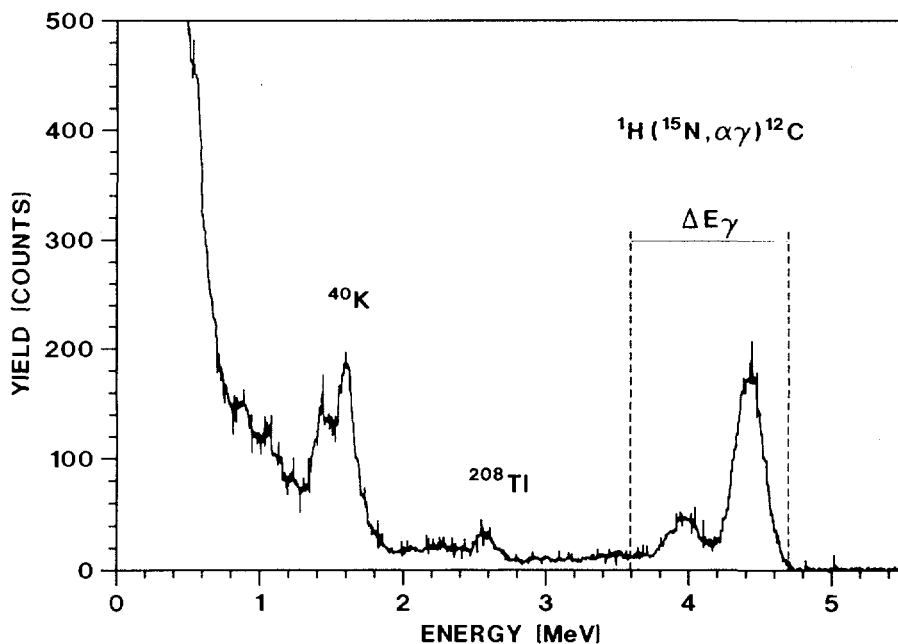


**Fig. 34.** Typical gamma ray spectrum measured with a BGO detector during irradiation of a hydrogenated tantalum sample with  ${}^{15}\text{N}^+$  ions of 6.635 MeV. The full energy peak (4.43 MeV) and the first escape peak, indicated by the energy window  $\Delta E_\gamma$ , are used in the yield curve measurement

A thin sample, in which the beam energy loss is less than the resonance width, reflects the resonance form of the cross section as demonstrated in Fig. 35(a) showing the depth profile of a thin hydrogen layer on a silicon wafer surface. The continuous line is a Lorentzian fit to the measured yield curve (crosses). A thick sample, which causes an energy loss bigger than the resonance width, behaves like the resonance integral as can be seen in Fig. 35(b) showing the depth profile of a hydrogenated tantalum sample. The peak at  $E = E_R$  in this figure is due to

surface hydrogen contamination. Considering negligible the thickness of this contamination the measured energy resolution is 10.4 keV and a surface depth resolution  $\Delta x = 7$  nm for silicon and 3 nm for tantalum was derived.

H-ERDA : The installation was done in the existing NRA (Nuclear Reaction Analysis) chamber so that now a range of light elements (hydrogen, boron, carbon, nitrogen, oxygen) can be determined in the same system. First tests with plastic foils were performed. Fig. 36(a) shows an energy spectrum of hydrogen recoils measured at a scattering angle of  $30^\circ$  in reflection geometry (target beam angle =  $15^\circ$ ) by bombarding a polyimide foil on a tantalum substrate with  $^4\text{He}^+$  ions of 2.7 MeV energy. A 10  $\mu\text{m}$  thick aluminium absorber in front of the surface barrier detector was used to filter out the scattered helium projectiles. Preliminary results of a simulation are also presented in Fig. 36(a) (smooth curve) and in Fig. 36(b) for hydrogen profiling produced by the simulation process. The steep decrease of the hydrogen concentration around the depth of 1700  $\text{\AA}$  corresponds to the boundary between the polyimide foil and the tantalum. The tail of the hydrogen profile indicates a hydrogen diffusion into the tantalum bulk.

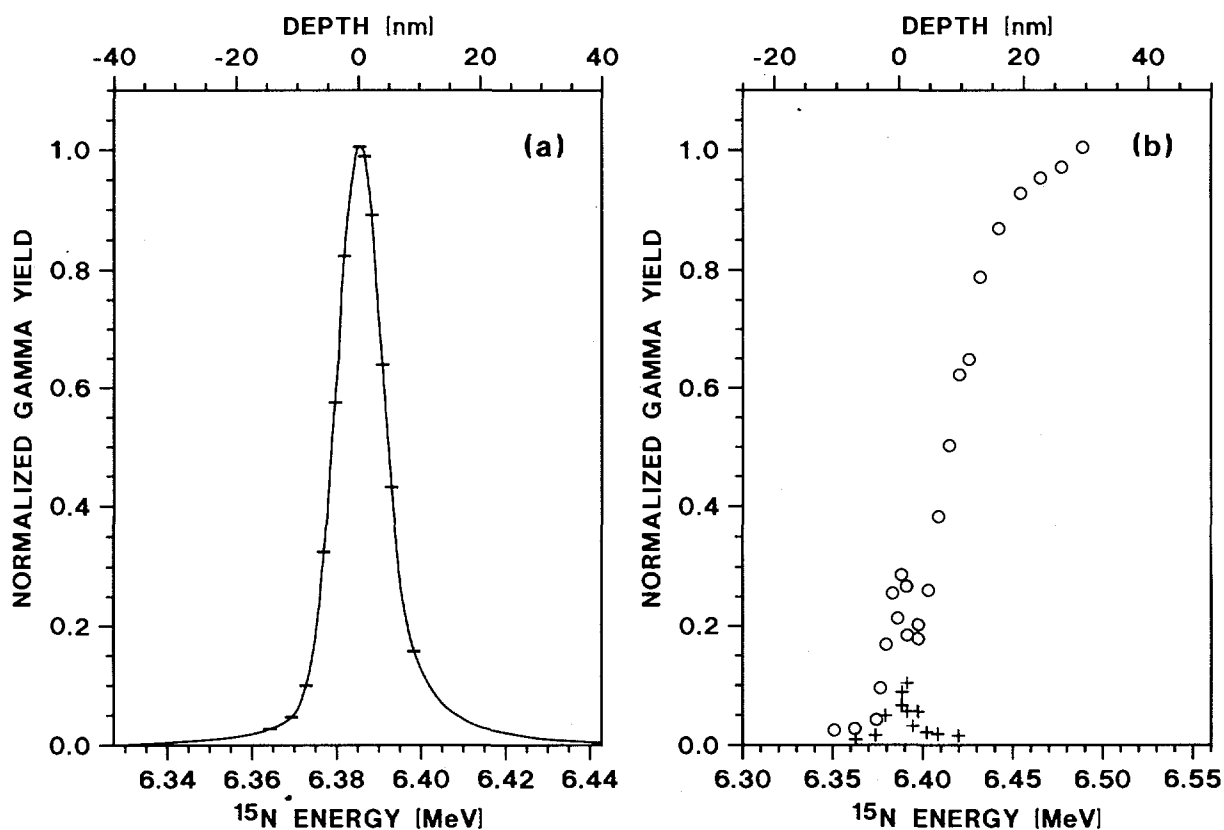
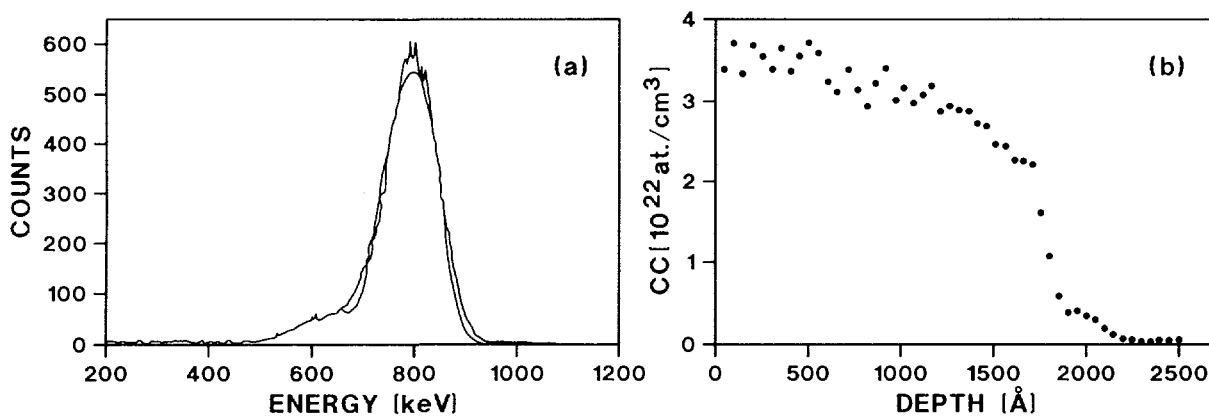


Fig. 35. Depth of (a) a thin hydrogen layer on a silicon wafer surface and (b) a hydrogenated (empty circles) and a blank (crosses) tantalum sample. The peaks in (b) are due to surface hydrogen contamination. The gamma ray yields (proportional to the hydrogen contents) were obtained by varying the energy of the incident  $^{15}\text{N}^+$  ions by steps between 2.5 and 10 keV



**Fig. 36.** *Measured energy spectrum of hydrogen recoils from the bombardment of a kapton foil on a tantalum substrate with  $^4\text{He}^+$  ions of 2.7 MeV energy (a) (noisy curve), simulation fit (a) (smooth curve) and hydrogen profile (b). The hydrogen concentration has a steep decrease at the boundary between kapton and tantalum and a diffusion tail into the tantalum bulk*

#### **IRMM Computer Network**

C. Cervini, T. Garcia, H. Horstmann, L. van Rhee

Two powerful RS/6000-3BT workstations have been connected to the IRMM network. They will be used for neutron data analysis and administrative applications, respectively. Z-mail, an e-mail user agent, and Xmgr, a graphics package, have been added to the UNIX environment.

IRMM has access to the Internet with a class C address.

For the future IRMM electronic mail system the installation of an IRMM mail server for SMTP and X.400 based on ISOCOR software is in preparation.

A PC network server has been ordered. This server is based on a Compaq Pentium system under UnixWare and with LanWorkplace as client software. DOS, OS/2, UNIX and MAC workstations will be supported.

#### **Modernizing and Standardising of Neutron Data Acquisition Systems**

G. Kelly

A comprehensive survey was made of the data acquisition systems used by neutron data physicists. This was based on detailed discussions with the users and practical demonstrations of the equipment used for each experiment. There are nine neutron experiments using different types of data acquisition computers.

The maximum event size was 22 bytes, highest event rate 5.000 events per second and typical deadtime of 1  $\mu$ sec. Single and multi-parameter spectra can be displayed although there are some limitations in multi-parameter mode.

Most users would like increased performance in terms of higher event rate (20.000 events per second), smaller deadtime (0.5  $\mu$ s) and capability to accept more ADC inputs in coincidence. Based on these requirements a specification for a new data acquisition system has been partially completed.

### ***The MP Family of Multi-Parametric Analysis Programs***

C. Bastian

The multiparametric acquisition setup using a microVAX 4000 was applied in the test phase to a neutron capture measurement program. The events were thereby coded by a 16-bit transputer in a multiplexer, and analysed by two 32 bit transputers connected to the host (microVAX). The results of the on-line analysis, consisting of histograms and/or a list of processed events were filed separately on the disk of the host.

A comprehensive file format \*.EPI was developed basing on this experience. It combines in one file all histogram and list mode data produced as well as the execution scheme followed during a MPA cycle. The analysis software was rewritten for this format whereby only the event coding is performed by external processors i.e. transputers. In this new program called MPACQ, the event processing and histogramming is completely executed in the host's central processing unit. MPACQ follows an analysis scheme described in an executive file \*.EPX compiled from a source written by the user in the EPL notation as developed in the Transputer/MPA project.

By moving the analysis program to the host, an improvement in execution speed by a factor of 4 has been realised. Furthermore, the off-line analysis of list data produced by MPACQ is now possible with a sister program MPSORT using the same EPI format for input, output, and executive files. MPACQ, MPSORT and utilities of the same family (MPMAKE, MPSCAN, MPVIEW) are written in C and are implemented as shell commands of the VMS and UNIX systems. This allows a seamless data transfer from the real time analysis programs to the off-line analysis programs on dedicated workstations.

***Gated Phase Lock for the Drive of the 7 MV Van de Graaff Post Buncher***

S. de Jonge

A phase lock circuit for the drive of the post buncher of the 7 MV Van de Graaff at 0.625 MHz has been designed. The reference signal for the phase lock is generated by a pick-off electrode and a zero cross detector. It is not present for every machine cycle due to amplitude variations. Nevertheless the locking conditions for a previous cycle are stored in an integrator driving a voltage controlled crystal oscillator. The phase lock condition remains established even if there is a loss of reference signals up to 90 %.

***Special Electronic Equipment for Laboratory Use***

S. de Jonge, J. Gonzalez, K. Hofmans, H. Mensch, H. Nerb, W. Stüber

A 0.5 ns time coder, two digital multiplexers for the connection of 4 ADCs and a timer circuit for switching the output current of a HP power supply have been built.

A VME interface for the DE time coder has been developed. This interface contains a 1024 word FIFO buffer generating an interrupt when the buffer is filled by 50%. A register supplies the run/stop signal to the time coder.

An adapter which enables the use of Silena ADCs in FAST or Canberra S100 data acquisition systems has been designed. The adapter permits the use of a spectrum stabilizer as well. An input buffer (512 words x 26 bits) for FAST systems has also been designed.

## LIST OF PUBLICATIONS

### CONTRIBUTION TO CONFERENCES

BERTHOLD, K., NAZARETH, C., ROHR, G., WEIGMANN, H.

Very high resolution measurements of the total section of natural iron.

Int. Conference on Nuclear Data for Science and Technology, Gatlinburg, May 9-13, 1994

BORTELS, G., HURTGEN, C., SANTRY, D.

Nuclide analysis on low-statistics alpha-particle spectra: an experimental verification for Pu isotopes.

Int. Symposium on Plutonium in the environment, Ottawa, July 6-8, 1994

BRUSEGAN, A., CRAMETZ, A., MACAVERO, E., SCHUBERT, W., VAN DER VORST, C., WATTECAMPS, E.

The total neutron cross section of  $^{10}\text{B}$  from 80 eV to 100 keV from 1 to 19 MeV.

Int. Conference on Nuclear Data for Science and Technology, Gatlinburg, May 9-13, 1994

BRUSEGAN, A., MACAVERO, E., VAN DER VORST, C.

Resonance parameters of  $^{138}\text{Ba} + n$  from high resolution transmission measurements.

Int. Conference on Nuclear Data for Science and Technology, Gatlinburg, May 9-13, 1994

BRUSEGAN, A., ROHR, G., SHELLEY, R., MACAVERO, E., VAN DER VORST, C., POORTMANS, F., MEWISSEN, L., VANPRAET, G.

Very high resolution transmission measurements and resonance parameters of  $^{58}\text{Ni}$  and  $^{60}\text{Ni}$ .

Int. Conference on Nuclear Data for Science and Technology, Gatlinburg, May 9-13, 1994

CORVI, F.

The measurement of neutron capture cross sections via prompt gamma-ray detection.

Specialists Meeting on Measurement, Calculation and Evaluation of Photon Production Data, Bologna, November 9-11, 1994

CORVI, F., GUNSING, F., POSTMA, H., POPOV, YU-P., SHARAPOV, E.

Spin assignments of neutron resonances for parity nonconservation experiments.

Int. Conference on Nuclear Data for Science and Technology, Gatlinburg, May 9-13, 1994

CORVI, F., MOXON, M.C., ATHANASOPOULOS, K.

Resonance neutron capture in  $^{58}\text{Ni}$ .

Int. Conference on Nuclear Data for Science and Technology, Gatlinburg, May 9-13, 1994

CORVI, F., MUTTI, P., ATHANASOPOULOS, K., BEER, H.

The stellar capture rate of  $^{208}\text{Pb}$ .

3rd Int. Symposium on Nuclear Astrophysics, Gran Sassa, July 8-13, 1994

CRAMETZ, A., SCHUBERT, W., WATTECAMPS, E.

Total neutron cross section measurements of  $^{232}\text{Th}$  from 1 to 19 MeV.

Int. Conference on Nuclear Data for Science and Technology, Gatlinburg, May 9-13, 1994

DEMATTE, L., WAGEMANS, C., D'HONDT, P., POMMÉ, S., DERUYTTER, A.  
New results on the energy and mass characteristics of  $^{242}\text{Pu}(\text{SF})$  and  $^{244}\text{Pu}(\text{SF})$  fragments.  
Workshop on Nuclear Fission and Fission-Product Spectroscopy, Seyssins, May 2-4, 1994

DERUYTTER, A., WEIGMANN, H., CARLSON, A., SMITH, D.  
International collaboration on measurement of differential nuclear data for energy applications in the frame of the NEA nuclear science committee.  
Int. Conference on Nuclear Data for Science and Technology, Gatlinburg, May 9-13, 1994

GIORGINIS, G., MISAEELIDES, P., CRAMETZ, A., CONTI, M.  
Nuclear reaction analysis of boron-nitride coatings.  
13th Int. Conference on Applications of Accelerators in Research and Industry, Denton, November 7-10, 1994

GUNSING, F., CORVI, F., ATHANASOPOULOS, K., POSTMA, H., POPOV, YU.P., SHARAPOV, E.I.  
Spin assignment of  $^{113}\text{Cd}$  neutron resonances.  
2nd Int. Seminar on Interactions of Neutrons with Nuclei, Dubna, April 26-28, 1994

HAMBSCH, F.-J., OBERSTEDT, A., JÄCKEL, B.S.  
LISA, a PV-WAVE application for scientific data analysis and visualization.  
PV-WAVE User Group Meeting, Stuttgart, October 5-6, 1994

HAMBSCH, F.-J., VAN AARLE, J., VOGT, R.  
Counting gas peculiarities observed for  $^{252}\text{Cf}(\text{sf})$ .  
Spring Meeting of the German Physical Society, München, March 21-25, 1994

HAMBSCH, F.-J., VAN AARLE, J., VOGT, R.  
Is there a pulse height defect for methane?  
Workshop on Nuclear Fission and Fission Product Spectroscopy, Seyssins, May 2-4, 1994

HAMBSCH, F.-J., VAN AARLE, J., VOGT, R.  
Peculiarities found by using different counting gases for  $^{252}\text{Cf}(\text{sf})$ .  
Int. Conference on Nuclear Data for Science and Technology, Gatlinburg, May 9-13, 1994

HAMBSCH, F.-J., VOGT, R.  
Feasibility study for a neutron fluence detector based on the n-p scattering process.  
Int. Conference on Nuclear Data for Science and Technology, Gatlinburg, May 9-13, 1994

MEISTER, A.  
Influence of lattice vibrations on the Doppler broadening of the 0.18 eV Cd neutron resonance cross section.  
Int. Conference on Nuclear Data for Science and Technology, Gatlinburg, May 9-13, 1994

MEISTER, A., ROLLIN, G., SCHUBERT, W., WATTECAMPS, E.  
Measurement of (n,n' $\gamma$ ) cross section for low-lying levels of palladium isotopes.  
Int. Conference on Nuclear Data for Science and Technology, Gatlinburg, May 9-13, 1994

MOXON, M., BÜRKHOLZ, K., WARTENA, J.A., WEIGMANN, H.

Inelastic scattering from  $^{238}\text{U}$ .

Int. Conference on Nuclear Data for Science and Technology, Gatlinburg, May 9-13, 1994

MOXON, M., WARTENA, J.A., WEIGMANN, H.

Analysis of  $n(\eta)$  measurements for  $^{235}\text{U}$  in the thermal neutron energy region.

Int. Conference on Nuclear Data for Science and Technology, Gatlinburg, May 9-13, 1994

MOXON, M., WARTENA, J.A., WEIGMANN, H.

Analysis of  $\eta$  measurements for  $^{235}\text{U}$  in the thermal neutron energy region.

Int. Conference on Nuclear Data for Science and Technology, Gatlinburg, May 9-13, 1994

MOXON, M., WARTENA, J.A., WEIGMANN, H., VAN PRAET, G.

Inelastic neutron scattering from  $^{238}\text{U}$ .

Int. Conference on Nuclear Data for Science and Technology, Gatlinburg, May 9-13, 1994

POSTMA, H.

Methods to determine spins and neutron-channel-spin mixing of p-resonances.

2nd Int. Symposium on Neutron Spectroscopy, Dubna, April 27, 1994

POSTMA, H., GUNSING, F., CORVI, F., ATHANASOPOULOS, K.

Neutron capture gamma-rays spectroscopy for spins of p-wave resonances

4th Int. Conference on Applications of Nuclear Techniques "Neutrons and Their Applications", Crete, June 13, 1994

REHER, D.F.G.

Metrology of  $^{192}\text{Ir}$  brachytherapy sources

World Congress on Medical Physics and Biomedical Engineering, Rio de Janeiro, August 21-26, 1994

REHER, D.F.G.

Metrology of  $^{192}\text{Ir}$  brachytherapy sources

EUROMET Workshop and Contact Persons Meeting, NPL, Teddington, October, 10-12, 1994

REHER, D.F.G.

EC-JRC-Institute for Reference Materials and Measurements

EUROMET Workshop and Contact Persons Meeting, NPL, Teddington, October 10-12, 1994

ROHR, G.

The parameters of the level density expression and their energy dependence tested with experimental data.

Int. Conference on Nuclear Data for Science and Technology, Gatlinburg, May 9-13, 1994

ROHR, G.

The parameters of the Bethe level density expression and their energy dependence tested with experimental neutron resonance data.

Int. Conference on Nuclear Data for Science and Technology, Gatlinburg, May 9-13, 1994

ROHR, G., SHELLEY, R., NAZARETH, C., MOXON, M.

Resonance parameters of  $^{27}\text{Al}+n$  from very high resolution transmission measurements.

Int. Conference on Nuclear Data for Science and Technology, Gatlinburg, May 9-13, 1994

SIEGLER, P., HAMBSCH, F.-J., THEOBALD, J.  
Investigation of the fission reaction  $^{237}\text{Np}(n,f)$  for incident neutron energies from 0.3 MeV to 5.5 MeV  
Int. Conference on Nuclear Data for Science and Technology, Gatlinburg, May 9-13, 1994

SIEGLER, P., HAMBSCH, F.-J., THEOBALD, J.P.  
Investigation of the fission reaction  $^{237}\text{Np}(n,f)$  for incident neutron energies from 0.3 MeV to 5.5 MeV.  
Spring Meeting of the German Physical Society, München, March 21-25, 1994

SIEGLER, P., HAMBSCH, F.-J., THEOBALD, J.P.  
Neutron induced fission of  $^{237}\text{Np}(n,f)$  in the neutron energy range 0.3 MeV to 5.5 MeV.  
Workshop on Nuclear Fission and Fission Product Spectroscopy, Seyssins, May 2-4, 1994

SIEGLER, P., HAMBSCH, F.-J., THEOBALD, J.P.  
Measurements of mass and kinetic energy distributions of fission fragments from the reaction  $^{237}\text{Np}(n,f)$ .  
2nd Int. Seminar on Interaction of Neutrons with nuclei, Dubna, April 26-28, 1994

TSABARIS, C., WATTECAMPS, E., ROLLIN, G.  
Double differential (n, x alpha) and (n,xp) cross section ratio measurements of  $^{27}\text{Al}$ ,  $^{58}\text{Ni}$ , and  $^{63}\text{Cu}$  at 6.5, 8.0, 9.0 and 15.5 MeV.  
International Conference on Nuclear Data for Science and technology, Gatlinburg, May 9-13, 1994

VAN AARLE, J., HAMBSCH, F.-J., VOGT, R.  
Correlations of fission fragments with prompt gamma-emission in  $^{252}\text{Cf}(sf)$ .  
Workshop on Nuclear Fission and Fission Product Spectroscopy, Seyssins, May 2-4, 1994

WAGEMANS, C., DRUYTS, S., BARTHÉLÉMY, R.  
Recent (n,p)- and (n, alpha)-measurements of relevance to astrophysics.  
3rd Int. Symposium on Nuclear Astrophysics "Nuclei in the Cosmos", Gran Sasso, July 8-13, 1994

WAGEMANS, C., POMMÉ, S.  
New results on ternary fission : Part I : Theoretical backgrounds, Part II : Experimental results.  
Workshop on Nuclear Fission and Fission-product Spectroscopy, Seyssins, May 2-4, 1994

## SCIENTIFIC OR TECHNICAL ARTICLES

DENECKE, B.  
Absolute activity measurements with the windowless  $4\pi$ -CsI(Tl)-sandwich spectrometer.  
Nucl. Instrum. Methods Phys. Res. A 339 (1994) 92

DRUYTS, S., WAGEMANS, C., GELTENBORT, P.  
Determination of the  $^{35}\text{Cl}(n,p)^{35}\text{S}$  reaction cross section and its astrophysical implications.  
Nucl. Phys. A 573 (1994) 291

- GUNSING, F., CORVI, F., ATHANASOPOULOS, K., POSTMA, H. MAURI, A.  
Spin assignment of  $^{238}\text{U}$  p-wave resonances.  
In : Proc. 8th International Symposium on Capture Gamma-ray Spectroscopy and Related Topics, J. Kern (ed.), World Scientific, 1994, p. 797
- HAEBERLÉ, O., RULLHUSEN, P., SALOMÉ, J.-M., MAENE, N.  
Calculations of Smith-Purcell radiation generated by electrons of 1-100 meV.  
Phys. Rev. E49 (1994) 3340
- OBERSTEDT, A., HAMBSCH F.-J.  
LISA - a powerful program package for LIstmode and Spectral data Analysis.  
Nucl. Instrum. Methods, Phys. Res. A 340 (1994) 379
- OBERSTEDT, S., THEOBALD, J.P., WEIGMANN, H., WARTENA, J.A.,  
BÜRKHOLZ, C.  
Limits on the half life of the shape isomer in  $^{239}\text{Pu}$ .  
Nucl. Phys. A 573 (1994) 467
- OBERSTEDT, S., THEOBALD, J.P., WEIGMANN, H., WARTENA, J.A.,  
BÜRKHOLZ, C.  
Intermediate structure and the shape isomet in  $^{223}\text{Th}$ .  
Nucl. Phys. A 578 (1994) 31
- REHER, D.F.G., AALBERS, A.H.L., BJERKE, H., DRUGGE, N., GENKA, T.,  
ROSSITER, M.J., SANTRY, D., SEPHTON, J.P., SIBBENS, G., SEUNTJENS, J.,  
THIERENS, H., VERHAEGEN, F., WILLIAMS, T.T., WOODS, M.J.  
Second EUROMET comparison of air kerma rate and activity measurements of  $^{192}\text{Ir}$  brachytherapy wires.  
Nucl. Instrum. Methods, Phys. Res. A 339 (1994) 386
- REHER, D.F.G., DENECKE, B., DE ROOST, E., VAN DER MEER, K.  
Standardization of a 50 GBq  $^{152,154}\text{Eu}$  extended volume source.  
Nucl. Instrum. Methods, Phys. Res. A 339 (1994) 334
- SOLÉ, V.A., DENECKE, B., MOUCHEL, D., BAMBYNEK W.  
Measurement of  $P_k \omega_k$  in the decay of  $^{56}\text{Zn}$  and the K-shell fluorescence yield of copper.  
Appl. Radiat. Isotop., Int. J. Radiat. Appl. Instrum. A 45 (1994) 941
- STEINBAUER, E., BAUER, P., GERETSCHLÄGER, M., BORTELS, G.,  
BIERSACK, J.P., BÜRGER, P.  
Energy resolution of silicon detectors : approaching the physical limit.  
Nucl. Instrum. Methods, Phys. Res. B 85 (1994) 642
- STEINBAUER, E., BORTELS, G., BAUER, P., BIERSACK, J.P., BÜRGER, P.,  
AHMAD, I.  
A survey of the physical processes which determine the response function of silicon detectors to alpha particles.  
Nucl. Instrum. Methods, Phys. Res. A 339 (1994) 102
- STÜBER, W.  
Oszillatoren - per Langwelle kalibriert.  
Elektronik 8 (1994) 80
- URITANI, A., GENKA, T., MORI, C., REHER, D.F.G.  
Analytical calculations on radioactivity measurements of  $^{192}\text{Ir}$  metallic sources with a calibrated ionization chamber.  
Nucl. Instrum. Methods, Phys. Res. A 339 (1994) 377
- WORDEL, R., MOUCHEL, D., SOLÉ, V.A., HOOGEWERFF, J., HERTOGEN, J.  
Investigation of the natural radioactivity of volcanic rock samples using a low background gamma-ray spectrometer.  
Nucl. Instrum. Methods, Phys. Res. A 339 (1994) 322

## SPECIAL PUBLICATIONS

HANSEN, H.H. (ed.)  
Annual Report 93. EUR 15659 EN (1994)

HANSEN, H.H. (ed.)  
Annual Progress Report on Nuclear Data 1993  
NEA/NSC/DOC(94)22;INDC (EUR) 028/G; EUR 15822 EN (1994)

## GLOSSARY

A E R E	Atomic Energy Research Establishment, Harwell (UK)
A N L	Argonne National Laboratory, Argonne (USA)
B I P M	Bureau International des Poids et Mesures, Sèvres (F)
C B N M	Central Bureau for Nuclear Measurements (now IRMM)
C E A	Commissariat à l'Energie Atomique, Paris (F)
C E C	Commission of the European Communities
C E R N	Centre Européen pour la Recherche Nucléaire
C N R S	Centre National de la Recherche Scientifique
D F N	Deutsches Forschungsnetz
D F T	Density Functional Theory
D G	Direction Générale
E C	European Community
E C N	Energieonderzoek Centrum Nederland, Petten (NL)
E F F	European Fusion File
E F G	Electric Field Gradient
E N D F	Evaluated Nuclear Data File
E R D A	Elastic Recoil Detection Analysis
E T L	Electrotechnical Laboratory, Ibaraki (Japan)
E U	European Union
E W G R D	European Working Group on Reactor Dosimetry
F W H M	Full Width at Half Maximum
G E L I N A	Geel Electron Linear Accelerator
H F	Hartree-Fock
H O P G	Highly Oriented Pyrolytic Graphite
H P G e	High Purity Germanium
I A E A	International Atomic Energy Agency, Vienna (A)
I C R M	International Committee for Radionuclide Metrology
I L L	Institut Laue-Langevin, Grenoble (F)
I N D C	International Nuclear Data Committee
I N F N	Istituto Nazionale di Fisica Nucleare, Legnaro (I)
I N W	Instituut voor Nucleaire Wetenschappen
I R M M	Institute for Reference Materials and Measurements, Geel (B)
J A E R I	Japan Atomic Energy Research Institute, Tokai-Mura (Japan)
J E F	Joint European File
J E N D L	Japanese Evaluated Data Library
J I N R	Joint Institute for Nuclear Research, Dubna (Russia)
J R C	Joint Research Centre
K F A	Kernforschungsanlage, Jülich (D)

K F K	Kernforschungszentrum Karlsruhe, Karlsruhe (D)
K U	Katholieke Universiteit, Leuven (B)
L P R I	Laboratoire Primaire des Rayonnements Ionisants (F)
N B S	National Bureau of Standards, Gaithersburg (USA)
N E A	Nuclear Energy Agency, Paris (F)
N E A N D C	Nuclear Energy Agency's Nuclear Data Committee
N I S T	National Institute of Standards and Technology, Gaithersburg (USA)
N P L	National Physical Laboratory, Teddington (UK)
N R A	Nuclear Reaction Analysis
N R R A	Nuclear Resonant Reaction Analysis
N R C C	National Research Council of Canada
O R E L A	Oak Ridge Electron Linear Accelerator
O T R	Optical Transition Radiation
P N C	Parity Non Conservation
P T B	Physikalisch-Technische Bundesanstalt, Braunschweig (D)
R H F	Restricted Hartree-Fock
R P L	Radiation Physics Laboratory
R U G	Rijksuniversiteit Gent, Gent (B)
S C K / C E N	Studiecentrum voor Kernenergie/ Centre d'Etudes Nucléaires, Mol (B)
S I R	Système International de Référence
S M T	Standards, Measurements and Testing
S P	Smith-Purcell
T D P A D	Time Differential Perturbed Angular Distribution
T H	Technische Hochschule
T O F	Time of Flight
T R	Transition Radiation
T U	Technical University
T U I	Transuranium Institute (JRC Karlsruhe)
U H F	Unrestricted Hartree-Fock
W R E N D A	World Request List for Neutron Data Measurements

## CINDA ENTRIES LIST

ELEMENT		QUANTITY	TYPE	ENERGY		DOCUMENTATION		LAB	COMMENTS
S	A			MIN	MAX	REF VOL PAGE	DATE		
U	235	NF	EXP	30 + 4	20 + 5	INDC(EUR) 029-03	95	GEL	HAMBSCH-/H(N,N) SAMPLE CH.
Cf	252	SF	EXP			INDC(EUR) 029-03	95	GEL	VAN AARLE. CORR. GAMMA EMIS.
Np	237	NF	EXP	30 + 4	55 + 5	INDC(EUR) 029-11	95	GEL	SIEGLER - FISS. FR. M,E DISTR.
U	283	NG	EXP	20 + 0	80 + 1	INDC(EUR) 029-16	95	GEL	GUNSING ABOVE GSTATE OF U <sup>239</sup>
B	10	NT	EXP	80 + 0	18 + 6	INDC(EUR) 029-07	95	GEL	BRUSEGAN - CRAMETZ
Pu	242	SF	EXP			INDC(EUR) 029-17	95	GEL	WAGEMANS - FIS. FR. M,E DISTR.
Pu	244	SF	EXP			INDC(EUR) 029-17	95	GEL	WAGEMANS - FIS. FR. M,E DISTR.
U	235	NF	EXP	20-3	10 + 2	INDC(EUR) 029-18	95	GEL	WAGEMANS - TERNARY FISSION
Cd	113	NG	EXP	10 + 0	60 + 4	INDC(EUR) 029-32	95	GEL	CORVI - SPIN ASSIGNMENT
Ni	58	NT	EXP	14 + 0	30 + 6	INDC(EUR) 029-22	95	GEL	ROHR - SHELLEY HI. RES.
Ni	60	NT	EXP	14 + 0	30 + 6	INDC(EUR) 029-22	95	GEL	ROHR - SHELLEY HI. RES.
Ni	58	NG	EXP	15 + 3	26 + 4	INDC(EUR) 029-23	95	GEL	CORVI - RESONANCE ANALYSIS
Cl	35	NP	EXP	10 + 1	10 + 4	INDC(EUR) 029-30	95	GEL	WAGEMANS NUCLEOSYTH.
Cl	36	NP	EXP	10 + 1	10 + 4	INDC(EUR) 029-30	95	GEL	WAGEMANS NUCLEOSYTH.
Cl	36	NA	EXP	10 + 1	10 + 4	INDC(EUR) 029-30	95	GEL	WAGEMANS NUCLEOSYTH.
Ca	41	NA	EXP	10 + 2	10 + 5	INDC(EUR) 029-32	95	GEL	WAGEMANS, WEIGMANN
Ba	138	NT	EXP	80 + 0	20 + 4	INDC(EUR) 029-33	95	GEL	BRUSEGAN - RES. PAR. ANAL.
Pd	110	NNG	EXP	20 + 4	33 + 5	INDC(EUR) 029-35	95	GEL	WATTECAMPS - MEISTER
Mo	0	NNG	EXP	55 + 5	55 + 5	INDC(EUR) 029-37	95	GEL	WATTECAMPS - BIRN
U	238	NT	EXP	60-1	60-1	INDC(EUR) 029-39	95	GEL	TAGZIRIA, ROYER (D. BROAD.)
Pb	208	NG	EXP	10 + 2	90 + 4	INDC(EUR) 029-39	95	GEL	BEER, MUTTI NUCLEOSYTH
Fe	0	NT	EXP	20 + 4	20 + 6	INDC(EUR) 029-24	95	GEL	BERTHOLD - WEIGMANN HI. RES.
Al	27	NT	EXP	20 + 4	20 + 6	INDC(EUR) 029-25	95	GEL	SHELLEY - ROHR HI. RES.
V	0	NT	EXP	80 + 0	25 + 6	INDC(EUR) 029-26	95	GEL	SHELLEY - ROHR HI. RES.
Th	232	NT	EXP	15 + 5	18 + 6	INDC(EUR) 029-26	95	GEL	CRAMETZ - WATTECAMPS
Ni	58	NX	EXP	20 + 5	16 + 6	INDC(EUR) 029-27	95	GEL	WATTECAMPS - Ni <sup>58</sup> /Al <sup>27</sup>
Cu	63	NX	EXP	20 + 5	16 + 6	INDC(EUR) 029-27	95	GEL	TASBARIS - Cu <sup>63</sup> /Ni <sup>58</sup>

European Communities - Commission

EUR 16288 EN - ANNUAL PROGRESS REPORT ON  
NUCLEAR DATA 1994

Institute for Reference Materials and Measurements

H. H. Hansen (ed.)

Luxembourg: Office for Official Publications of the European Communities

1995 - pag. 75 - 21.0 x 29.7 cm

EN

## NOTICE TO THE READER

All scientific and technical reports published by the European Commission are announced in the monthly periodical '**euro abstracts**'. For subscription (1 year: ECU 60) please write to the address below.



OFFICE FOR OFFICIAL PUBLICATIONS  
OF THE EUROPEAN COMMUNITIES

L-2985 Luxembourg